

# CHALMERS



## Design with Regard to Blast- and Fragment Loading

*Master's Thesis in the Master's programme Structural Engineering and Building  
Performance Design*

KARL-JOHAN EK

PÄR MATTSSON

Department of Civil and Environmental Engineering  
*Division of Structural Engineering*

*Concrete Structures*

CHALMERS UNIVERSITY OF TECHNOLOGY

Göteborg, Sweden 2009

Master's Thesis 2009:81



MASTER'S THESIS 2009:81

# Design with Regard to Blast- and Fragment Loading

Master's Thesis in the *Master's programme Structural Engineering and Building Performance Design*

KARL-JOHAN EK

PÄR MATTSSON

Department of Civil and Environmental Engineering  
*Division of Structural Engineering*  
*Concrete Structures*

CHALMERS UNIVERSITY OF TECHNOLOGY

Göteborg, Sweden 2009

Design with Regard to Blast- and Fragment Loading  
Master's Thesis in the *Master's programme Structural Engineering and Building  
Performance Design*

KARL-JOHAN EK  
PÄR MATTSSON

© KARL-JOHAN EK & PÄR MATTSSON, 2009

Examensarbete 2009:81  
Department of Civil and Environmental Engineering  
Division of Structural Engineering  
Concrete Structures  
Chalmers University of Technology  
SE-412 96 Göteborg  
Sweden  
Telephone: + 46 (0)31-772 1000

Chalmers Reproservice /Department of Civil and Environmental Engineering  
Göteborg, Sweden 2009

## Design with Regard to Blast- and Fragment Loading

Master's Thesis in the *Master's programme Structural Engineering and Building Performance Design*

KARL-JOHAN EK

PÄR MATTSSON

Department of Civil and Environmental Engineering

Division of Structural Engineering

Concrete Structures

Chalmers University of Technology

### ABSTRACT

When a bomb detonates a blast wave is created and the case of the bomb is fragmentized into many fragments, which are released with a very high initial velocity. The fragmental impact is commonly considered in a simplified way, but studies carried out shows that fragments, combined with the blast load, can seriously damage a reinforced concrete structure if the detonation takes place close to a building. Hence, focus in this project is to simulate the fragments and their effects in a more advanced way and investigate how these results differ from simplified analyses.

A simply supported, reinforced concrete beam, with geometry and reinforcement configuration corresponding to a civil defence shelter wall, is to be analysed. The blast wave is consistently applied as an uniformly distributed load with a constant duration and amplitude. The fragmental impact on the other hand is analysed in various ways to see how the structural response in simplified analyses differ from more advanced ones. The fragmental impact and penetration into the concrete is also analysed, where the beam loses bearing capacity and mass.

To be able to analyse such a complex problem, transient, finite element analyses have been performed in the general finite element programme ADINA. The results obtained in these analyses have been compared to results obtained by single degree of freedom analysis and simplified hand calculation in order to verify the FE-results.

Concerning the impact of the fragmental loads appearance, it turned out that simplified and more advanced analyses, generates similar results. However, when the loss of stiffness and mass, due to fragmental penetration of the beam, are taken into account, this have significant influence on its dynamic behaviour.

Key words: Explosion, impulse load, fragment load, blast load, dynamics, single degree of freedom system (SDOF).

Dimensionering med Hänsyn till Stötvågs- och Splitterbelastning  
Examensarbete inom masterprogrammet Konstruktion och Byggnadsteknik  
KARL-JOHAN EK  
PÄR MATTSSON  
Institutionen för bygg- och miljöteknik  
Avdelningen för Konstruktionsteknik  
Betongbyggnad  
Chalmers tekniska högskola

## SAMMANFATTNING

När en bomb detonerar skapas en tryckvåg, varvid bombens mantel fragmenteras och mängder av splitter frigörs med mycket hög begynnelsehastighet. Splittrets påverkan på en konstruktion behandlas ofta på ett förenklat sätt men utförda studier visar att splitter tillsammans med stötvågen påtagligt kan skada en armerad betongkonstruktion som ligger i nära anslutning till explosionen. Fokus i detta projekt ligger därför på att simulera splitter och dess inverkan på ett mer nyanserat sätt för att kontrollera hur resultaten skiljer sig gentemot förenklade analyser.

En fritt upplagd, armerad betongbalk med geometri och armeringskonfiguration motsvarande en skyddsrumsvägg analyseras. Stötvågen behandlas konsekvent som en jämnt utbredd impulslast, med konstant varaktighet och amplitud, medan splittrets inverkan på balken analyseras på olika sätt för att undersöka hur responsen från förenklade analyser skiljer sig mot mer avancerade. Även splittrets anslag och inträngning i betongen analyseras, varvid balken förlorar lastkapacitet och massa.

För att kunna analysera sådana komplexa problem har tidsberoende, finita elementanalyser utförts i det generella finita elementprogrammet ADINA. Resultaten från dessa analyser har jämförts med förenklade enfrihetsgradsanalyser samt förenklade handberäkningar för att kunna verifiera resultaten.

Rörande inverkan av splitterlastens utseende visar sig förenklade och mer nyanserade analyser ge likvärdiga resultat. När balkens förlust av styvhet och massa, i samband med splitterinträngning, beaktas visar sig detta dock ha en betydande inverkan på balkens dynamiska beteende.

Nyckelord: Explosion, impulslast, splitterlast, stötvågslast, dynamik, enfrihetsgradsystem (SDOF).

# Contents

ABSTRACT	I
SAMMANFATTNING	II
CONTENTS	III
PREFACE	VII
NOTATIONS	VIII
1 INTRODUCTION	1
1.1 Background	1
1.2 Aim	1
1.3 Method	1
1.4 Limitations	1
1.5 Outline of the report	2
1.6 Comments about references	2
2 BASIC THEORY	4
2.1 Outline	4
2.2 Explosions	4
2.2.1 Orientation	4
2.2.2 Blast wave	4
2.2.3 Fragments	5
2.3 Dynamic modification of concrete	11
2.4 Materials	13
2.4.1 Material responses	13
2.4.2 Theory of plasticity and plastic hinges	16
2.5 Simply supported reinforced concrete beam	18
2.5.1 Mechanical properties	18
2.5.2 Analysis of cross-sections subjected to bending	20
2.6 Load-displacement relations for simply supported beam subjected to uniformly distributed load	25
2.7 Basic dynamics	26
2.7.1 Orientation	26
2.7.2 Force and pressure	26
2.7.3 Momentum, impulse and impulse intensity	26
2.7.4 Momentum and kinetic energy	27
2.7.5 Internal energy	28
2.7.6 The fundamental equation of motion	31
2.8 SDOF system	32
2.8.1 Orientation	32
2.8.2 Differential equation for an SDOF system	33
2.8.3 Transformation factors	34

2.9	The central difference method	36
3	THE STUDIED CASE	38
3.1	Orientation	38
3.2	Geometry	38
3.3	Material	40
3.4	Load	41
3.4.1	Orientation	41
3.4.2	Reference bomb	41
3.5	Blast load	42
3.6	Fragment loads	43
3.6.1	Fragmental impact on the beam	47
3.6.2	Combination of fragment and blast load	48
3.6.3	Simulation of fragments	50
3.6.4	Fragmental load angle	56
3.6.5	Fragment arrival time	57
3.6.6	Comments about load angle and arrival time	58
4	THE FE-MODEL	59
4.1	General description	59
4.2	Beam element model	60
4.2.1	Material properties	60
4.2.2	Elastic analysis	61
4.2.3	Elasto-plastic analysis	62
4.3	2D-solid element model	63
4.3.1	Element mesh and material properties	63
4.3.2	Elastic analysis	64
4.3.3	Elasto-plastic analysis	64
4.4	Simulation of removal of concrete due to fragmental impact	65
5	RESULTS	68
5.1	Orientation	68
5.2	Linear elastic analysis	68
5.2.1	Beam element model	68
5.2.2	Conclusion	75
5.3	Plastic analysis	76
5.4	Bilinear elasto-plastic analysis	77
5.4.1	Conclusion	85
5.5	SDOF results	85
5.6	2-D solid model	87
5.6.1	Comparison with beam element	87
5.6.2	Results when removing concrete due to the fragmental impact	89

6	CONCLUSIONS	91
7	REFERENCES	92
APPENDIX A	INPUT DATA IN ANALYSIS	93
APPENDIX B.1	CALCULATION OF CRACKING MOMENT	94
APPENDIX B.2	CALCULATION OF YIELDING MOMENT	95
APPENDIX B.3	CALCULATION OF ULTIMATE MOMENT	96
APPENDIX C	LOAD-DISPLACEMENT RELATION	98
APPENDIX D	MATERIAL AND CROSS SECTION CONSTANTS	99
APPENDIX E	HAND CALCULATION FOR DISPLACEMENTS	101
APPENDIX F	ERRORS IN ADINA WHEN USING EXPLICIT SOLVER	104
APPENDIX G	DIFFERENT RESULTS DUE TO NUMBER OF ELEMENTS	106
APPENDIX H	MOMENT AND REACTION FORCES	108
APPENDIX I	HAND CALCULATION WHEN MASS IS REDUCED	113
APPENDIX J	METHOD TO DERIVE TRANSFORMATION FACTORS	116
APPENDIX K	SDOF - TRANSITION FROM ELASTIC TO PLASTIC	117
APPENDIX L	INDATA FILE FOR ADINA	120



## Preface

In this Master's Thesis, blast- and fragmental load obtained by an explosion is analysed in accordance to a reference case from Räddningsverket (2006). Focus has been on the fragment load and how it should be considered. The project has been carried out in cooperation between the Division of Structural Engineering, Concrete Structures, at Chalmers University of Technology and Reinertsen Sverige AB. We had the opportunity to work at their office in Göteborg. It is a continuation of a previous Master's Thesis performed by Ulrika Nyström, 2006. The major part of this thesis have been carried out during the period from February to October 2009 and the report was finalized in August 2010.

Morgan Johansson, PhD from Reinertsen Sverige AB has been our supervisor in this project and we gratefully thank him for his commitment and engagement during the project. We would also like to thank the rest of the staff at Reinertsen for contributing to a nice working climate and for answering many questions during the project.

Our opponent, Jonas Ekström, has throughout the project contributed and given us good ideas and we would like to thank him. We would also like to thank Patrik Johansson and Håkan Lantz, who also did their Master's Thesis at Reinertsen, for great support and help during the project.

Finally, we would like to thank our adorable girlfriends for their support.

Göteborg August 2010

Karl-Johan Ek & Pär Mattsson

# Notations

## Roman upper case letters

$A$	Area
$A_I$	Equivalent area in state 1
$A_{II}$	Equivalent area in state 2
$A_{cc}$	Area of concrete
$A_s$	Area of reinforcement in tension zone
$A_s'$	Area of reinforcement in compression zone
$B$	Width of cross section
$E$	Young's modulus
$E_{cm}$	Young's modulus for concrete, mean value
$E_{c,fict}$	Fictive Young's modulus for the beam, concerning state 1 and 2
$E_s$	Young's modulus for steel
$F$	Force
$F_c$	Concrete force
$F_{cr}$	Load when first crack appears
$F_e$	Equivalent load
$F_{pl}$	External load corresponding to the plastic capacity
$F_{spl}$	Load when the reinforcement starts to yield
$F_s$	Steel force in tensioned reinforcement bars
$F_s'$	Steel force in compressed reinforcement bars
$M_R$	Internal resisting moment
$H$	Height of cross section
$I$	Impulse, moment of inertia
$I_I$	Moment of inertia for state 1
$I_{II}$	Moment of inertia for state 2
$I_{III}$	Moment of inertia for state 3
$K$	Stiffness
$K'$	Stiffness in the elasto-plastic range
$K_I$	Stiffness in state 1
$K_{II}$	Stiffness in state 2
$L$	Length
$M$	Mass, Moment
$M_A$	Fragment distribution factor
$M_e$	Equivalent mass
$M_h$	Bomb shell mass
$M_R$	Internal resisting moment
$M_y$	Moment when the reinforcement starts to yield
$P$	Pressure
$P^+$	Positive peak pressure
$P^-$	Negative peak pressure
$Q$	Load, mass of explosive
$R$	Internal resisting force, distance from the detonation to the structure under consideration
$R_e$	Equivalent resisting force
$R_M$	Maximum internal resisting force
$R_{stat}$	Internal static force

$R_{dyn}$	Internal dynamic force
$T^+$	Duration of positive phase
$T^-$	Duration of negative phase
$W_e$	External energy
$W_i$	Internal energy
$W_k$	Kinetic energy
$Z$	Flexural resistance
$Z_{el}$	Elastic flexural resistance
$Z_{pl}$	Plastic flexural resistance

### Roman lower case letters

$a$	Acceleration
$c$	Damping constant
$d$	Effective height of cross section
$d'$	Distance between the top reinforcement and the compressed edge
$e$	Height of the elastic zone of the cross-section
$f_{cc}$	Compressive strength for concrete
$f_{cy}$	Yield stress for concrete
$f_{ctm}$	Stress for which concrete cracks
$f_{yk}$	Characteristic yield stress for reinforcement
$i$	Impulse intensity
$i^+$	Positive impulse intensity
$i^-$	Negative impulse intensity
$m$	Mass
$m_i$	Fragment mass
$n$	Number of fragments
$p$	Momentum
$p_0$	Atmospheric pressure
$q$	Distributed load
$t$	Time
$t_a$	Arrival time for the pressure wave
$\Delta t$	Time increment
$u$	Displacement
$u_{cr}$	Displacement when first crack appears
$u_{el}$	Elastic displacement
$u_{pl}$	Displacement corresponding to the ultimate load
$u_{spl}$	Displacement when the reinforcement starts to yield
$\dot{u}$	Displacement velocity
$\ddot{u}$	Acceleration
$v$	Velocity
$v_0$	Initial velocity
$x$	Coordinate, height of compression zone
$x_{gc}$	Centre of gravity
$y$	Coordinate
$z$	Coordinate, distance from neutral axis to a certain level of the cross-section
$z_s$	Distance between reinforcement in tensile zone and the neutral axis

$z_s'$  Distance between reinforcement in compressive zone and the neutral axis

### Greek lower case letters

$\alpha$	Relation between the Young's modulus between concrete and reinforcement, parameter considering the shape of the blast wave
$\alpha_c$	Stress block factor
$\beta_c$	Stress block factor
$\varepsilon$	Strain
$\dot{\varepsilon}$	Strain rate
$\varepsilon_c$	Strain in concrete
$\varepsilon_{c1}$	Strain in compressed concrete
$\varepsilon_{c2}$	Strain in tensioned concrete
$\varepsilon_{cu}$	Ultimate compressive strain in concrete
$\varepsilon_s$	Steel strain
$\varepsilon_s'$	Steel strain in compressed reinforcement
$\varepsilon_{sy}$	Yield strain in steel
$\Delta\varepsilon$	Difference in strain
$\gamma$	Reduction factor for the elasticity of modulus
$\kappa_K$	Transformation factor for the internal force
$\kappa_{KF}$	Combined transformation factor for the internal force and external load
$\kappa_M$	Transformation factor for the mass
$\kappa_{MF}$	Combined transformation factor for the mass and external load
$\kappa_F$	Transformation factor for the external load
$\rho$	Density
$\phi$	Diameter
$\sigma$	Stress
$\sigma_c$	Concrete stress
$\sigma_{c1}$	Concrete stress in compressive zone
$\sigma_{c2}$	Concrete stress in tensile zone
$\sigma_{fict}$	Stress when the beam goes from linear elastic to ideally plastic response
$\sigma_s$	Steel stress
$\sigma_s'$	Steel stress in compressed reinforcement
$\sigma_y$	Yield stress
$\omega$	Angular frequency





# **1 Introduction**

## **1.1 Background**

Explosives are used for many different purposes in today's society. In the building industry explosives are used as an efficient method to demolish structures and to make space for roads and railways. Explosives play, in this context, an important role in order to improve the infrastructure.

Explosions can, on the other hand, also be a threat for both society and for human beings and explosives are unavoidable tools during war and terrorist attacks. An explosion can also occur by accident and cause large damage. These kinds of actions may be devastating and there is a need to improve the knowledge about explosions in order to make society more resistant against such events.

Swedish Rescue Service Agencies (Räddningsverket) has for several years run projects concerning explosions and their impacts. In previous projects most of the focus has been either on the blast wave or on fragment loading, while the combined load part from these two often has been either neglected or simplified approximately. However, it has been discovered by recent research (Leppänen, 2009 and Nyström, 2008) that the fragmental load plays a substantial part of the total damage obtained by the blast- and fragment loads.

## **1.2 Aim**

The main goal for this work is to increase the knowledge about how explosions affect concrete structures. A structure subjected to combined blast load and impact loading is studied, but focus will be on how fragments from a bomb should be considered when a structure is subjected to an explosion. In this thesis different ways to apply the fragmental load are studied and should result in recommendations and guidelines about how fragments should be taken into account.

## **1.3 Method**

Literature studies have been done in order to obtain knowledge and understanding how structures behave when they are exposed to dynamic loadings. The studied case is taken from the Swedish shelter regulations, Räddningsverket (2006), and is analysed using a SDOF system (single degree of freedom) and hand calculations and compared to the "true" behaviour which is obtained by a commercial finite element software.

## **1.4 Limitations**

Concrete is a complex material, which requires advanced calculations, and hence simplified material behaviors have been used in this project. These are linear elastic, ideally plastic and bi-linear elasto-plastic material properties. Material effects such as shrinkage, creep, temperature and the dead weight is not considered in the concrete calculations.

A reference case from Räddningsverket (2006) is used in this thesis where a civil shelter is exposed to impact from an explosion. The geometry and material requirements are chosen in accordance to the regulations stated in Räddningsverket (2006).

The fragmental impact which occurs during the penetration phase will not be analysed in this project, instead an approximated method used, which simulates the removal of concrete, is used.

## **1.5 Outline of the report**

The outline of the report can be divided into basic theory (Chapter 2), conditions and choices (Chapter 3), FE-model (Chapter 4), Results (Chapter 5) and conclusions (Chapter 6).

Chapter 2 is an introduction to explosions and in a comprehensive way describes the loads and their effects. It also describes important parts in a general way for a good understanding in the rest of the report, such as: materials, basic concrete material properties and how to analyse it, basic dynamics, and single degree of freedom-system.

Chapter 3 can be seen as a continuation of chapter 2, the conditions and choices for further analysis is presented. A more careful description of the loads is presented and also how the subdivision of the fragment loads is performed.

Chapter 4 describes the FE models, the input data and how the models are built up.

Chapter 5 presents the results from the analysis, for the linear elastic, plastic as well as the elasto-plastic response. Displacements are mainly presented and compared to the results obtained by SDOF and simplified hand calculations. The results from the removal of material due to the loads are also presented in chapter 5. After each section in this chapter, a conclusion regarding the result is presented.

Finally, Chapter 6 is a discussion where the results are concluded and the authors give their own reflections and recommendations about how the fragmental load should be considered.

## **1.6 Comments about references**

Large parts of the theories presented in this report are based on, and sometimes directly collected from other reports. This means that the reader is sometimes not referred to the main source but referred to a report where material from the main source is used and where the reference to the main source can be found. The theory presented in this report is mainly based on the following reports; Johansson and Laine (2009), Leppänen (2009), Nyström (2006) and Nyström (2008).

Material has also been collected from Räddningsverket (2006), in swedish: Myndigheten för samhällsskydd och beredskap, denoted as MSB in this report. This is an authority responsible for unifying, coordinating, and supportive tasks prior to, during and after emergencies in Sweden. This authority was formed from three existing national government authorities on the 1st January 2009. Former reports might refer to the Swedish Rescue Services Agencies which was one out of the three

former authorities. MSB has published the Swedish Shelter Regulation (SR) which will be an important reference in this work.

## 2 Basic theory

### 2.1 Outline

A structure subjected to an explosion will have a complex behaviour. Good knowledge about the properties of the load, the material response, the dynamical behaviour of the structure and analytical tools is necessary in order to analyse the response of the structure. Basic theory within these subjects is presented in this chapter.

### 2.2 Explosions

#### 2.2.1 Orientation

A bomb consists of a charge with a certain amount of explosives and a shell with a certain mass. A bomb can be seen as stored potential energy which will be transformed into mechanical work when the bomb detonates. The impact on a structure from an explosion can be divided into impact from the blast wave and impact from fragments which are released when the bomb case cracks.

#### 2.2.2 Blast wave

When the charge detonates, a blast wave with high pressure and temperature will spread out from the centre of the detonation, see Figure 2.1. The pressure will decrease with increasing distance from the detonation centre and the pressure front, referred to as the blast wave, will travel in supersonic speed. A blast wave consists of a positive and a negative phase and an idealized wave is illustrated in Figure 2.2. As can be seen, the positive phase is followed by a negative one.

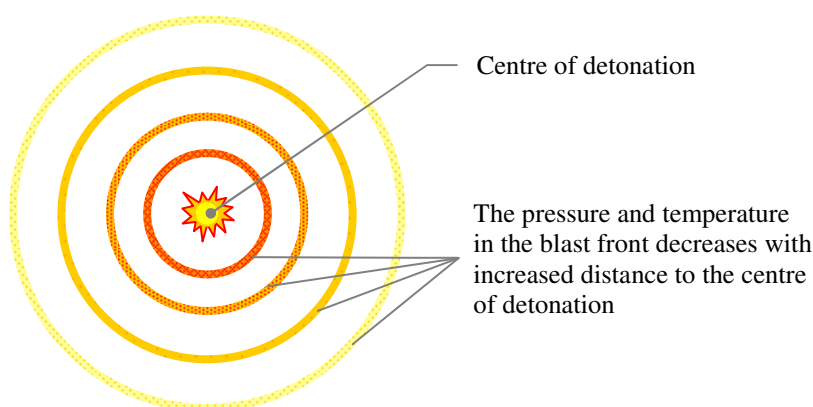


Figure 2.1 Schematic figure for detonation in air .

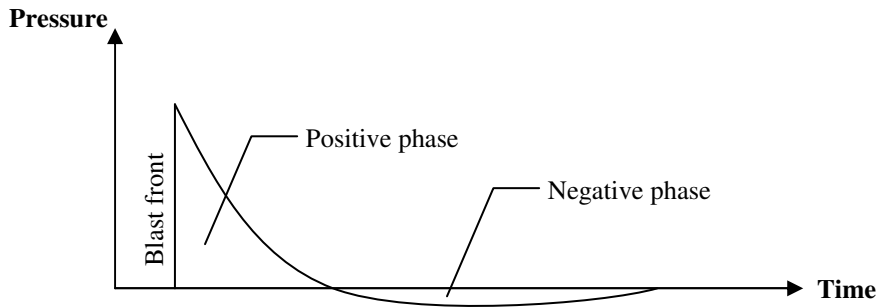


Figure 2.2 Idealized blast wave

The duration of the shock wave is very short and the load is applied very sudden. The loading velocity for a shock wave can be compared to other types of loads, see Figure 2.3. The reference case is a static load which is equal to 1 and for example, the creep is 100-1000 times smaller and a blast load is up to 100 million times larger.

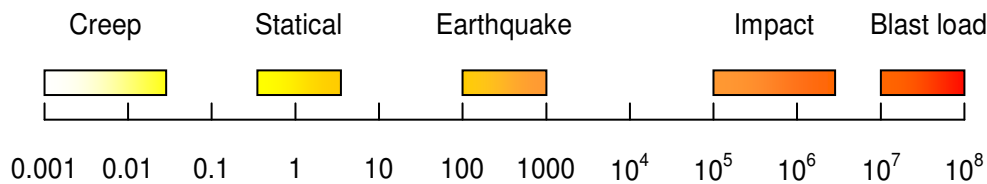


Figure 2.3 Difference in loading velocity between different types of loading, the values are obtained in relation to static load. From R ddningsverket (2006).

## 2.2.3 Fragments

### 2.2.3.1 Fragmentation

In addition to the blast wave, fragments will be released during the explosion. The appearance of the fragmentation process is directly affected by the properties of the bomb. This is why the properties and geometry of the bomb has to be known in order to predict the fragmentation.

When the bomb detonates, very high pressure is generated inside the bomb. The case will expand and tensile stresses are generated causing the envelope to crack into small fragments, see Figure 2.4.

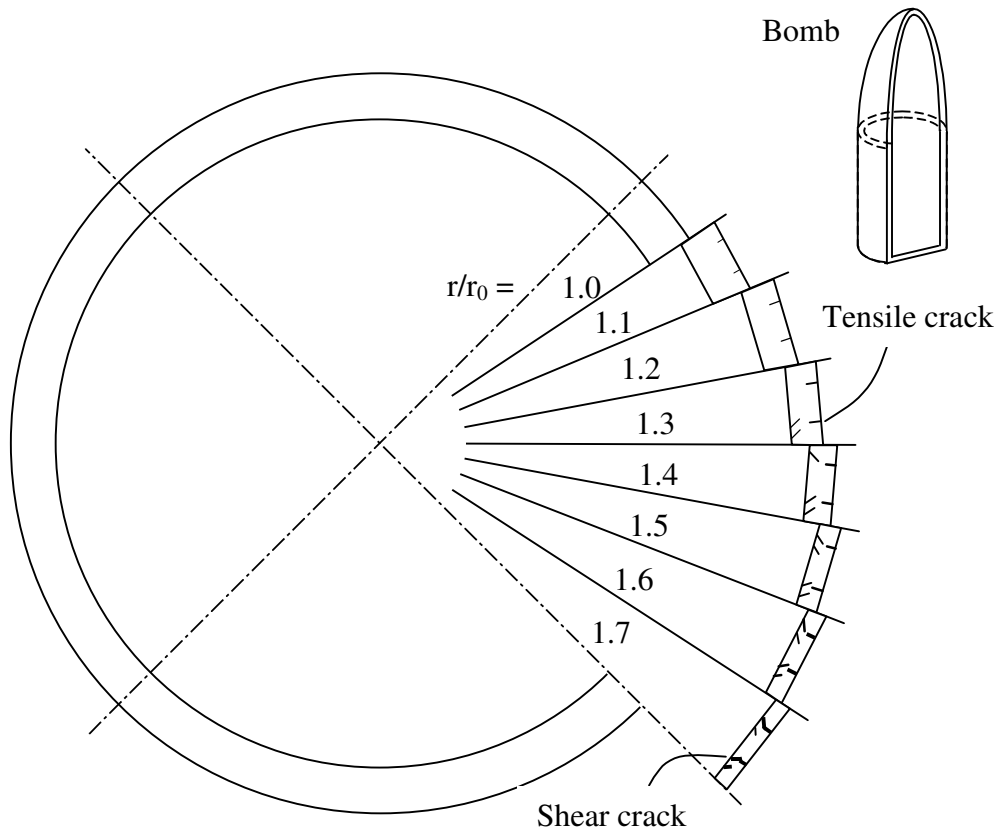


Figure 2.4 Fragmentation process of the case, Leppänen (2009).

A bomb consists of a charge with a certain amount of explosives and a case, see Figure 2.5. The case consists of a nose, a tail and an envelope. The distance from the surface of the bomb to the outer parts of the charge is normally much thicker in the nose and the tail compared to the envelope, something that also affect the fragmentation process.

The fragments will be thrown out at high velocities in directions indicated by the light grey segments in Figure 2.5. The nose and tail will be separated from the bomb and thrown out in opposite directions as indicated by the darker arrows in Figure 2.5.

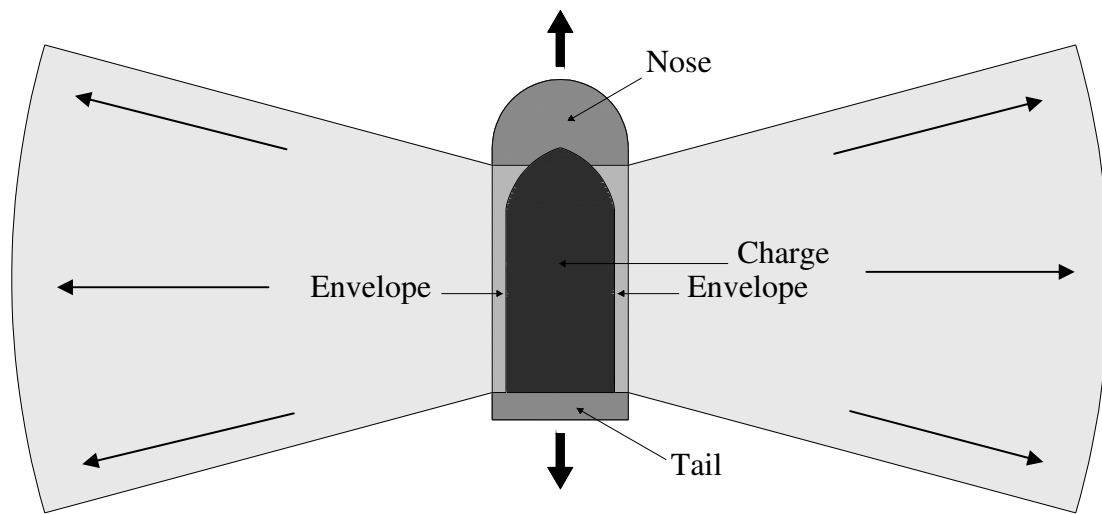


Figure 2.5 Schematic geometry of a bomb with the charge and the parts of the case with direction for how these parts behave when the charge detonates.

A structure that is hit by fragments will be exposed to an impact load that not only will increase the load on the structure but also locally damage the structure. How the structure is damaged depends on the magnitude of the fragmental impact and the properties of the structure itself. Three phenomenon can occur; penetration, perforation and scabbing. These will be explained in the following sections with a schematic description in Figure 2.6.

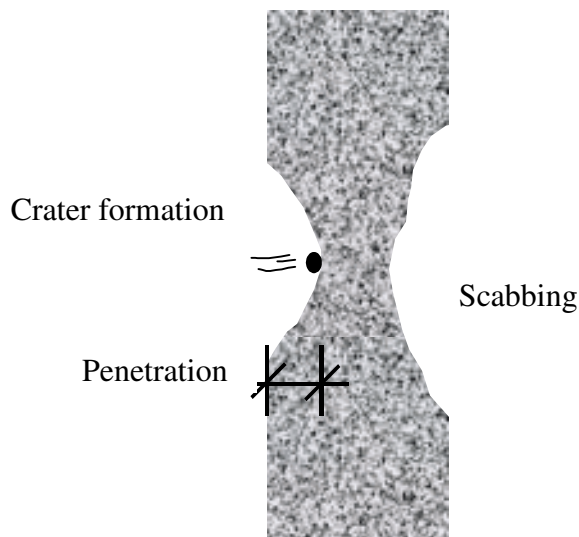


Figure 2.6 Different fragmental impacts, Leppänen (2009).

### 2.2.3.2 Penetration

A fragment that hits a concrete structure will penetrate into the structure. The concrete close to the surface will crush and a crater is formed i.e. spalling. In regions close to the crater the concrete will substantially crack and the effective height of the structural part will decrease, resulting in a reduced bearing capacity for the structural part. The reinforcement can also be cut off or get damaged, and the bond between concrete and reinforcement may decrease due to vibrations in the concrete during the penetration.

The penetration depth can, according to Leppänen (2009) be approximated as:

$$x = \frac{26.9 \cdot m_f^{0.37} \cdot v_f^{0.9}}{f_c^{0.25}} \quad \text{for} \quad x \leq 117 \cdot m_f^{1/3}$$

and

$$x = \frac{4.35 \cdot m_f^{0.4} \cdot v_f^{1.8}}{f_c^{0.5}} + 40.6 \cdot m_f^{1/3} \quad \text{for} \quad x > 117 \cdot m_f^{1/3} \quad (2.1)$$

where  $m_f$  is the mass of the fragment in [kg],  $v_f$  is the velocity of the fragment when it hits the structure in [m/s] and  $f_c$  is the compressive strength of concrete in [Pa].

Penetration depths as function of the velocity for fragments with different mass are presented in Figure 2.7.

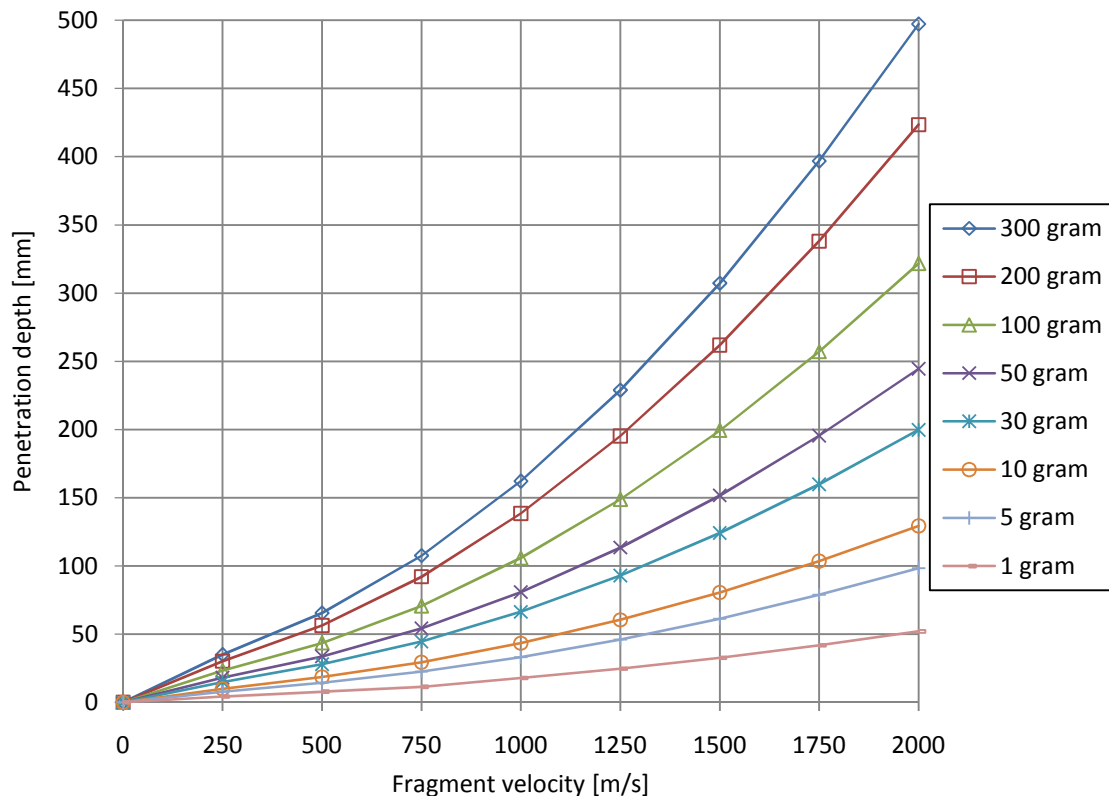


Figure 2.7 Penetration depths as a function of velocity for different fragment masses.

### 2.2.3.3 Perforation

Perforation is the same as penetration with the difference that the fragment penetrates through the beam. As a rule of thumb Leppänen (2009) means that, if 70 % of the concrete member is penetrated, perforation will occur.

### 2.2.3.4 Scabbing

When the fragment hits a concrete structure, extruding at the back side may occur, so called scabbing. This happens because the pressure wave in the concrete created by the fragment impact will be transformed into a tension wave at the back side of the beam, causing the concrete to crack. This is a phenomenon also influenced by the blast wave.

Leppänen (2009) refers to Krauthammer, who means that as a rule of thumb can be used what concerns scabbing, which follows: if fragments are penetrating 50 % or more of the members' thickness, scabbing will occur.

### 2.2.3.5 Fragmental distribution

The complexity of the geometrical properties of a bomb results in a non uniformly distribution of fragment when the charge detonates. As mentioned in section 2.2.3.1, the tail and the nose will remain fairly intact and thrown out as large masses in opposite directions, see Figure 2.8. The small fragments released from the envelope will be thrown out as a relatively concentrated swarm. According to Leppänen (2009) it is a good estimation to say that 60 percent of the total mass of the case will be thrown out as small fragments within an angle of 40 degrees as shown in Figure 2.8, which shows a simplified bomb compared to Figure 2.5.

The fragmental impact from a bomb on a structure will be very different depending on the position of the bomb when it detonates, i.e. if the structure is exposed to the small fragments within the swarm or for the large fragments made up of the nose and tail.

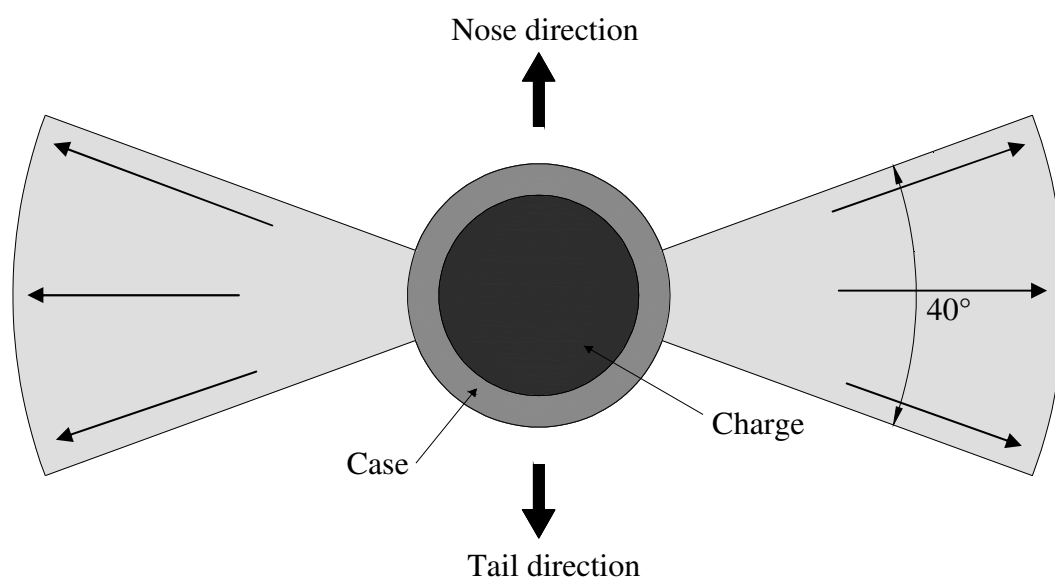


Figure 2.8 Simplified figure of a bomb with fragmental distribution after detonation.

### 2.2.3.6 Fragment velocity

The initial velocity of a fragment directly after the fragmentation is a function of the amount of explosives inside the bomb and the mass of the case and can, according to Leppänen (2009), be calculated as:

$$v_0 = 2400 \cdot (1 - e^{-2 \cdot Q / M_h}) \quad (2.2)$$

where  $Q$  is the mass of the explosives and  $M_h$  is the mass of the bomb shell.

The velocity of a fragment is decreased by the air resistance as a function of the distance from the centre of the detonation and the mass of the fragment itself. The velocity of a fragment at a certain distance from the centre of the detonation is, according to Leppänen (2009), defined as:

$$v_{i(r,m_i)} = v_0 \cdot e^{-0,0456 \cdot R / \sqrt[3]{m_i}} \quad (2.3)$$

where  $R$  is the distance from the centre of the detonation and  $m_i$  is the mass of the fragment. Fragment velocities as function of fragment mass at a distance of 5 meters are presented in Figure 2.9.

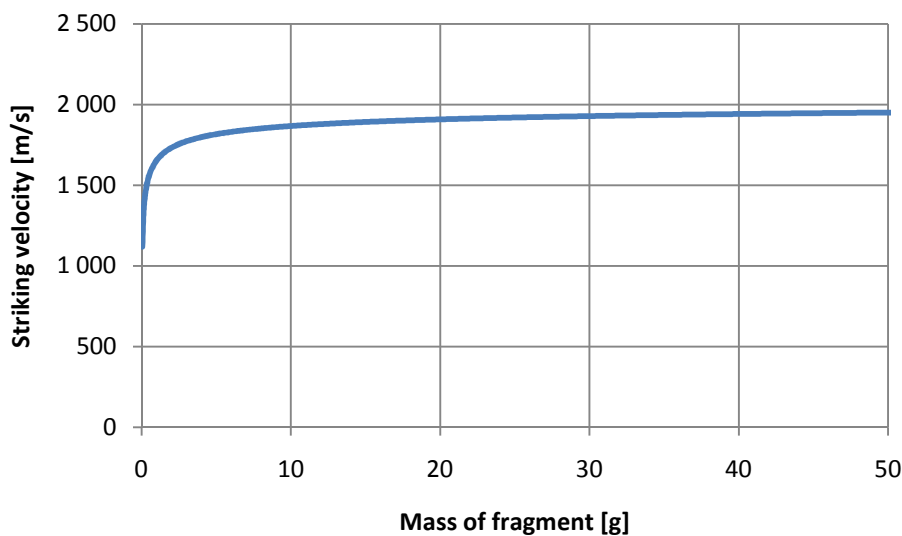


Figure 2.9 Relation between striking velocities and mass for a distance  $R=5$  m, initial velocity of 1950 m/s and 125 kg TNT.

It can be observed that fragments with larger mass will have higher velocity at a certain distance than fragment with smaller mass. This is due to that the air resistance can decelerate a lighter fragment more efficiently. The effect is most obvious when the fragmental weight is less than about 5 gram.

### 2.2.3.7 Fragment mass distribution

When the bomb envelope cracks, fragments with different mass (i.e size since the envelope consists of homogenous material) are released. The mass distribution of these fragments is different for different kinds of bombs.

Leppänen (2009) uses the following empirical expression to calculate the mass distribution:

$$n_{(m_s)} = \frac{M_h}{2 \cdot M_A} e^{-\sqrt{\frac{m_s}{M_A}}} \quad (2.4)$$

where  $n_{(m_s)}$  is the number of fragments with a mass larger than  $m_s$ ,  $M_h$  is the total mass of the case and  $M_A$  is a fragment distribution factor depending on the type of bomb.

## 2.3 Dynamic modification of concrete

A concrete structure exposed to dynamic load behaves different compared to a structure exposed to static load, especially for an intense impulse load with very short duration. This can partly be described by the structural response which behaves differently due to the time effects and also the material properties changes substantially.

The strain velocity  $\dot{\varepsilon}$  describes how fast the material deforms and is defined as the strain per unit time:

$$\dot{\varepsilon} = \frac{\Delta\varepsilon}{\Delta t} \quad (2-5)$$

The faster the load is applied to the structure, the higher the strain rate will be. In experimental tests it has been discovered that for increased strain rates the dynamic magnification factor, defined as the relation between the dynamic and the static strength, increases for concrete in both compression and tension. The dynamic magnification factors are presented in Figure 2.10 and Figure 2.12 for compression and tension respectively with varying strain velocities.

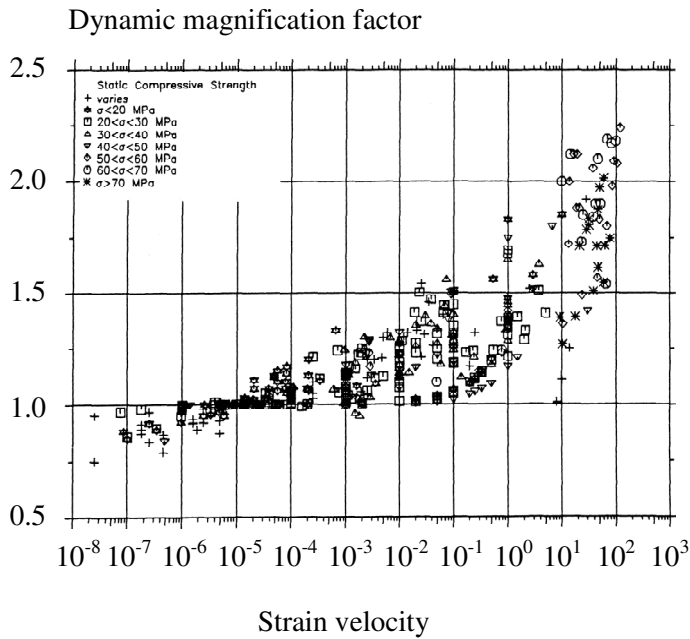


Figure 2.10 Relation between dynamic magnification factor and strain velocity for compressed concrete. Räddningsverket (2006).

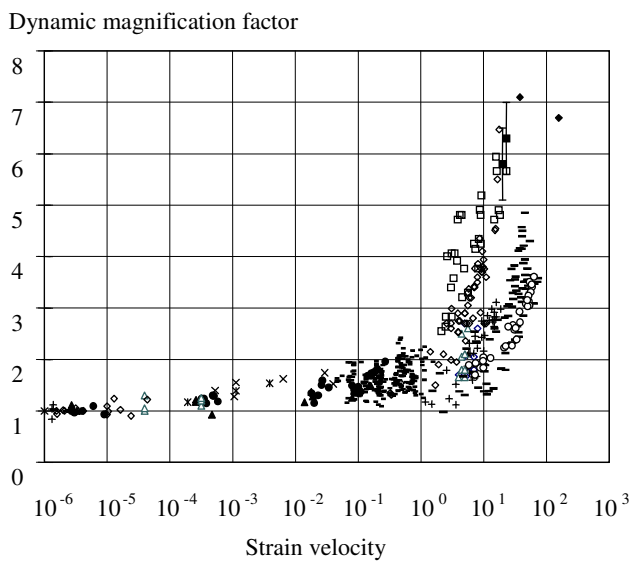


Figure 2.11 Relation between dynamic magnification factor and strain velocity for tensioned concrete. Räddningsverket (2006).

The behaviour can be explained by study the crack paths when the material cracks, see Figure 2.12. When a concrete structure is exposed to a static load, the material will find the most energy efficient way to reach failure. Since the aggregates are stronger than the paste, in normal strength, the crack will go through the paste and around the aggregate to find “the weakest way” when static loading is applied. For a dynamic load with short duration the material will find the fastest way to reach failure. The crack will now go straight through the paste and the aggregate. More energy is consumed in the latter case and this is one reason for an increased resistance can be assumed for a dynamic load with short duration.

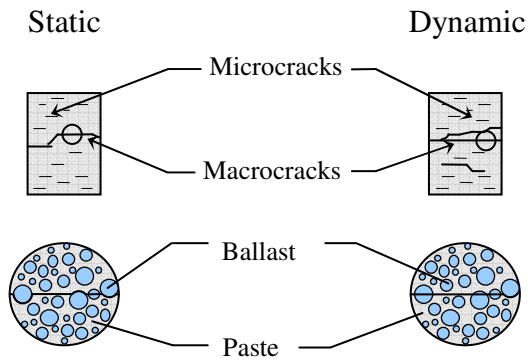


Figure 2.12 Principle crack paths for static and dynamic loads respectively. Based on R ddningsverket (2006).

A concrete beam subjected to a dynamic load will behave different compared to a static case. When the load is applied very fast there can be local failures in the beam before other parts of the beam and the supports even are aware of the load. This can be explained by that it takes a certain time for the information to be spread out along the beam. The velocity for which information is spread in concrete is approximately 3500 m/s. Hence, for a beam with a length of 2.7 m it will take  $2.7/(2 \cdot 3500) \approx 0.39$  ms for the information of a load acting in the mid section to reach the support. Hence, it will take a total of 0.78 ms for the information to go to the support and back to the loaded midsection again. The phenomenon is illustrated in Figure 2.13 where a typical example of direct shear failure is shown.

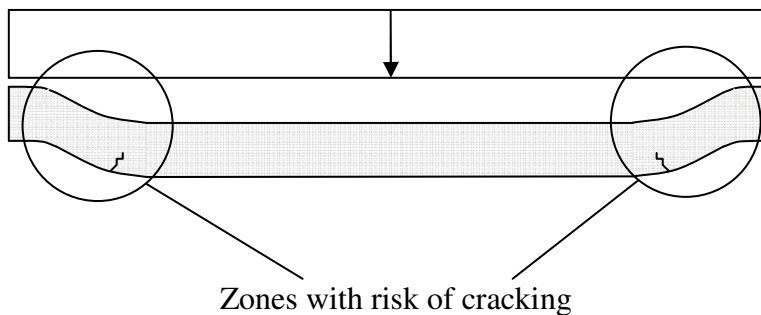


Figure 2.13 Principle initial behaviour of beam subjected to a dynamic uniformly distributes load.

## 2.4 Materials

### 2.4.1 Material responses

The response of a structural system when subjected to a certain load depends on the material responses in the structural parts and the boundary conditions between the parts. This is why it is important to predict the material response in a structural part in order to predict the global response of the structural system.

The true response of a building material exposed to a load is often complex with both linear and non-linear stages. It is, however, possible to simplify the behaviour in a satisfactory way. Ideally elastic, plastic or elasto-plastic responses are examples of

simplifications of a complex material response. These three responses will be explained in the following sections. Of these simplifications, the bilinear elasto-plastic is the most realistic response of a reinforced concrete structure and closest to the true behaviour, but the elastic and plastic are also analysed in order to increase the understanding.

#### 2.4.1.1 Linear elastic material

The relation between stress and strain in the linear elastic material response can be seen in Figure 2.14. The stress,  $\sigma$ , is linearly proportional to the strain,  $\varepsilon$ , and the curve originates from Hook's law:

$$\sigma = E \cdot \varepsilon \quad (2-6)$$

where  $E$  is the Young's modulus.

When the load is removed for a structure with linear elastic response the member will go back to its original position and the material will not gain any permanent deformations.

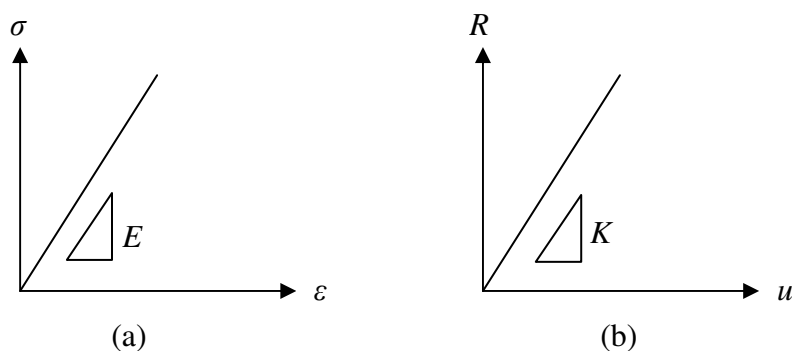


Figure 2.14 Linear elastic material response, where (a) is the material response and (b) the structural response.

Since the material properties are linear, the internal resisting force will also behave linearly. That means the resisting force,  $R$ , which the structure gains when it deflects, is linearly proportional to the deflection,  $u$ , i.e.:

$$R = K \cdot u \quad (2-7)$$

where  $K$  is the system's stiffness.

#### 2.4.1.2 Ideal plastic material

The relation between stress and strain in the ideal plastic material response can be seen in Figure 2.15. The body will stay undeformed as long as the applied stress is lower than the yield stress,  $\sigma_y$ . Once the yield stress is reached, though, the strain will increase without increased stress.

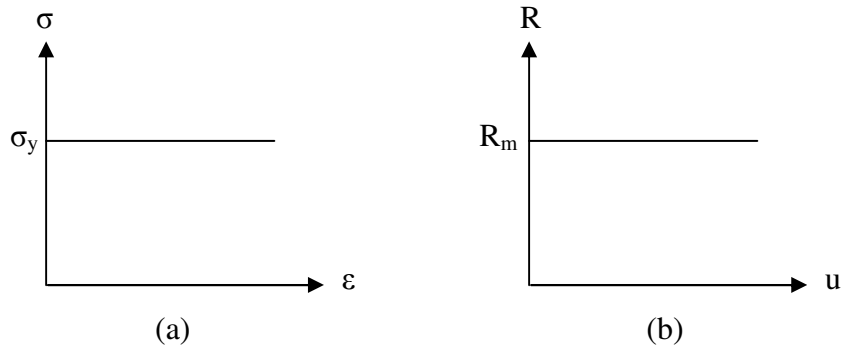


Figure 2.15 Ideal plastic material response, where (a) is the material response and (b) the structural response.

The internal resisting force,  $R$ , for a body with plastic material response that is exposed to a load,  $F$ , can be expressed as:

$$R = F \quad \text{for} \quad F < R_m \quad \text{i.e.} \quad u = 0 \quad (2-8)$$

$$R = R_m \quad \text{for} \quad F \geq R_m \quad \text{i.e.} \quad u \neq 0$$

where  $R_m$  is the maximum internal force.

### 2.4.1.3 Bilinear elasto-plastic material

The bilinear elasto-plastic material response is a combination of the linear elastic and plastic response and is equal to the linear elastic response until the material/materials yields. As can be seen in Figure 2.17 the material response will be plastic after yielding is initiated. The deformation after yielding is unlimited assuming ideal plastic material behavior. When the structure is unloaded after the yield stress is passed, the response will follow the linear elastic stiffness as shown in Figure 2.17.

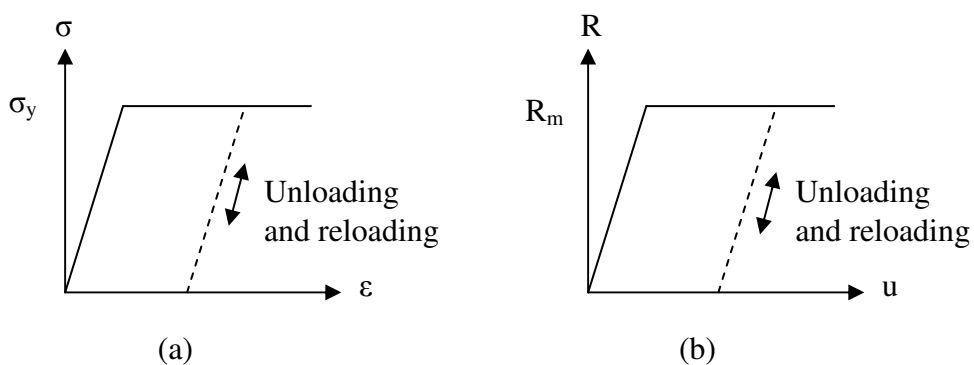


Figure 2.16 Bilinear elasto-plastic material response where (a) is the material response and (b) the structural response.

In the plastic response the structure will, if passing the yield strength, gain permanent deformations and also consume much more energy compared to the linear elastic response for the same load.

The expression for the internal force needs to be divided into two intervals, one for the elastic part and another one for the plastic part, see equations (2-9).

$$R = K \cdot u \quad \text{For } F(t) < R_m \quad (2-9)$$

$$R = R_m \quad \text{For } R_m \leq F(t)$$

where  $K$  is the stiffness of the systems and  $R_m$  is the maximum value of the resisting force.

## 2.4.2 Theory of plasticity and plastic hinges

A beam with elasto-plastic material response that is exposed to a bending moment will start to yield when the moment give rise to stress in the outer fibres in the most critical section that is equal to the yielding stress of the material. The material will have elastic response until yielding is reached. As can be seen in Figure 2.17a the stress distribution will be linearly distributed over the height of the cross section as long as the stress is equal to or less than the yielding stress in the outer fibres. When the moment increases further, more fibres has to yield in the cross-section in order to increase the internal resisting moment, see Figure 2.17b. When all fibres over the height of the cross section have reach the yielding stress, see Figure 2.17c, the maximal internal moment is reached, the plastic moment.

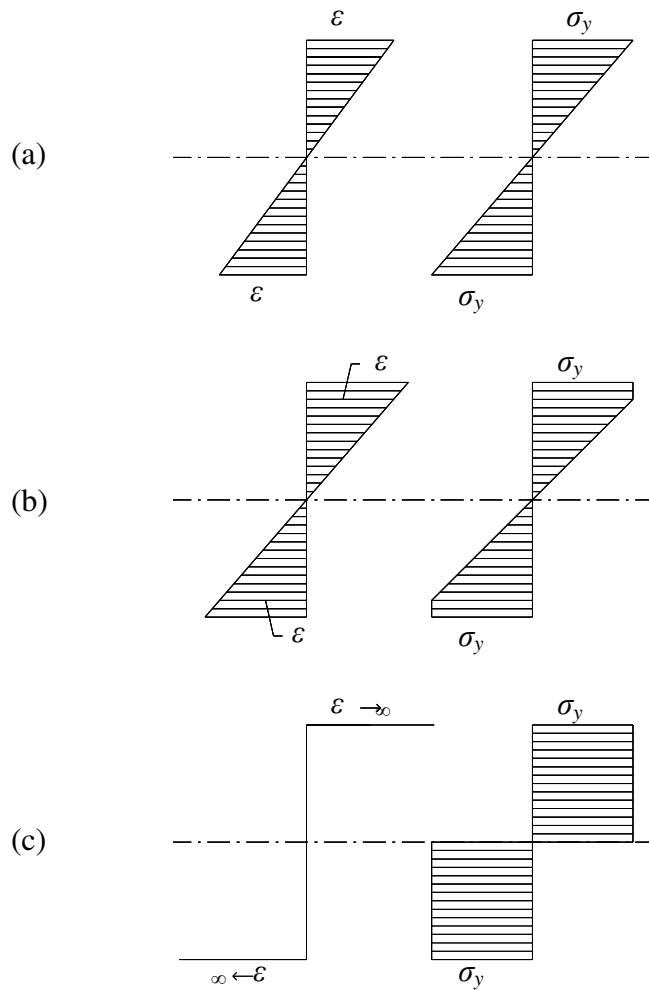


Figure 2.17 Stress and strain distribution for beam subjected to pure bending when a) yielding starts in the outer, most stressed fibres, b) parts of the cross section has yielded and c) the whole section has yielded.

The internal resisting moment can be calculated as:

$$M_R = Z \cdot \sigma_y \quad (2-10)$$

where  $Z$  is the flexural resistance and  $\sigma_y$  is the yield stress.

The flexural resistance can for a partly plastic section be calculated according to equation (2-11) and Figure 2.18.

$$Z = B \cdot \left( \frac{H^2}{4} - \frac{e^2}{12} \right) \quad (2-11)$$

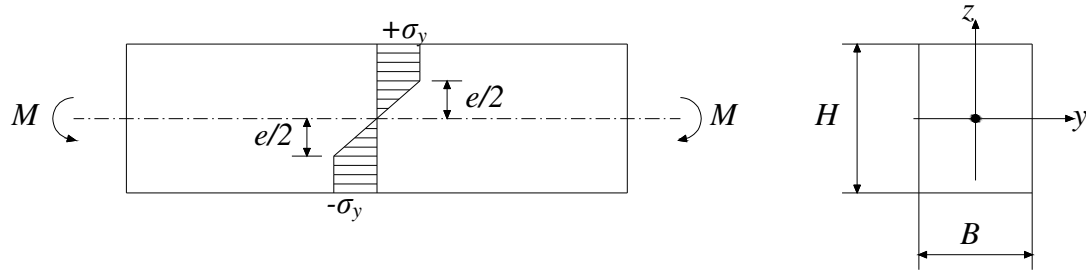


Figure 2.18 Stress distribution when the cross section goes from elastic to fully plastic.

When the material starts to yield, Figure 2.17a, the stress distribution is equal to the elastic stress distribution and the flexural resistance is:

$$Z_{el} = B \cdot \left( \frac{H^2}{4} - \frac{H^2}{12} \right) = \frac{BH^2}{6} \quad (2-12)$$

The flexural resistance for a fully plastic section, Figure 2.17c, is:

$$Z_{pl} = \frac{BH^2}{4} \quad (2-13)$$

When the beam reaches its fully plastic capacity in the most stressed section, the majority of the deformations will occur in this region, which will generate a large plastic rotation. This rotation will be rather concentrated, which makes it possible to assume that all the deformation takes place in this region. A small, deformable element over which all the deformations occurs is called a plastic hinge and for a simply supported beam a failure mechanism is formed when one plastic hinge is created in the most critical section, i.e. the mid section, see Figure 2.19.

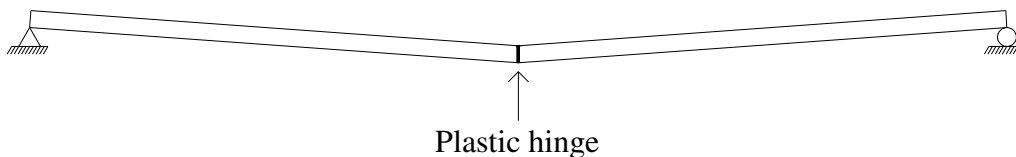


Figure 2.19 Plastic hinge for a simply supported beam.

## 2.5 Simply supported reinforced concrete beam

### 2.5.1 Mechanical properties

A simply supported, reinforced concrete beam will have different behaviour for different load magnitudes. The stiffness of the beam for a certain load magnitude will be strongly influenced by the material properties of concrete and steel and the geometrical properties of the cross section. Three different states: uncracked, cracked and failure, can be distinguished for the beam. The behaviour of a reinforced concrete beam can be described by the load versus displacement relation shown in Figure 2.20 with its various states.

As long as the beam is uncracked, i.e. the tensile stress in the concrete is lower than the tensile strength, the bending stiffness of the beam is high and the reinforcement has small influence on the member's stiffness. The displacement will increase linearly for an increased load and the beam is said to be in state I.

The concrete cracks when the tensile stress in the most critical section reaches the tensile strength for concrete. Tensile forces will now be carried by the reinforcement and the stiffness in the cracked sections will decrease. When the load increases, more and more sections will crack but the displacement will still increase linearly for increased load. The beam is said to be in state II.

When the load is further increased, the tensile stress in the reinforcement will finally reach the yielding stress. The beam will now get a plastic behaviour and the displacements increases for almost constant load amplitude. A small increase of the load is possible due to strain hardening in the reinforcement and/or increased internal lever arm due to reduced height of the compression zone. Either, the compressive stress in the concrete will exceed the maximum capacity and the concrete will get crushed in compression or the tensile strength in the reinforcement is passed and a tensile rupture occurs in the beam. The beam is said to be in state III.

Finally, the beam cannot endure the load and there will be a flexural failure. The failure can be either ductile or brittle depending on the relation between the quality and arrangement of reinforcement and the quality of the concrete.

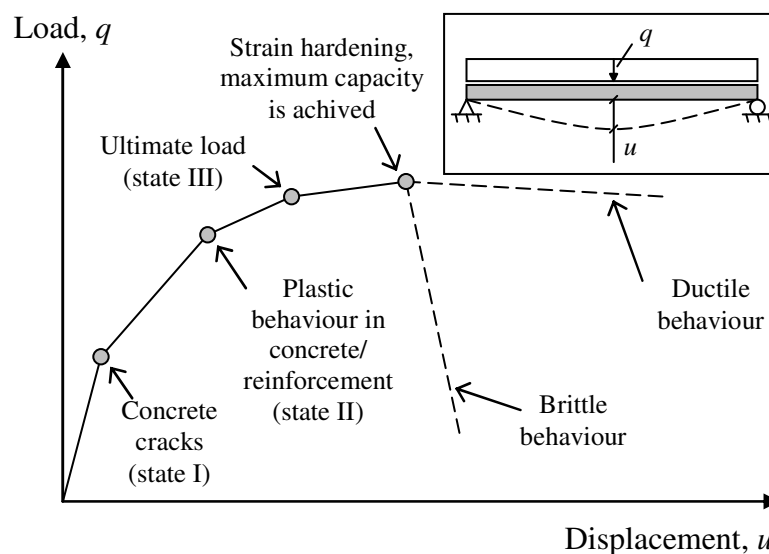


Figure 2.20 Schematic figure of the response of a reinforced concrete beam with ductile as well as brittle behaviour, based on Johansson and Laine, (2008).

The load versus displacement relation in Figure 2.20 may be simplified in order to simplify the calculations. Figure 2.21b shows a common choice of a simplified tri-linear load versus displacement relation.  $F_{cr}$  is the load for when cracking occurs and  $u_{cr}$  the corresponding displacement and  $F_{pl}$  is the value for the load when the ultimate capacity of the concrete is reached and  $u_{pl}$  the corresponding displacement. The curve can be even more simplified by a bi-linear load versus displacement curve, see Figure 2.21a. Such a simplification is possible to do when the displacements are known to be large. The area under the load-displacement curve can be seen as

consumed energy while the beam deflects and the difference in consumed energy between the tri-linear the bi-linear curve will be relatively small when the displacements are relatively large. In Nyström (2006), it is stated that the effect of using a tri-linear material response compared to a bilinear response is very small and that is also why the bilinear material response is adopted in this thesis.

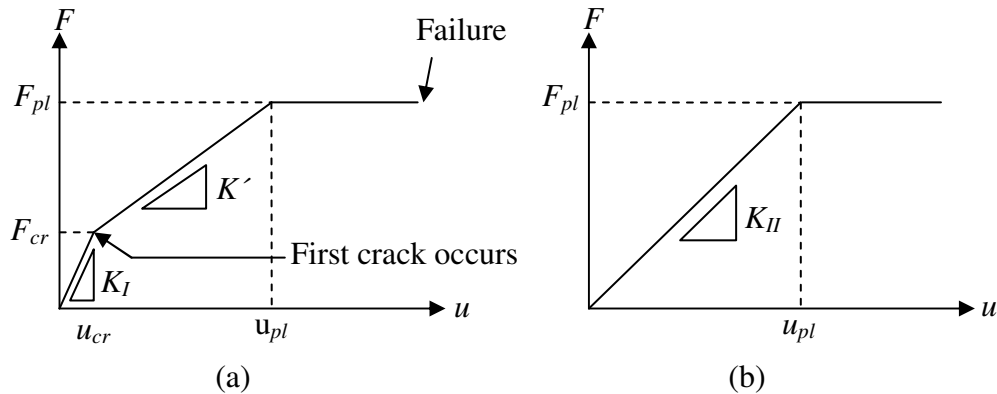


Figure 2.21 Simplified load versus displacement relations; a) common choice of simplified load versus displacement curve, b) load versus displacement curve used in this report.

## 2.5.2 Analysis of cross-sections subjected to bending

### 2.5.2.1 Orientation

Analysis of a reinforced concrete section has to be performed for each state since the behaviour of the cross section changes when the concrete cracks and when the reinforcement yields. Assumptions and theories for analysis in each state are presented in the following sections.

### 2.5.2.2 Assumptions

The following assumption has been made in order to calculate the response for a cross section:

- The section is assumed to be subjected to pure bending which means that no axial force is present.
- The strain distribution is assumed to be linearly distributed over the cross-section with full interaction between concrete and steel.
- Concrete in tension will be neglected for a cracked section even if the concrete can carry a small part of the tensile forces.
- It is assumed that the steel will yield before the ultimate capacity of the concrete in the compressed edge is reached.
- In state I and state II linear elastic response is assumed for both steel and concrete:

$$\sigma_c = E_{cm} \cdot \varepsilon_c \quad (2-14)$$

$$\sigma_s = E_s \cdot \varepsilon_s \quad (2-15)$$

### 2.5.2.3 Reinforced cross section in state I

Figure 2.22 shows a double symmetric cross section in state I subjected to pure bending. The centre of gravity will coincide with the neutral axis (where the normal stress is zero). The tensioned reinforcement is placed in the tensile zone at a distance  $z_s$  from the neutral axis.

$$z_s = d - x_{gc} \quad (2-16)$$

The compressed reinforcement is placed in the compressed zone at a distance  $z'_s$  from the neutral axis.

$$z'_s = d' - x_{gc} \quad (2-17)$$

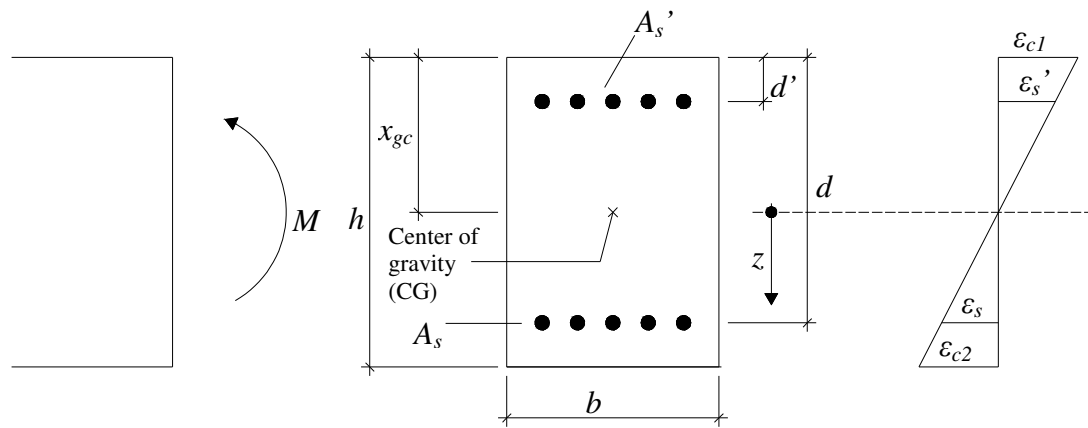


Figure 2.22 Double symmetric cross section in state I with strain distribution, subjected to pure bending.

The moment of inertia for a cross section in state I can be calculated by neglecting the relatively small contribution from the reinforcement:

$$I_I = \frac{bh^3}{12} \quad (2-18)$$

The stress in the concrete at a certain level  $z$  is calculated as:

$$\sigma_c(z) = \frac{M}{I_I} z \quad (2-19)$$

The stress in the steel is calculated as:

$$\sigma_s = \alpha \cdot \sigma_c(z_s) \quad (2-20)$$

$$\sigma'_s = \alpha \cdot \sigma_c(z'_s) \quad (2-21)$$

where  $\alpha$  is the ratio between the Young's modulus of steel and concrete:

$$\alpha = \frac{E_s}{E_c} \quad (2-22)$$

The section will start to crack when the stress in the most tensioned edge reaches the concrete tensile strength,  $f_{ct}$ , and the moment for which cracking occurs can now be calculated by rearranging the terms in equation (2-19).

$$M_{cr} = \frac{f_{ct} \cdot I_I}{h - x_{cg}} \quad (2-23)$$

#### 2.5.2.4 Reinforced cross section in state II

In state II the section is assumed to be cracked and concrete in tension is neglected, see Figure 2.23.

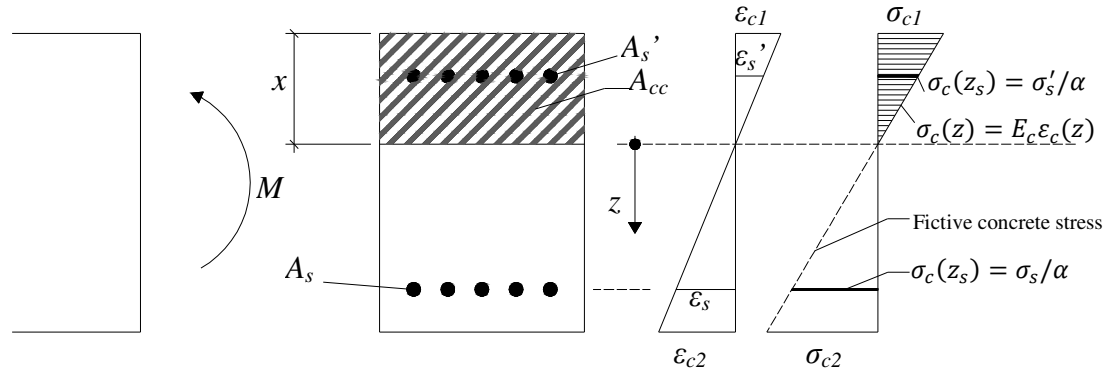


Figure 2.23 Double symmetric cross section in state II with strain distribution, subjected to pure bending.

Calculations in state II is often simplified by replacing the steel and concrete with an equivalent cross section. The expression of the equivalent area for a double symmetric cross-section in state II is written as:

$$A_{II} = A_{cc} + (\alpha - 1)A'_s + \alpha \cdot A_s \quad (2-24)$$

where  $A_{cc}$  is the area for the compressed zone, i.e.

$$A_{cc} = b \cdot x \quad (2-25)$$

For a cross section subjected to pure bending, i.e. no normal forces, the height  $x$  of the compressed zone will coincide with the centre of gravity of the transformed cross section, i.e.

$$x = x_{CG} \quad (2-26)$$

The expression for the centre of gravity can be written by considering an equilibrium condition as:

$$x_{CG} = \frac{bx \frac{x}{2} + (\alpha - 1)A'_s d' + \alpha A_s d}{A_{II}} \quad (2-27)$$

The expression for the height of the neutral layer can now be written by combining equation (2-24) and equation (2-27) and rearrange the terms as:

$$b \cdot \frac{x^2}{2} + (\alpha - 1)A'_s(x - d') - \alpha \cdot A_s(x - d) = 0 \quad (2-28)$$

where  $x$  can be determined by solving the second order equation (2-28). The moment of inertia for a concrete section in state II is calculated as:

$$I_{II} = \frac{bx^3}{3} + (\alpha - 1)A'_s(x - d')^2 + \alpha A_s(d - x)^2 \quad (2-29)$$

The concrete stress at a certain distance  $z$  from the neutral layer can now be calculated in the same way as for the section in state I:

$$\sigma_c(z) = \frac{M}{I_{II}} z \quad (2-30)$$

The steel will start to yield when the stress in the tensioned reinforcement reaches the characteristic yielding stress. The fictive concrete stress can be calculated at the reinforcement layer as:

$$\sigma_c(z_s) = \frac{M}{I_{II}} z_s \quad (2-31)$$

The yield stress,  $f_y$ , can now be expressed as:

$$f_y = \alpha \cdot \sigma_c(z_s) \quad (2-32)$$

By inserting equation (2-31) into equation (2-32) and rearrange the terms the expression for the moment when the tensile reinforcement yields,  $M_y$ , can be written as:

$$M_y = \frac{f_y I_{II}}{\alpha z_s} \quad (2-33)$$

### 2.5.2.5 Reinforced cross section in state III

In state III the reinforcement in tension has reached yielding. The compressive stress in the concrete will increase and the assumption about linear stress distribution is no longer valid for concrete. The non-linear stress distribution however can be simplified with a rectangular stress distribution by using a factor  $\alpha_c$  and a factor  $\beta_c$  which takes into account the average stress and the location of the force resultant for the concrete respectively, see Figure 2.24.

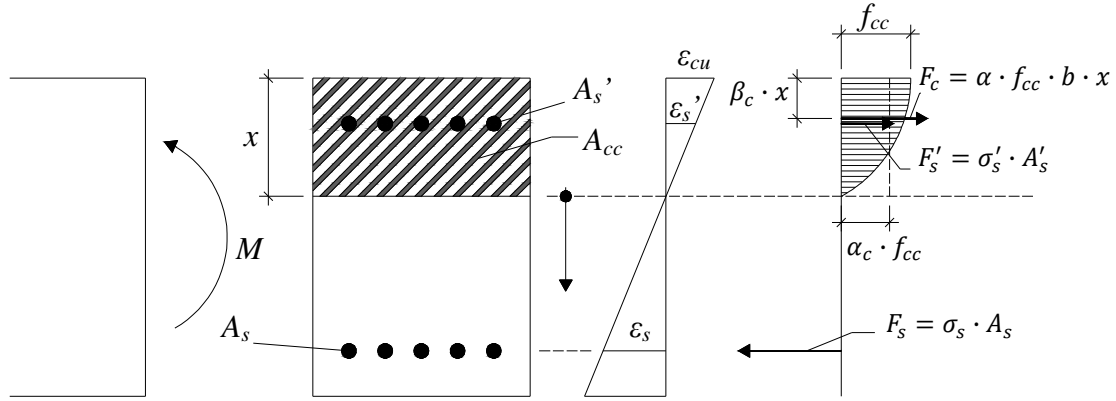


Figure 2.24 Double symmetric cross section in state III with strain distribution, subjected to pure bending.

The failure criteria for a cross-section with flexural cracks and hot-rolled reinforcing steel subjected to pure bending is limited by the maximum compressive strain in the concrete,  $\varepsilon_{cu}$ .

$$\varepsilon_{cu} = 3.5 \cdot 10^{-3} \quad (2-34)$$

When this maximum value of the compressive strain in concrete is reached, the cross-section is about to fail and has reached its ultimate limit.

The parameters  $\alpha_c$  and  $\beta_c$  are functions of the strain in the compressed concrete. The values for these parameters when the maximum strain is reached in the concrete C25/30 is:

Table 2.1 Concrete parameters in ultimate limit state for classes C12/15-C50/60, Engström (2008).

$\alpha_c$	0.81
$\beta_c$	0.416

The height of the compression zone  $x$  can be calculated from the condition that the sum of the forces  $F_c$  in the compressed concrete,  $F_s$  in the tensile reinforcement and  $F_s'$  in the compressed reinforcement (assumed to be compressed) should be equal to zero, i.e.:

$$f_c \cdot b \cdot \alpha_c \cdot x + \sigma_s' \cdot A_s' - f_y \cdot A_s = 0 \quad (2-35)$$

The stress in the compressed reinforcement is calculated as a function of the ultimate strain in concrete and the location of the compressed reinforcement.

$$\sigma_s' = E_s \cdot \frac{(x - d')}{x} \cdot \varepsilon_{cu} \quad \text{when} \quad \varepsilon_s' \leq \varepsilon_{sy} \quad (2-36)$$

$$\sigma_s' = f_y \quad \text{when} \quad \varepsilon_s' \geq \varepsilon_{sy} \quad (2-37)$$

where yield strain for the reinforcement can be calculated as:

$$\varepsilon_{sy} = \frac{f_y}{E_s} \quad (2-38)$$

The moment,  $M_u$ , when the ultimate limit of the cross-section is reached can now be calculated by considering the moment around the tensile reinforcement as:

$$M_u = \alpha_c \cdot f_c \cdot b \cdot x \cdot (d - \beta_c \cdot x) + \sigma_s' \cdot A_s' \cdot (d - d') \quad (2-39)$$

## 2.6 Load-displacement relations for simply supported beam subjected to uniformly distributed load

Consider the simply supported beam in Figure 2.25. The beam is subjected to a uniformly distributed load  $F=q \cdot L$ .

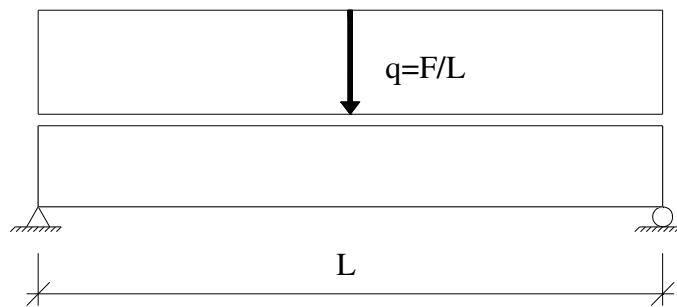


Figure 2.25 Simply supported beam with uniformly distributed load.

The maximum moment will occur in the mid section of the beam and can be calculated as:

$$M = \frac{F}{2} \cdot \frac{L}{2} - \frac{F}{L} \cdot \frac{L}{2} \cdot \frac{L}{4} = \frac{F \cdot L}{8} \quad (2-40)$$

If a restriction concerning the moment in the mid section is known, the corresponding load can be calculated as:

$$F = \frac{8 \cdot M}{L} \quad (2-41)$$

The stiffness  $K$  for the beam in Figure 2.25 can be calculated according to linear elastic theory as:

$$K = \frac{384EI}{5L^3} \quad (2-42)$$

The deflection  $u$  in the mid section can be expressed as a function of the applied load and the stiffness as:

$$u = \frac{F}{K} \quad (2-43)$$

## 2.7 Basic dynamics

### 2.7.1 Orientation

In order to understand how an explosion affects a concrete structure, good knowledge in dynamics is necessary. Basic dynamic expressions will be presented and explained in the following sections.

### 2.7.2 Force and pressure

A force can be seen as the capability to accelerate mass. The relation between Force,  $F$ , mass,  $m$ , and acceleration,  $a$ , is defined according to Newton's law of acceleration:

$$F = m \cdot a \quad (2-44)$$

Pressure,  $P$  is defined as force per unit area,  $A$ , as:

$$P = \frac{F}{A} \quad (2-45)$$

### 2.7.3 Momentum, impulse and impulse intensity

For a body with mass  $m$  and velocity  $v$ , the momentum  $p$  is defined as:

$$p = m \cdot v \quad (2-46)$$

If the body is subjected to a force,  $F=F(t)$ , during a certain time, see Figure 2.26, the new momentum can be written:

$$m \cdot v_1 = m \cdot v_0 + \int_{t_0}^{t_1} F(t)dt \quad (2-47)$$

The integral in equation (2-47) is the change of momentum and is defined as the impulse,  $I$ , transmitted to the body.

$$\Delta p = I = \int_{t_0}^{t_1} F(t)dt \quad (2-48)$$

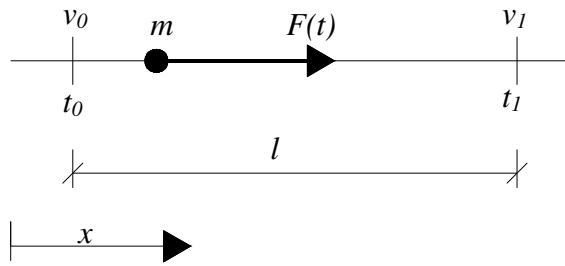


Figure 2.26 Force acting on a body.

For pressure loads the term *impulse intensity* is used and is equal to the impulse over a certain area:

$$i = \frac{I}{A} = \int_{t_0}^{t_1} P(t) dt \quad (2-49)$$

### 2.7.4 Momentum and kinetic energy

Consider a collision between two bodies where the first body has a mass  $m_1$  and velocity  $v_1$  and the second body has a mass  $m_2$  and velocity  $v_2$ . Assuming that the two bodies are attached to each other after the collisions, see Figure 2.27.

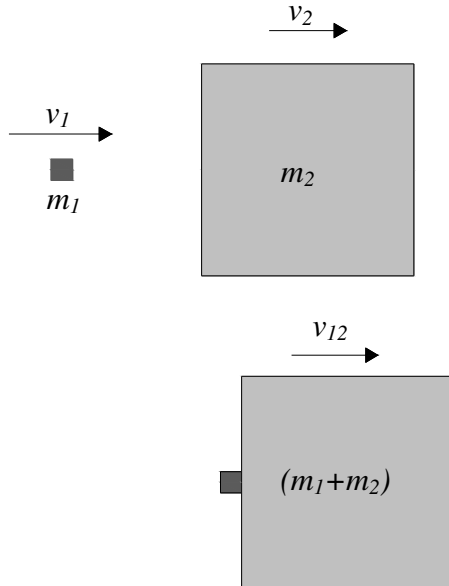


Figure 2.27 Collision between two bodies.

The law of conserved momentum yields:

$$m_1 v_1 + m_2 v_2 = (m_1 + m_2) v_{12} \quad (2-50)$$

The unknown velocity for the two bodies, attached to each other, can be calculated as:

$$v_{12} = \frac{m_1 v_1 + m_2 v_2}{m_1 + m_2} \quad (2-51)$$

If the initial velocity of the second body is equal to zero, the law of conserved momentum yields:

$$v_{12} = \frac{m_1}{m_1 + m_2} \cdot v_1 \quad (2-52)$$

If  $m_2$  is much larger than  $m_1$ , equation (2-52) can be simplified to:

$$v_{12} = \frac{m_1 v_1}{m_2} \xrightarrow{\text{yields}} m_1 v_1 = m_2 v_2 \quad (2-53)$$

The larger body will stop the movement of the smaller body with a certain force, during a certain time. This can also be seen as that impulse is transmitted from the smaller body to the larger body during the collision.

The kinetic energy for the larger body is:

$$W_k = \frac{m_2 v_2^2}{2} \quad (2-54)$$

Which, by use of equation (2-53) can be written as:

$$W_k = \frac{(m_1 \cdot v_1)^2}{2m_2} = \frac{I^2}{2m_2} \quad (2-55)$$

The kinetic energy can be seen as external energy and in order to stop the movement, an equally large internal resisting energy is required.

## 2.7.5 Internal energy

### 2.7.5.1 Concept

In order to stop the movement, or the deflection, in a structural system exposed to an impulse load, the applied external energy has to be resisted by internal energy. The internal energy in a resisting structure is provided by a combination of deformation and internal resisting forces. A large deflection requires smaller internal forces than a small deflection in order to create the same internal energy. The energy equivalence will in the following be described for linear elastic, plastic, and bilinear elasto-plastic material response.

### 2.7.5.2 Elastic Response

For an elastic material, the internal resisting force for an elastic response can be written as:

$$R(u) = Ku \quad (2-56)$$

where  $K$  is the stiffness and  $u$  the displacement.

The internal resisting energy can be expressed as the area under the curve in Figure 2.28 (b) and is equal to:

$$W_i = \frac{R(u) \cdot u_{el}}{2} = \frac{K \cdot u_{el}^2}{2} \quad (2-57)$$

where  $u_{el}$  is the required displacement in order to equalize the internal energy to the external energy.

A combination of equation (2-55) and (2-57) yields the expression for the elastic displacement:

$$u_{el} = \frac{I}{m\omega} \quad (2-58)$$

where  $\omega$  is the angular frequency, equal to:

$$\omega = \sqrt{\frac{K}{m}} \quad (2-59)$$

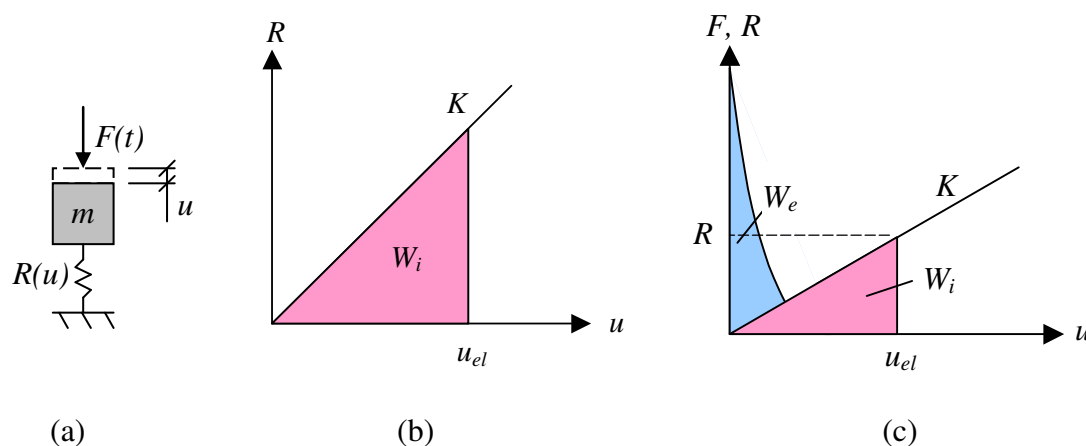


Figure 2.28 System with elastic response: (a) Single degree of freedom system, (b) Force displacement relation, (c) Energy equilibrium between external,  $W_e$ , and internal energy,  $W_i$ .

### 2.7.5.3 Plastic response

For a plastic material behavior, the material capacity is limited. Thus, the maximum internal resisting force in the structural system is also limited. A large displacement capacity in the system is therefore the only way to increase the internal energy. This is why a ductile behavior is to be preferred for a plastic material exposed to a dynamic impulse load.

The internal resisting force,  $R$ , is constant in a plastic system, see Figure 2.30, and equal to:

$$R(u) = R \quad (2-60)$$

The internal resisting energy can be written as:

$$W_i = R(u_{pl}) \cdot u_{pl} = R \cdot u_{pl} \quad (2-61)$$

where  $u_{pl}$  is the required displacement in order to equalize the internal energy to the external.

The plastic displacement can be calculated by combining equation (2-55) and (2-61).

$$u_{pl} = \frac{I^2}{2mR} \quad (2-62)$$

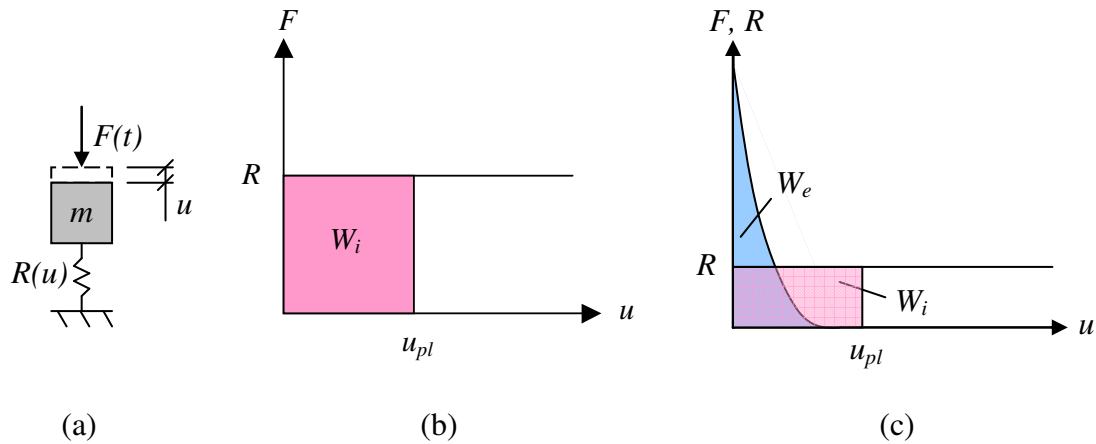


Figure 2.29 System with plastic response: (a) Single degree of freedom system, (b) Force displacement relation, (c) Energy equilibrium between external,  $W_e$ , and internal energy,  $W_i$ .

#### 2.7.5.4 Elastic-plastic response

An elastic-plastic material response is a combination of elastic and plastic behavior. The internal resisting forces will increase as a function of the displacement up to a certain limit where plastic behavior is reached.

The internal resisting force is defined as:

$$R(u) = \begin{cases} Ku, & u \leq u_{el,1} \\ R, & u > u_{el,1} \end{cases} \quad (2-63)$$

where  $u_{el,1}$  is the limit for when the material behavior goes from elastic to plastic, defined as:

$$u_{el,1} = \frac{R}{K} \quad (2-64)$$

The internal energy can now be calculated:

$$W_i = \frac{R}{2} (u_{el,1} + 2u_{pl,1}) \quad (2-65)$$

The required plastic displacement in order to equalize the internal and external energy can now be calculated by combining equation (2-55) and (2-65).

$$u_{pl,1} = \frac{I^2}{2mR} - \frac{u_{el,1}}{2} = u_{pl} - \frac{u_{el,1}}{2} \quad (2-66)$$

where  $u_{pl}$  is the response for an ideally plastic system. The total displacement can now be calculated as:

$$u_{tot} = u_{el,1} + u_{pl,1} = u_{pl} + \frac{u_{el,1}}{2} \quad (2-67)$$

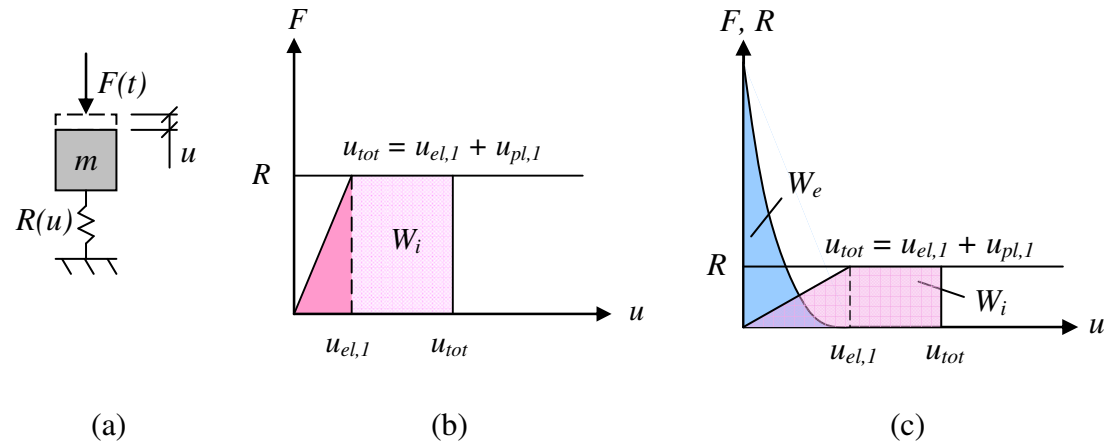


Figure 2.30 System with elasto-plastic response: (a) Single degree of freedom system, (b) Force displacement relation, (c) Energy equilibrium between external,  $W_e$ , and internal energy,  $W_i$ .

## 2.7.6 The fundamental equation of motion

A beam subjected to a load  $F(t)$ , can be seen as a body with a certain mass subjected to internal and external forces where  $F(t)$  is the external force acting on the body. When the beam deflects, an internal resisting force proportional to the deflection will appear. This force can be seen as a static force.

$$R_{stat} = K \cdot u \quad (2-68)$$

where  $K$  is a constant which depends on the support conditions and material properties, and  $u$  is the displacement.

In addition to the static resistance, a dynamic resistance will be created proportional to the velocity. This force can be seen as internal friction when the beam deflects, see equation (2-69).

$$R_{dyn} = c \cdot \dot{u} \quad (2-69)$$

where  $c$  is the damping constant and  $\dot{u}$  is the velocity for the displacement.

The equilibrium condition according to Newton equation now yields:

$$m\ddot{u} + c\dot{u} + ku = F(t) \quad (2-70)$$

This equation is referred to as the fundamental equation of motion.

In order to simplify calculations regarding the maximum deflection, the dynamic internal resistance can be neglected if it is small enough, i.e. if it marginally affects the displacement for the time period of interest. This is the case for an explosion in which the time to maximum displacement is short and the equation of motion will be simplified to:

$$m\ddot{u} + ku = F(t) \quad (2-71)$$

## 2.8 SDOF system

### 2.8.1 Orientation

A simply supported beam can be divided into an infinite number of sections. For an applied load, each of these sections will deflect with different magnitude, i.e. the beam has an infinite number of degrees of freedom. By simplifying the problem and only imitating the first bending mode, see Figure 2.31, the global shape of the deflection is approximated in such a way that it is possible to transform the beam into a single degree of freedom system, a so called SDOF system, see Figure 2.32.

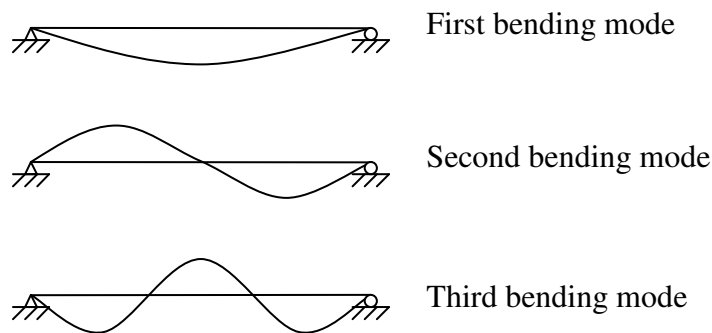


Figure 2.31 The three first bending modes.

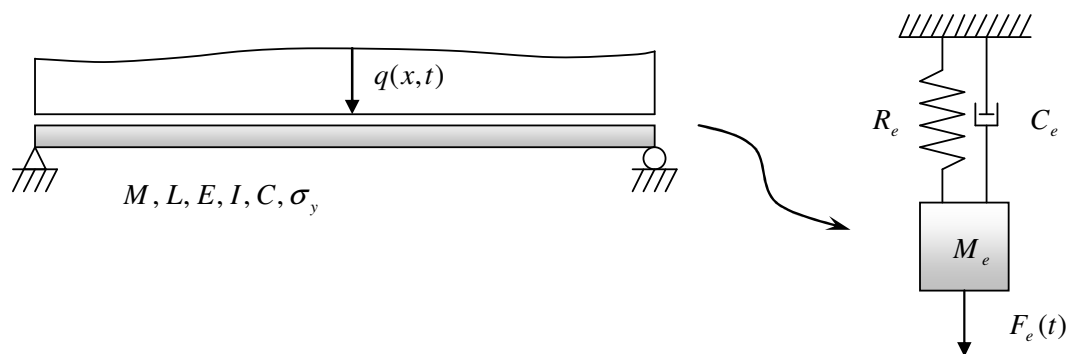


Figure 2.32 Transformation of the beam into a single degree of freedom system.

The main goal when transforming the beam into an SDOF system is to describe a motion in a certain point. This point is called the system point. It can be chosen anywhere over the length of the beam but since the maximum deflection often is of interest, the system point is usually chosen to be in the mid span in case of a simply supported beam.

The SDOF system consists of a single mass, an applied load, an internal resistance and a damping which all have to reflect the real system in a satisfied way. The damping will decrease the amplitude of the oscillation as function of the mass velocity and its influence will only have considerable effects after a certain periods. This is why the damping often can be neglected when a beam is exposed to a load originated from an explosion since it is the largest deflection during the first period that is of interest. In order to transform the beam into an SDOF-system equivalent mass, force and resistance have to be used. Transformation factors are derived from assumptions regarding energy equivalence between the SDOF and the real system. The transformation factors will be explained (and derived) in the following sections.

## 2.8.2 Differential equation for an SDOF system

If neglecting the damping, the differential equation for an SDOF system is:

$$M_e \ddot{u}_s + R_e = F_e(t) \quad (2.72)$$

where notation  $e$  denotes equivalent mass, resistance and load, respectively.

Equation (2.72) can also be written by means of transformation factors as:

$$\kappa_M M \ddot{u}_s + \kappa_K R = \kappa_F F(t) \quad (2.73)$$

where  $M$ ,  $R$  and  $F(t)$  is the real mass, resistance and load respectively.

The definition of transformation factors is given by equations (2.74), (2.75) and (2.76).

$$\kappa_M = \frac{M_e}{M} \quad (2.74)$$

$$\kappa_K = \frac{R_e}{R} \quad (2.75)$$

$$\kappa_F = \frac{F_e}{F} \quad (2.76)$$

Equation (2.73) can be further simplified by introducing another two transformation factors:

$$\kappa_{MF} = \frac{\kappa_M}{\kappa_F} \quad (2.77)$$

$$\kappa_{KF} = \frac{\kappa_K}{\kappa_F} \quad (2.78)$$

It can be shown that  $\kappa_K$  is equal to  $\kappa_F$  which result in that  $\kappa_{KF}$  will be equal to one, Nyström (2006). The final fundamental equation of motion for the SDOF system can now be written:

$$\kappa_{MF} M \ddot{u}_s + R = F(t) \quad (2.79)$$

## 2.8.3 Transformation factors

### 2.8.3.1 Orientation

Nyström (2006) derives the transformation factors for the mass, load and internal force, which all were defined in section 2.8.2. A basic knowledge about how to calculate these factors is, however, necessary in order to better understand problems that may occur when transforming a beam into an SDOF system. A fundamental discussion about how to derive the transformation factors will therefore be presented in this section. The reader is referred to Nyström (2006) for a complete derivation of the transformation factors.

### 2.8.3.2 Transformation factor for the mass

The transformation factor for the mass can be calculated using the condition that the oscillation of the equivalent mass in the SDOF system has to generate the same amount of kinetic energy as for the real beam.

$$W_k^{SDOF} = W_k^{Beam} \quad (2.80)$$

The kinetic energy for the SDOF system can easily be stated but with the equivalent mass and its velocity as unknown. The kinetic energy for the beam can be calculated by summing up the contribution from all infinitesimal sections along the beam. The mass is here known but the velocities for the sections are unknown.

The velocity, or the displacement during a very short time, for the system point in the beam has to be the same as the velocity of the mass in the SDOF system. The deformed shape of the beam is, for a point load or a distributed load, known since the first bending mode is assumed. When the bending shape of the beam is known, the deflection in all points along the beam can be expressed as function of the deflection of the system point. Both sides of equation (2.80) can now be divided by the deflection of the system point and the relation between the equivalent and the real mass can be calculated.

The transformation factor for the mass depends thus, for a certain load case, on the deflection shape of the beam and can be calculated according to equation (2.81).

$$\kappa_M = \frac{1}{M} \int_{x=0}^{x=L} \left( \frac{u(x,t)}{u_s(t)} \right)^2 \rho A dx = \frac{1}{L} \int_{x=0}^{x=L} \left( \frac{u(x,t)}{u_s(t)} \right)^2 dx \quad (2.81)$$

where  $M$  is the mass,  $u$  is displacement,  $\rho$  is density and  $A$  is the cross section area.

### 2.8.3.3 Transformation factor for the load

The transformation factor for the load can be derived from the condition that the equivalent load in the SDOF system should create the same amount of work as the total load in the real system does.

The work is defined as the force acting on a body during a certain distance. In the SDOF system the load and the unknown deflection is the same as for the system point in the real system.

The load in the real system is known, and the deflection shape is assumed for a given load. The deflection for all sections can now be written as function of the deflection of

the system point. The total work in the beam can thus be calculated by integrating the contribution from all infinitesimal section, over the length of the beam. When calculating the transformation factor for the mass, both sides can be divided by the system point's deflection, leaving the equivalent force as the only unknown.

The transformation factor for the load can be calculated according to equation (2.82).

$$\kappa_F = \frac{\int_{x=0}^{x=L} \left( \frac{u(x,t)}{u_s(t)} \right) q(x,t) dx}{\int_{x=0}^{x=L} q(x,t) dx} \quad (2.82)$$

#### 2.8.3.4 Transformation factor for the resistance

The transformation factor for the internal resistance can be derived from the condition that the equivalent internal force in the SDOF system should perform the same work as the internal resistance in the real system does.

The resisting force depends on material behavior and is for an elastic material a function of the stiffness and constant for a plastic material.

The total internal work in a beam is a sum of the work performed by moment, shear and normal forces. The work performed by shear and normal force, though, is relatively small and can often be negligible. The work performed by the moment can be calculated by integrating the contribution from every infinitesimal section over the length of the beam.

The reader is referred to Nyström (2006) for a complete derivation of the transformation factor for the resistance. The factor can be calculated according to equation (2.83).

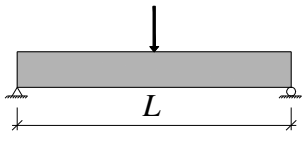
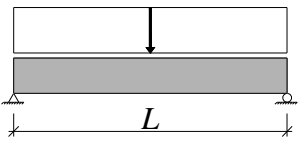
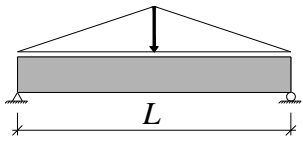
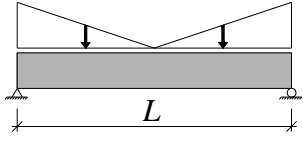
$$\kappa_K = \frac{1}{Ku_s^2} \int_{x=0}^{x=L} M(x)u''(x) dx = \frac{1}{u_s} \frac{\int_{x=0}^{x=L} M(x)u''(x) dx}{\int_{x=0}^{x=L} q(x,t) dx} \quad (2.83)$$

#### 2.8.3.5 Transformation factors for simply supported beam

Nyström (2006) derives transformation factors for load and mass for a simply supported beam with point load and distributed load; see case 1 and 2 in Table 2.2. Two additional load situations have been considered in this work; see case 3 and 4 in Table 2.2. These are of interest since they are two likely load situations for fragmental loading that may occur when a bomb detonates and the fragments are released. Derivation of the transformation factors for the two latter cases can be found in Appendix J.

The tabled values enable a possibility for simplified hand calculations when having an elastic or ideally plastic material response. For a bilinear elasto-plastic material response however, it is not possible to directly use the elastic transformation factor for the elastic part and the plastic transformation factor for the plastic part since a sudden change of transformation factor will result in a sudden loss of energy. That is why an incremental transition needs to be used. Information about how this transition has been considered in this thesis can be found in Appendix K.

Table 2.2 Transformation factors for a simply supported beam.

		Material	$\kappa_F$	$\kappa_M$	$\kappa_{MF}$
Case 1		Elastic	1.0	0.486	0.486
		Plastic	1.0	1/3	1/3
Case 2		Elastic	0.640	0.504	0.787
		Plastic	0.5	1/3	2/3
Case 3		Elastic	0.810	0.499	0.616
		Plastic	2/3	1/3	0.5
Case 4		Elastic	0.475	0.512	1.077
		Plastic	1/3	1/3	1

## 2.9 The central difference method

In this project, the *Central Difference Method* is used as solution procedure. The method is a special case of the Newmark Method with certain values for the parameters  $\alpha$  and  $\delta$ , which are determined in order to obtain integration accuracy and stability. The Newmark method is a direct integration solution method where the equation of motion is integrated using a numerical stepwise procedure. By the term “direct” it is meant that no transformation of the equations into a different form is carried out before the numerical integration.

The *Central Difference Method* is, according to Craig and Kurdila (2006), perhaps the most fundamental algorithm for the approximate numerical solution of second order differential equations in structural dynamics. They argue that it is a simple method which is easy to understand and deal with, and also is an accurate second order algorithm. And by vast experience they mean that second order algorithm is often

required in many engineering problems. The method is also a conditionally stable algorithm, provided that the time step,  $\Delta t$ , is selected to be smaller than a critical time step  $\Delta t_{cr}$ , which depends on the eigenvalues of the iteration matrix.

In the Newmark method the velocity and displacement at time  $t_{n+1}$  are assumed to be:

$$\dot{u}_{n+1} = \dot{u}_n + ((1 - \delta)\ddot{u}_n + \delta\ddot{u}_{n+1})\Delta t \quad (2.84)$$

$$u_{n+1} = u_n + \dot{u}_n\Delta t + ((1 - 2\alpha)\ddot{u}_n + 2\alpha\ddot{u}_{n+1})\frac{\Delta t^2}{2} \quad (2.85)$$

When the parameters  $\alpha = 0$  and  $\delta = 0.5$  the Central difference method is obtained.

To be able to establish the expression for the *Central Difference Method* the equation of motion needs to be recalled from section 2.7.6.

$$M\ddot{u} + C\dot{u} + Ku = f(t) \quad (2.86)$$

The foundation of the *Central Difference Algorithm* is the simple finite- difference expression:

$$\dot{u}_n = \frac{u_{n+1} - u_{n-1}}{2h} \quad (2.87)$$

The derivative at time  $t_n$  is approximated by the slope of the line passing through the values of the function at  $t_{n-1}$  and  $t_{n+1}$ . In order to maintain the consistency of the approximation, the value of the second derivative is calculated as the difference of the first-order forward and backward finite differences.

$$\ddot{u}_n = \frac{u_{n+1} - 2u_n + u_{n-1}}{h^2} \quad (2.88)$$

When the equations (2.87) and (2.88), are inserted into the equation of motion the following expression is obtained and evaluated at time,  $t_n$ :

$$\left(\frac{1}{h^2}M + \frac{1}{2h}C\right)u_{n+1} + \left(K - \frac{2}{h^2}M\right)u_n + \left(\frac{1}{h^2}M - \frac{1}{2h}C\right)u_{n-1} = f_n \quad (2.89)$$

In case of neglecting the damping the equation (2.89) will look like:

$$\frac{1}{h^2}Mu_{n+1} + \left(K - \frac{2}{h^2}M\right)u_n + \frac{1}{h^2}Mu_{n-1} = f_n \quad (2.90)$$

For a more accurate establishment of the expressions for *The Newmark Method* and *The Central Difference Method* and a working scheme for the methods the reader is referred to Nyström (2006).

## 3 The studied case

### 3.1 Orientation

In order to increase the knowledge about how an explosion affects a structural part, a specific case has been studied. Choices regarding the geometry of the structure and the properties of the bomb follow the Swedish shelter regulations, stated by the Swedish Civil Contingencies Agency (MSB), the authority which controls regulations of civil shelters in Sweden. Other choices and assumption are based on the theory presented in chapter two.

### 3.2 Geometry

Räddningsverket (2006) proposes a standard case schematically shown in Figure 3.1 with the minimal thicknesses of structural members for the ground slab, walls and the roof and also the considered distance between the detonation and the affected wall. In this project, the height where the bomb detonates is assumed to be at a height equal to half the wall's height to simulate a worst case scenario. Since the wall is a member of the civil structure that will get hit by the blast- and fragment loads, a wall strip consisting of one meter in width is to be analysed.

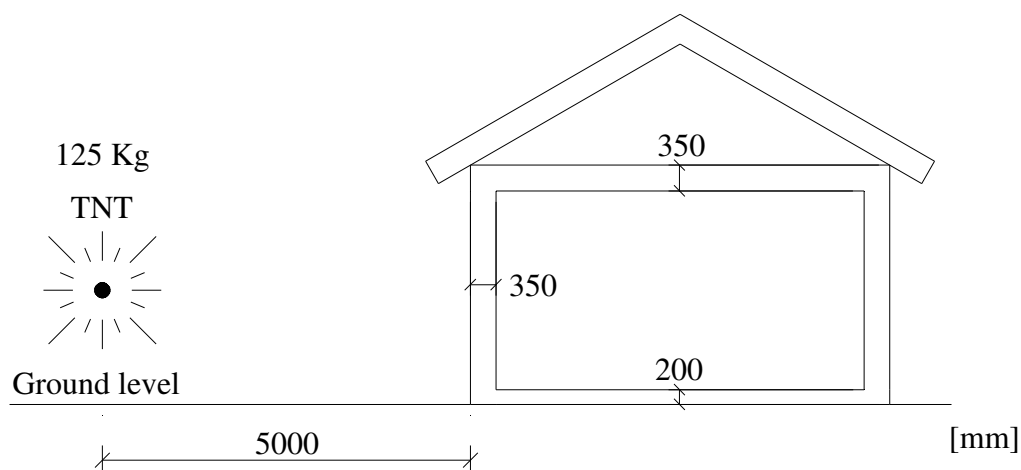


Figure 3.1 Studied case concerning explosion proposed by Räddningsverket (2006).

According to Räddningsverket (2006), the wall thickness needs to be at least 350 mm, and in previous research, Leppänen (2009), Nyström (2008), the height of the wall is set to be 2.7 m and is so in this thesis as well. All the measures and data concerning the beam's geometry are shown in Figure 3.2 and Figure 3.3.

Due to the structural response obtained by dynamic loading the wall has to be reinforced in both the external and the internal edge of the wall, with a maximum spacing of 200 mm between the bars and no shortening of the reinforcement in the field is allowed.

The reinforcement amount at each edge should be in the following interval:

$$0,14 \% < \rho < 1,1 \% \quad (3.1)$$

where  $\rho$  is:

$$\rho = \frac{A_s}{b \cdot d} \quad (3.2)$$

$A_s$  = Reinforcement area

$b$  = width of the wall strip

$d$  = effective height

Leppänen (2009) has chosen the amount of reinforcement to be  $5\phi 16$  with a spacing of 200 mm. This corresponds to an area of  $1005 \text{ mm}^2/\text{m}$  and  $\rho = 0.335 \%$ . The cross section can be visualized in Figure 3.2. This amount and arrangement of reinforcement is also adopted in this thesis.

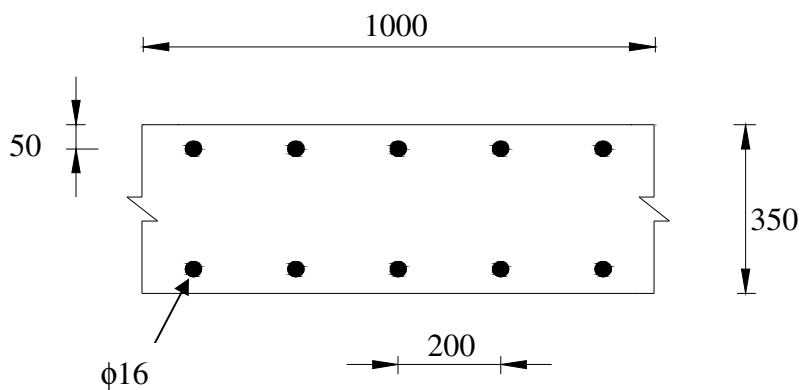


Figure 3.2 Cross section of the analysed beam.

In the calculations the wall strip is treated as a simply supported beam, see Figure 3.3. This does not correspond to the true support condition in the civil defence shelter. The real condition is something between simply supported and fixed, but it is a simplification that makes the calculations easier and is good enough for the purposes in this thesis.

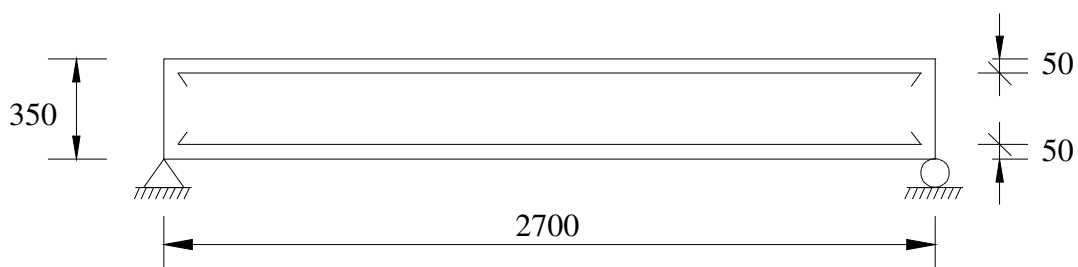


Figure 3.3 The simply supported wall strip that is analysed.

### 3.3 Material

According to R ddningsverket (2006), civil defence shelters should be built of reinforced concrete with some material specific data. The material data used in this project is presented in Table 3.1 and Table 3.2 for the concrete and the reinforcement respectively.

Table 3.1 Concrete data used in the calculations.

Concrete data	
Class	C 25/30
$f_{cc}$	25 MPa
$E_c$	31 GPa
$\rho$	2400 kg/m <sup>3</sup>

Table 3.2 Reinforcement data used in calculations.

Reinforcement data	
Class	B 500 BT
$F_y$	500 MPa
$E_s$	200 GPa

In this report three simplified material responses are established with the real behaviour under consideration. These three responses are: linear elastic, ideally plastic and bilinear elastic-plastic.

A simplified bilinear load-deflection curve to describe the complex behaviour of concrete is introduced in section 2.5.1. An expression for how to calculate the ultimate moment together with an expression for the load-displacement relation is presented in the same section 2.5.1. The load versus deflection curve for an elasto-plastic material can be seen in Figure 3.4 and the corresponding calculations are performed in Appendix C.

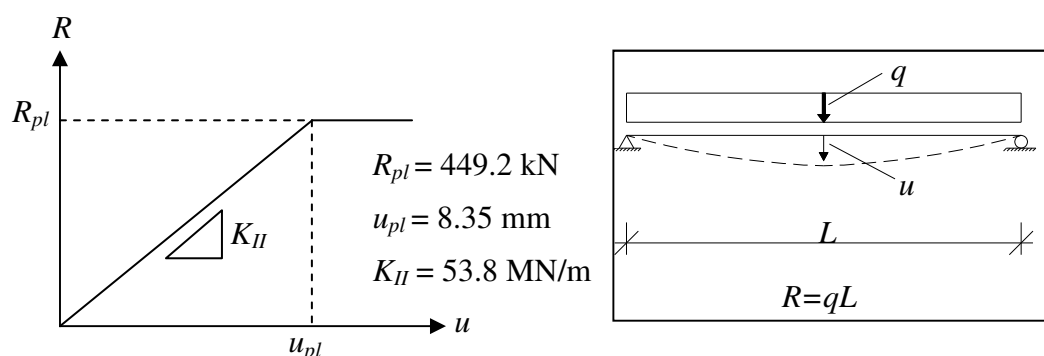


Figure 3.4 Load-displacement curve for simplified bi-linear elasto-plastic material response.

When having elastic response the same stiffness as for the elastic part of the elasto-plastic material response is used. The load-displacement curve will look like Figure 3.5.

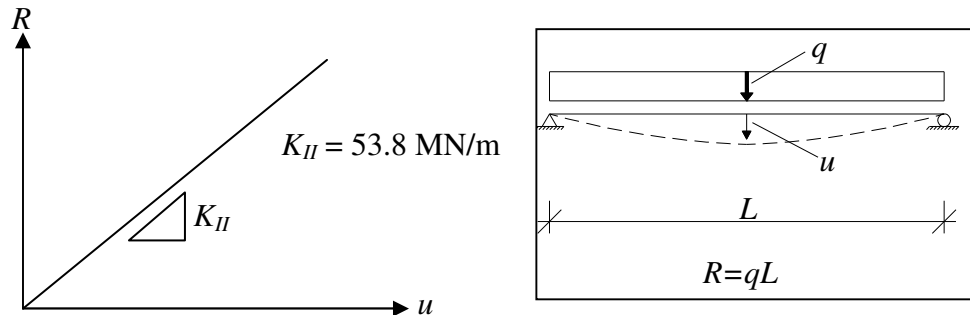


Figure 3.5 Load-displacement curve for linear elastic material response.

For an ideal plastic material response the maximum internal force is chosen to be the same as for the elasto-plastic material response. The load-deflection curve can be seen in Figure 3.6.

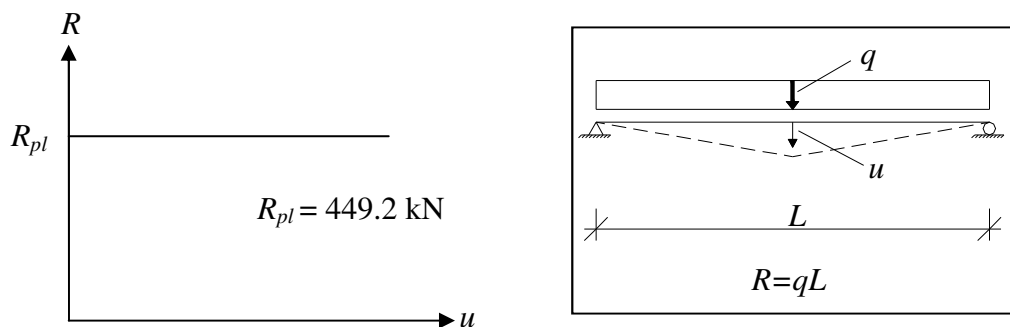


Figure 3.6 Load-displacement curve for ideal plastic material response.

### 3.4 Load

#### 3.4.1 Orientation

As mentioned in section 2.2.1, the impact of an explosion on a structure can be divided into impact from the blast wave and from the fragments. The properties of the bomb will affect the magnitude and characteristic of these impacts considerably. R ddningsverket (2006) uses a reference bomb to define the load conditions. This reference bomb, together with impact from the blast and fragments, will be treated in the following sections.

#### 3.4.2 Reference bomb

The bomb has a total weight of 250 kg, 125 kg out of these are TNT explosives and the remaining 125 kg is shell mass (fragments). As described in Figure 3.1, the bomb detonates 5.0 m from the wall at a height of 1.55 m.

### 3.5 Blast load

Basic theory about the blast load was presented in section 2.2.2. An idealized blast wave was also presented in the same section, this blast wave is presented once again in Figure 3.7.

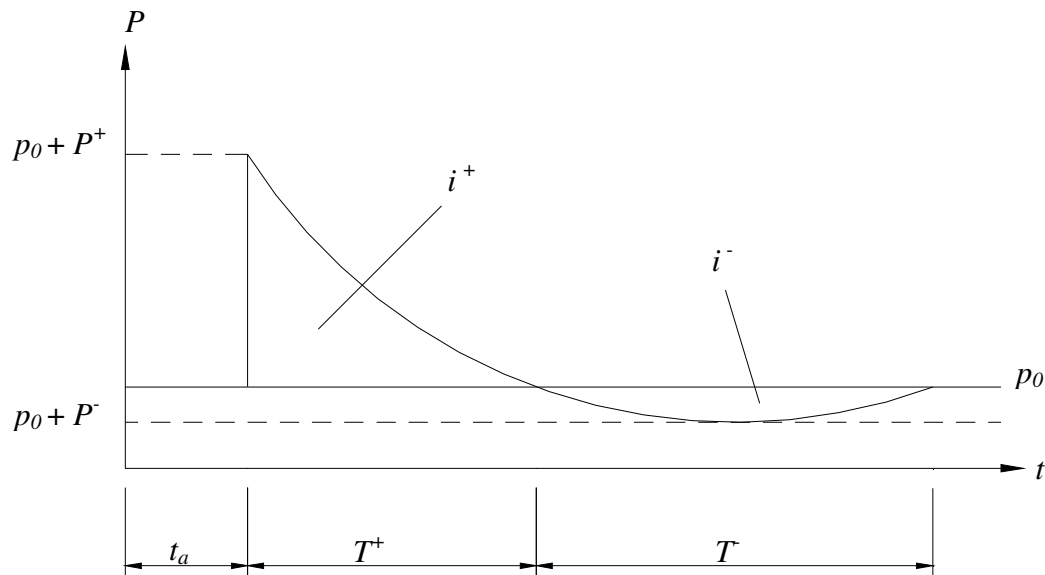


Figure 3.7 Idealized blast wave.

The blast wave, or the pressure as function of time curve, consists of a positive phase, followed by a negative phase. The effect of the negative phase is often neglected and will not be considered in this thesis.

The shape of the curve for the positive part can, according to Ekengren et al. (2004), be approximated as:

$$P(t) = p_0 + P^+ \left( 1 - \frac{t - t_a}{T^+} \right) e^{-t - \frac{t_a}{\alpha}} \quad (3.3)$$

$P^+$  is the pressure in the front of the pressure wave,  $t_a$  is the arrival time,  $T^+$  is the time for which the pressure is positive and  $\alpha$  is a parameter considering the shape of the pressure curve. The atmospheric pressure  $p_0$  is often not considered in equation (3.3) since the difference in pressure over boundaries for a structural part is of interest.

For the reference case presented earlier  $P_r^+$  is equal to 5000 kPa,  $T^+$  is equal to 8.974 ms,  $t_a$  is equal to 2.66 ms and  $\alpha$  is equal to 0.5983 in accordance with Leppänen (2009). The resulting impulse intensity for the positive part is equal to 2800 Pas.

The impulse intensity  $i^+$  is the area under the time versus pressure curve for the time  $T^+$  and can be calculated by excluding  $p_0$  from equation (3.3) and integrate the expression over the time  $T^+$ .

The pressure versus time relation for the positive phase in Figure 3.7 has, in this thesis, been even more simplified by a triangular curve, see Figure 3.8 and equation (3.4). The impulse intensity, the arrival time and the peak pressure is the same as for

the equation used by Leppänen. Furthermore, the peak pressure  $P^+$  will occur after 0,1 ms since a too large increment of the load can result in numerical problems in the FE analysis.

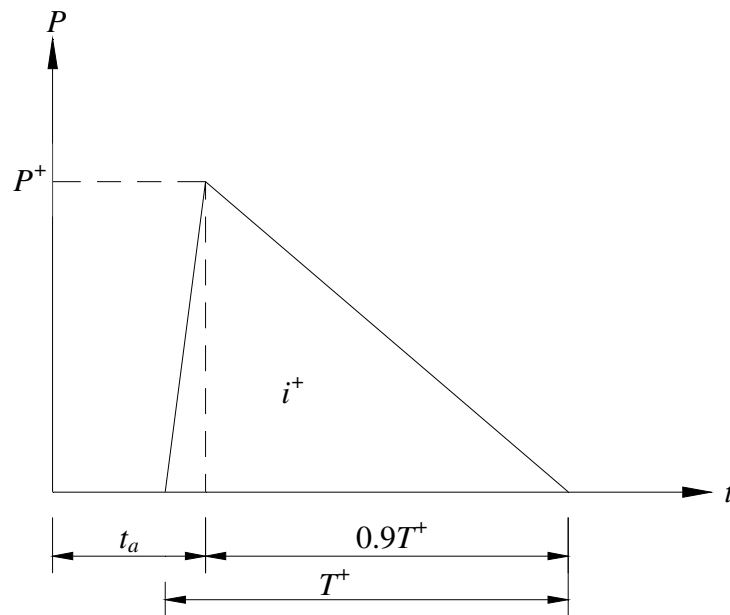


Figure 3.8 Simplified pressure versus time relation used in calculations made in this report.

$$\begin{aligned}
 P(t) &= 0 & \text{when} & \quad 0 \leq t < (t_a - 0.1 \cdot T^+) \\
 P(t) &= \frac{P^+}{0.1 \cdot T^+} (t - (t_a - 0.1T^+)) & \text{when} & \quad (t_a - 0.1 \cdot T^+) \leq t < t_a \\
 P(t) &= P^+ - \frac{P^+}{0.9 \cdot T^+} (t - t_a) & \text{when} & \quad t_a \leq t < (t_a + T^+) \\
 P(t) &= 0 & \text{when} & \quad (t_a + T^+) \leq t < \infty
 \end{aligned} \tag{3.4}$$

The time  $T^+$  for the simplified curve can be calculated from the condition that the impulse should remain the same:

$$T^+ = \frac{2 \cdot i^+}{P^+} = \frac{2 \cdot 2800}{5000 \cdot 10^3} 1.12 \text{ ms} \tag{3.5}$$

### 3.6 Fragment loads

Basic theory about fragments and the fragmentation process was presented in section 2.2.3.1. It is assumed, in this thesis, that the bomb detonates with its nose downwards and its tail upwards which implies that the beam (wall strip) will be exposed to a swarm of relatively small fragments.

As mentioned in section 2.2.3.5, 60 percent of the case mass will strike in a segment of 40 degrees. From Figure 3.9.a. and equation (3.6) it can be concluded that the total height of the wall will be within these 40 degrees for the studied reference case.

The percentage of the total case mass hitting a wall strip of 1,0 m in width can now be calculated by also consider Figure 3.9.b. and equations (3.6) and (3.7).

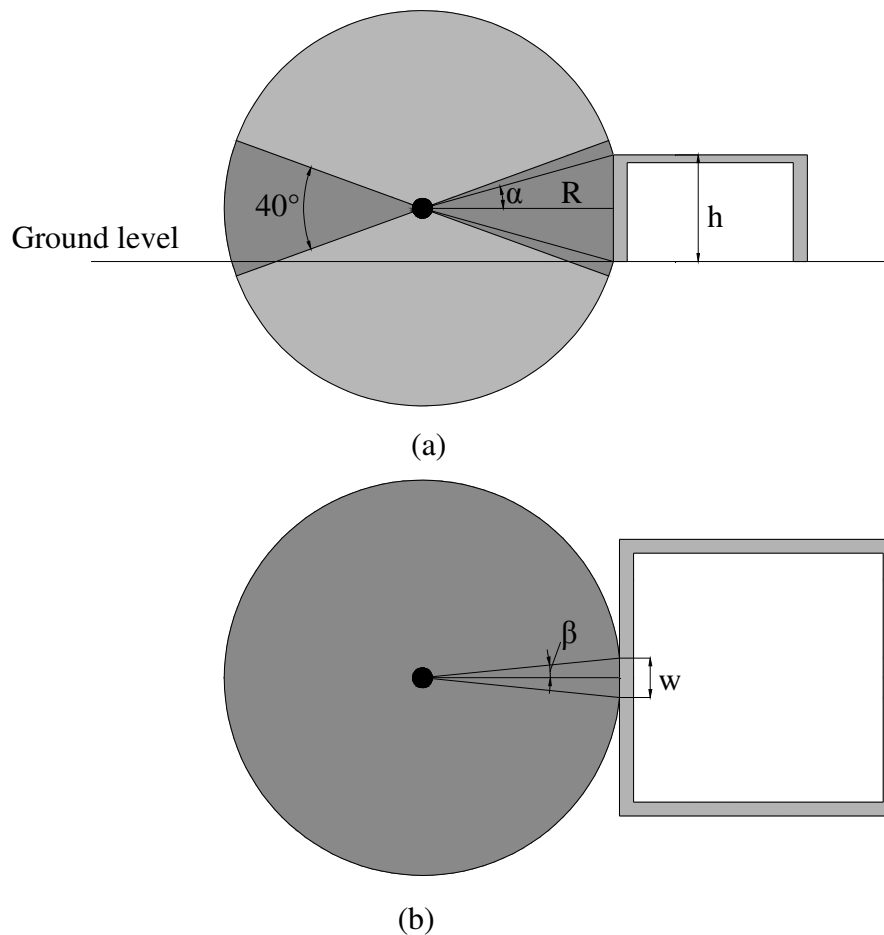


Figure 3.9 Fragmental distribution from (a), side and from (b), above

$$\alpha = \tan^{-1} \left( \frac{h}{2R} \right) = [h = 2.7 \text{ m}, R = 5 \text{ m}] = 15,11^\circ \quad (3.6)$$

$$\beta = \tan^{-1} \left( \frac{w}{2R} \right) = [w = 1 \text{ m}] = 5,71^\circ \quad (3.7)$$

The total amount of fragments striking 1 meter of the wall then becomes:

$$M_h \cdot \left( \frac{2 \cdot \alpha}{40^\circ} \right) \cdot 0.6 \cdot \left( \frac{2 \cdot \beta}{360^\circ} \right) = 0.0144 \cdot M_h = 0.0144 \cdot 125 \text{ kg} = 1.8 \text{ kg} \quad (3.8)$$

The total mass hitting the wall strip will thus be 1.8 kg which, for a wall of height 2.7 m, is equal to 0.67 kg/m<sup>2</sup>.

An empirical equation for how to calculate the mass distribution of the fragments for a certain bomb was presented in section 2.2.3.7. The same expression is once again presented:

$$n_{(m_s)} = \frac{M_h}{2 \cdot M_A} e^{-\sqrt{\frac{m_s}{M_A}}} \quad (3.9)$$

The fragment distribution,  $M_A$ , factor depends on the shape and the properties of the bomb. This parameter is not defined for the reference bomb. However, a similar bomb (American GP-bomb Mk82) can be used to estimate the value of  $M_A$  and Nyström (2008) estimates this parameter to be 1.758 g.

The total amount of fragments is obtained by putting  $m_s$  to zero in equation (3.9) and is equal to 35 552 fragments. The number of fragments, larger than a certain mass can be seen in Figure 3.10.

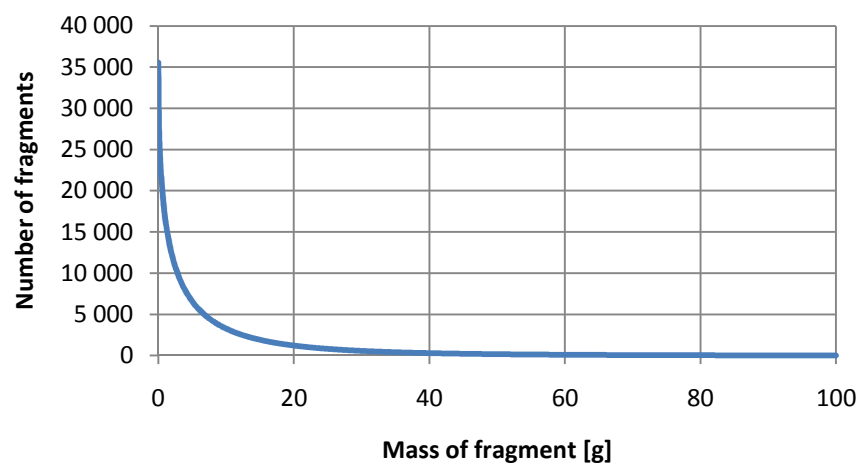


Figure 3.10 Number of fragments larger than a certain mass.

According to equation (3.8) only 1.44 % of these fragments will strike the wall which gives a total number of 526 fragments.

The mass distribution for the fragments can be obtained by dividing the total amount of fragments into 0.1 g intervals:

$$m = [0, 0.1, 0.2, 0.3, \dots, 100] \text{ [g]}$$

The average mass in each interval is calculated according to equation (3.10).

$$m_{av_i} = \frac{m_i + m_{i+1}}{2} \quad (3.10)$$

Equation (3.10) is a simplification of the real distribution but it is assumed to be a good enough approximation since the mass intervals are relatively small.

The amount of fragments in each interval is calculated according to equation (3.11).

$$n_{int_i} = (n_{(m_i)} - n_{(m_{i+1})}) \cdot 0.0144 \quad (3.11)$$

The total mass in each interval can now be calculated as:

$$m_{tot_i} = m_{av_i} \cdot n_{int_i} \quad (3.12)$$

which gives a mass distribution according to Figure 3.11.

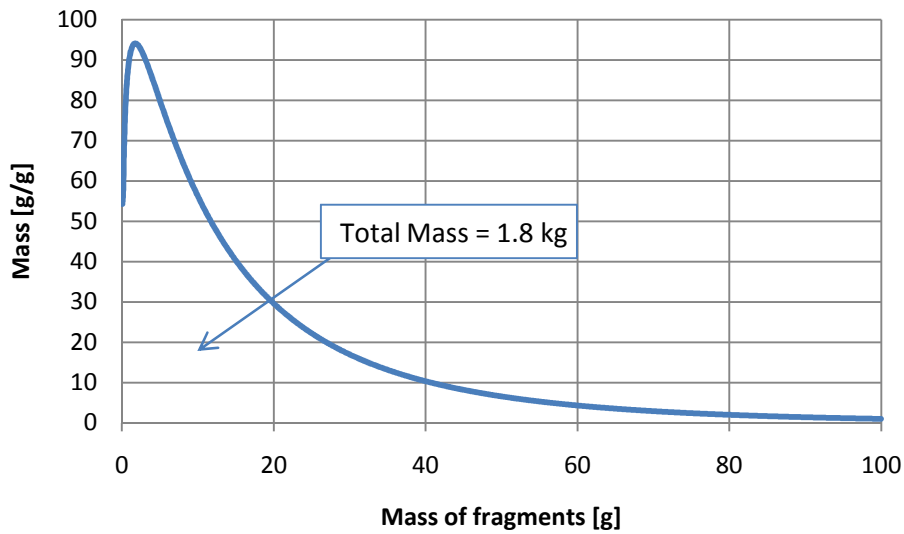


Figure 3.11 Fragment mass distribution for the studied case.

Striking velocities for the average mass in each interval can be calculated by equation (2.3) and the impulse for each interval can now be expressed as:

$$I_i = v_i \cdot m_{tot_i} \quad (3.13)$$

This gives an impulse distribution according to Figure 3.12.

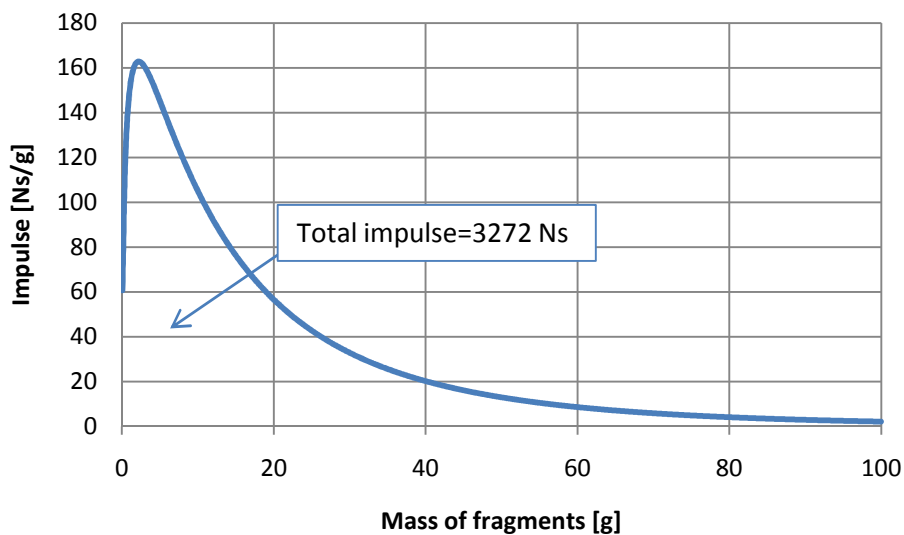


Figure 3.12 Impulse distribution from fragments for the studied case.

### 3.6.1 Fragmental impact on the beam

The fragmental impact on the beam can be seen as impulse loading since the fragments hits the beam at very high velocities and will be decelerated by the beam during a very short time.

As mentioned in section 2.2.3.2 the fragments will also penetrate the beam. Penetration depths as function of the fragment mass when the bomb detonates at a distance of 5 meters are presented in Figure 3.13 below. These penetration depths are, compared to more advanced simulations in Nyström (2008), rather high but nevertheless show a principal relation between penetration depth and fragment mass.

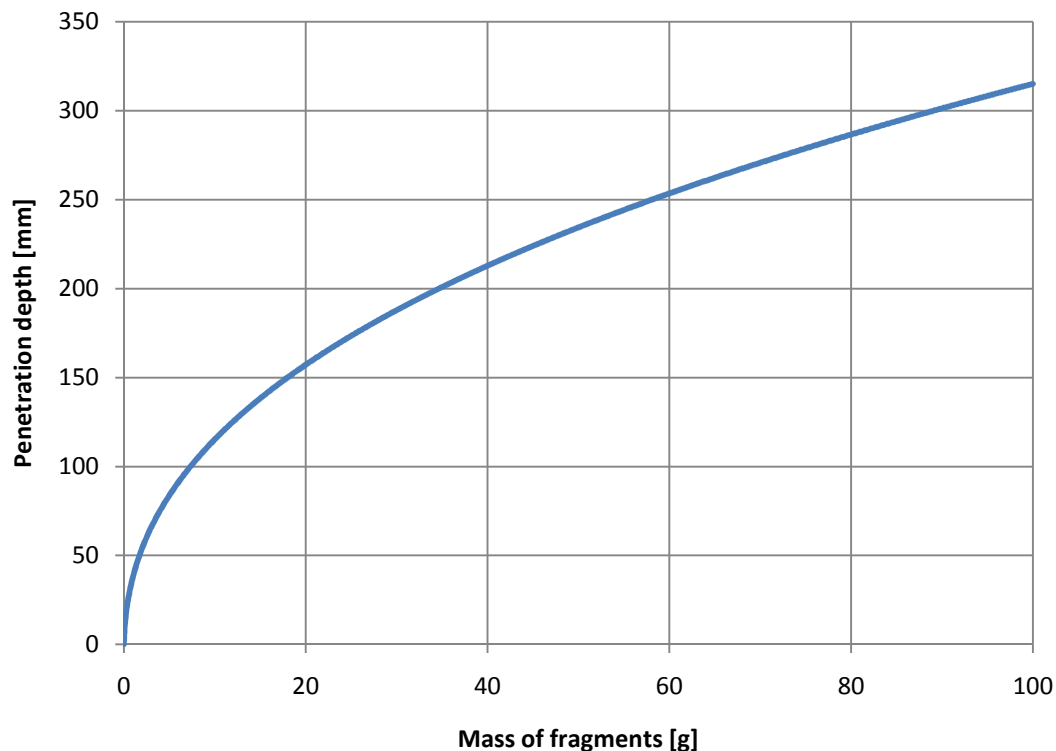


Figure 3.13 Penetration depth as function of fragment mass at a distance  $R=5m$ .

The duration from when the fragment strikes the wall until it has been fully stopped by the wall can be calculated by considering the penetration depth and the average velocity during the penetration, assuming linear retardation, as:

$$T_f = \frac{x}{v_{av_i}} = \frac{2 \cdot x}{v_i} \quad (3.14)$$

where  $x$  is the penetration depth which depends on the velocity, mass and shape of the fragment.

Leppänen (2009) estimates this time for a 6 gram fragment to be 0.1 ms. This value will also be used as an approximation for the fragment load duration for all fragments, independently of mass in this thesis.

The time from when the bomb detonates until the fragment reach the surface of the beam can be calculated by assuming linear retardation of the fragment in the air as:

$$t_{a_i} = \frac{R}{v_{av_i}} \quad (3.15)$$

$$v_{average} = \frac{v_0 + v_i}{2} \quad (3.16)$$

By assuming a force-time relation according to Figure 3.14 the peak force for a fragment can be calculated as:

$$F_{peak} = \frac{2 \cdot I_i}{t} = \frac{2 \cdot m_i \cdot v_i}{t} \quad (3.17)$$

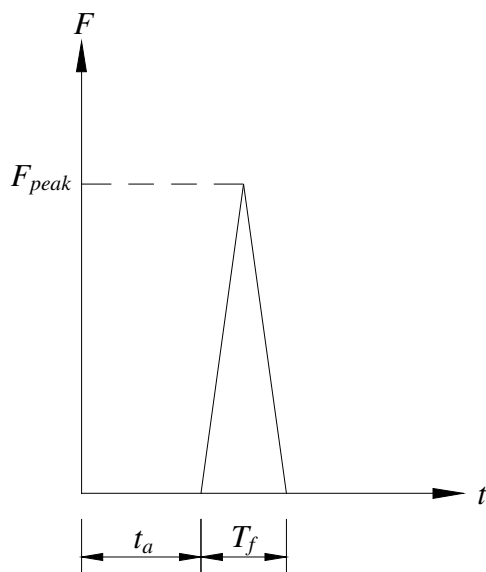


Figure 3.14 Load versus time relation for fragments.

### 3.6.2 Combination of fragment and blast load

Figure 3.15 shows the arrival time for the blast wave and for a 50 gram fragment as function of the distance to the centre of the detonation. It can be observed that at a distance of five meters the fragment and the blast wave will hit the wall at approximately the same time, according to Nyström (2008) which is a worst case scenario. Since the mass of the fragments are not constant the arrival time for a single fragment might deviate a little from Figure 3.14. It can however be assumed that the total amount of fragments will hit the wall within a relatively short time period.

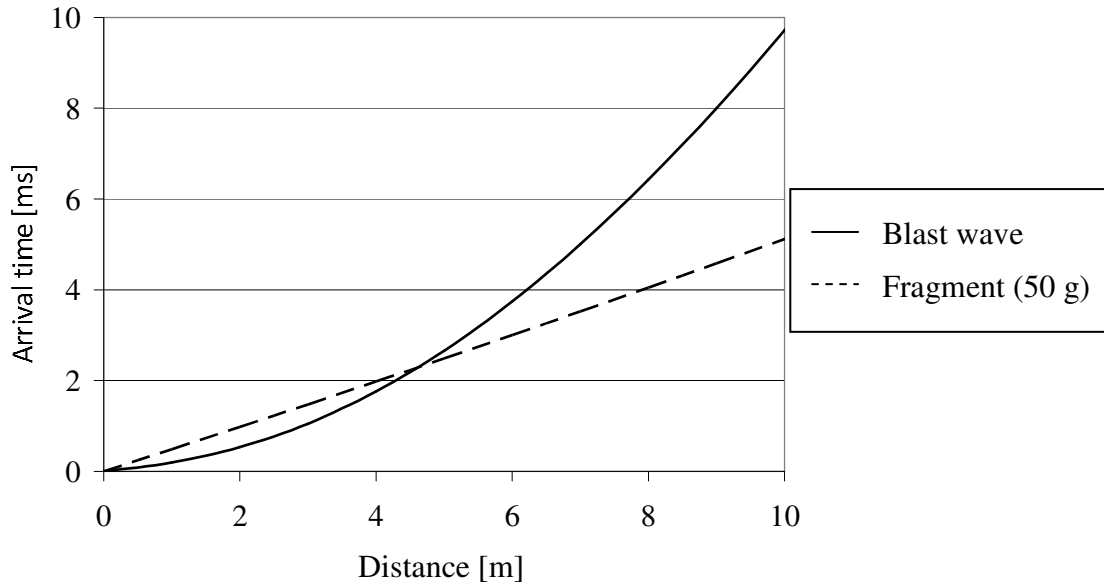


Figure 3.15 Time when the fragment and the blast wave reaches the beam as function of the distance to the bomb, Leppänen (2009).

The fragmental impact will later on be simulated as several point loads and as one (simplified) uniformly distributed load. When the fragments are simulated as point loads the real arrival time and load amplitude will be calculated for each point load, i.e. for each fragment. However, the duration for the load will still be kept to 0.1 ms. When the fragments on the other hand are simulated as one distributed load the arrival time has to be chosen. A conservative assumption is to say that the peak value from the blast load and the distributed fragment load will occur at the same time. This is also a scenario relatively close to reality and will be used in this work.

Figure 3.16 and Figure 3.17 show the pressure versus time relation for the blast load and for the fragment load respectively and Figure 3.18 shows the total load versus time relation.

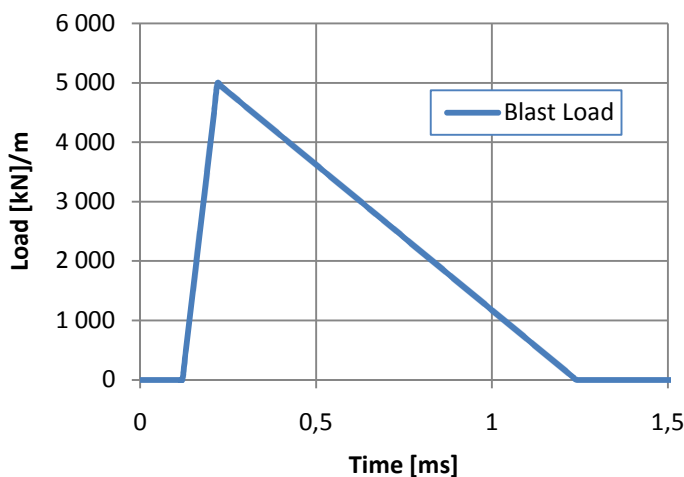


Figure 3.16 Load versus time relation for blast load.

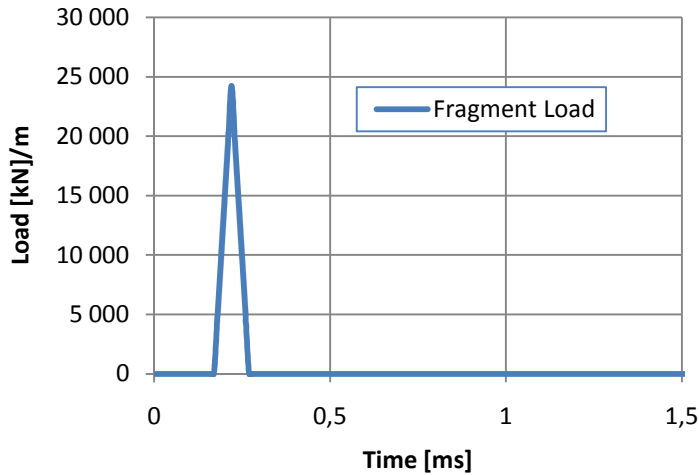


Figure 3.17 Pressure versus time relation for fragment load when applied as simplified uniformly.

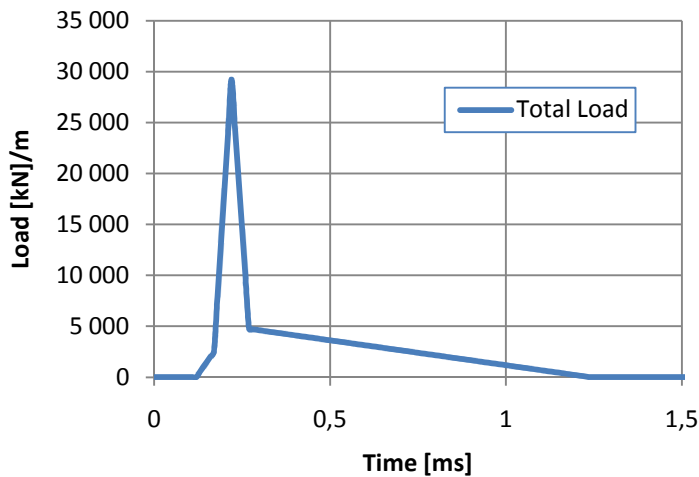


Figure 3.18 Total load versus time relation for blast- and fragment load.

In order to use the same time functions throughout all simulations, a gap of 0.12 ms between zero to the time when the blast load starts has been left since a large fragment could hit before the blast load arrives when all fragment are simulated as separate point loads.

### 3.6.3 Simulation of fragments

The simulation of fragments is usually simplified in calculations by distributing the total impulse from the fragments as a uniform pressure over the beam. Another possible simplification, very conservative and extreme, is to simulate the total impulse of the fragments as one point load acting in the middle of the beam, which would lead to a maximum displacement in mid span. The most realistic simulation, though, would be to use a random generator and let fragments with different size and velocity strike the wall in different points. In order to see how simulations of the fragments affect the response of the beam, different simulations has to be run in between the two extreme cases.

According to R ddningsverket (2006), shelters do not need to be designed for fragments with a mass larger than 50 gram. Therefore, fragments with mass larger

than 50 gram will not be considered in the study carried out here. However, the impulse generated by these larger fragments will be taken into consideration.

The choice of how to simulate the fragments in between the two extreme cases can be made in many different ways. However, the main goal in this project has been to imitate the reality as good as possible but still be able to see how a proper simulation, close to reality, may differ from a more theoretical one. By considering the amount of fragments in different mass intervals and also consider the total impulse in each interval a good base for how to simulate the fragments is achieved.

By use of equation (3.9) the amount of fragments with mass up to 50 grams can be calculated and is equal to 511 pieces. A good way to simulate these fragments would be to use a random generator based on the mass distribution but in such a case the impulse intensity will not be the same for different runs. Hence, if the impulse shall be constant, which is the objective here, the masses of the fragments has to be chosen in advance. In this report, eight different groups of fragments have been chosen in the interval from zero to fifty grams, see Figure 3.19.

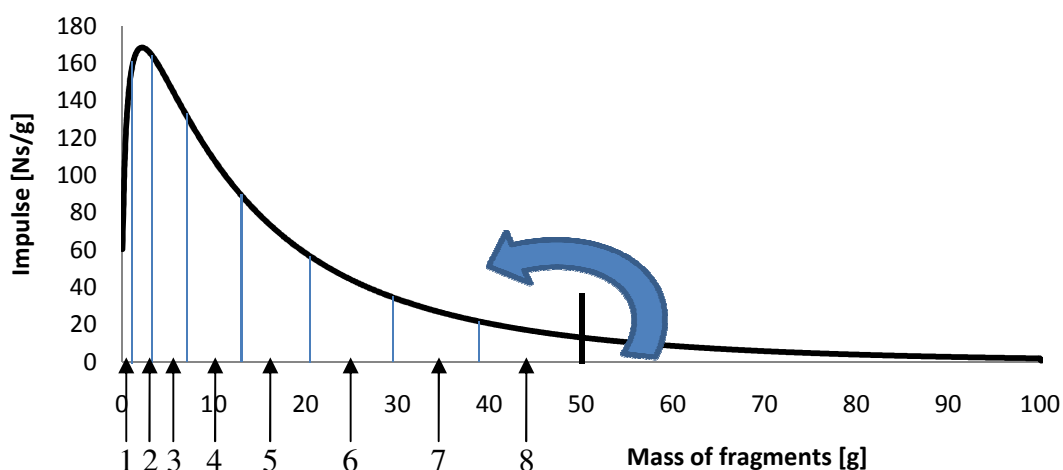


Figure 3.19 Subdivision of fragments into eight groups. The total mass of fragments larger than 50 g has been transformed to fragments with less mass.

Each group contains a certain amount of fragments with the same mass. The mass and amount of fragments will furthermore be different for all the groups. As a first simulation, all of the fragments from the same group will be thrown out in one, randomly chosen, point on the beam. In the second run, each group will be divided into two equally sized sub groups and each sub group will be thrown out in two randomized points. This simulation will continue until each subgroup contains only one fragment, see Figure 3.20.

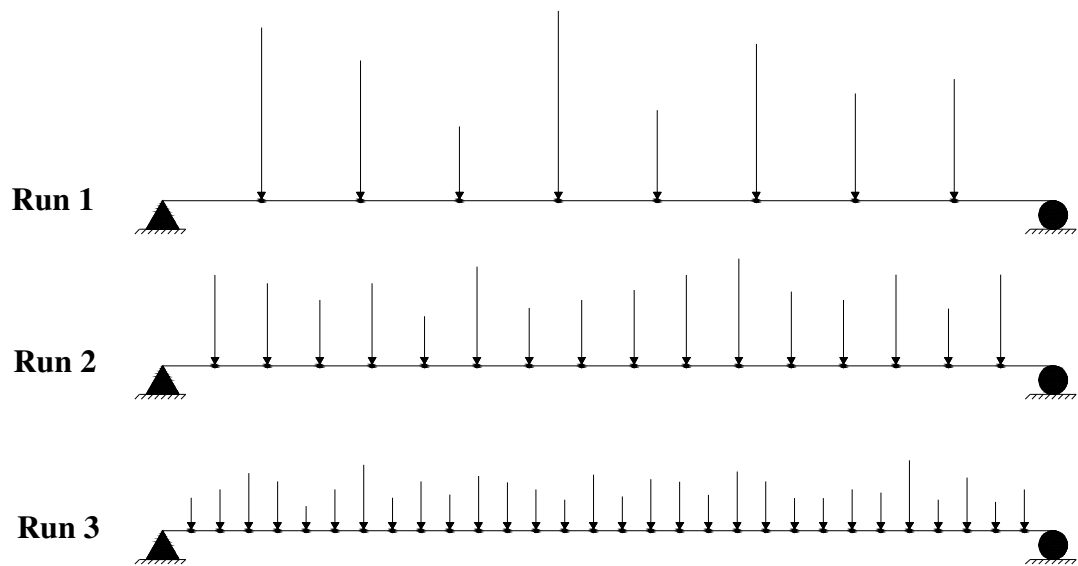


Figure 3.20 Simulation of fragments in the three first runs, containing 8, 16 and 32 groups of fragments.

Since groups and subgroups will be divided into 2, the amount of fragments in each group has chosen to be multiples of 2. The number of fragment per group in Table 3.3 gives a similar distribution to reality.

Table 3.3 Mass intervals for the subdivided groups comparing the columns 2 and 3 which is the true subdivision and in 5 and 6 the division used in this project.

Reality			Chosen division in this work		
Mass interval [g]	Fragments	% of total	Group	Fragments	% of total
0 – 0.9	261	51.1%	1	256	50.2%
0.9 – 3.4	125	24.5%	2	128	25.1%
3.4 – 7.6	63	12.3%	3	64	12.5%
7.6 – 13.4	32	6.0%	4	32	6.3%
13.4 – 20.8	16	3.1%	5	16	3.1%
20.8 – 29.6	8	1.6%	6	8	1.6%
29.6 – 39.4	4	0.8%	7	4	0.8%
39.4 - 50	2	0.4%	8	2	0.4%
Total amount	511		Total amount	510	

The size of fragments in each group can be calculated by respecting the condition that the real impulse should remain the same between the mass interval and the corresponding group. Even if masses over 50 g not will be taken into consideration, the impulse of these fragments will. The impulse for these larger fragments will be added to the mass interval as function of how large impulse each group contains in relation to the total impulse up to 50 g. The total impulse and corresponding choice of mass for the groups can be seen in Table 3.4 and Table 3.5. The choice of mass for the fragments in Table 3.5 has been made by respecting the condition that the impulse for the different groups should be the same as for the corresponding mass intervals.

*Table 3.4 The impulse for the various intervals including the extra impulse obtained from the fragments larger than 50 g.*

Mass interval [g]	Impulse [Ns]	% of impulse from 0-50 g	Impulse for fragments larger than 50 g [Ns]	Total impulse
0 – 0,9	101,3	3,4%	9,5	110,8
0,9 – 3,4	398,9	13,3%	37,4	436,3
3,4 – 7,6	590,4	19,7%	55,4	645,8
7,6 – 13,4	592,2	19,8%	55,6	647,8
13,4 – 20,8	500,4	16,7%	47	547,4
20,8 – 29,6	375,2	12,6%	35,2	410,5
29,6 – 39,4	258,8	18,7%	24,3	283,1
39,4 - 50	173,6	5,8%	16,3	189,9
Total impulse 0–50 g	2991		281	3272
Impulse for fragments larger than 50 g	280,8			

Table 3.5 The chosen mass for the various runs with corresponding velocity and impulse.

Group	Fragments	Mass [g]	Velocity [m/s]	Impulse [Ns]
1	256	0,3	1473	110,8
2	128	2,0	1730	436,3
3	64	5,5	1824	645,8
4	32	10,8	1872	647,8
5	16	18,0	1902	547,4
6	8	26,7	1923	410,5
7	4	36,5	1937	283,1
8	2	48,7	1950	189,9
Total impulse				3272

A total number of 9 different runs are prepared, see Table 3.6. In each run, the same number of striking points as loads will be chosen. These points will be equally distributed over the length of the beam. Furthermore, each load will be assigned to one single, randomly chosen, point.

Each run will be performed five times in order to see how the distribution affects the deflection of the loaded beam.

Table 3.6 Number of fragments and loads in the different runs. The subgroups in the grey marked zone consist of one fragment and can therefore not be further subdivided.

	run 1		run 2		run 3		run 4		run 5		run 6		run 7		run 8		run 9	
	subgroups	fragments																
Group 1	1	256	2	128	4	64	8	32	16	16	32	8	64	4	128	2	256	1
Group 2	1	128	2	64	4	32	8	16	16	8	32	4	64	2	128	1	128	1
Group 3	1	64	2	32	4	16	8	8	16	4	32	2	64	1	64	1	64	1
Group 4	1	32	2	16	4	8	8	4	16	2	32	1	32	1	32	1	32	1
Group 5	1	16	2	8	4	4	8	2	16	1	16	1	16	1	16	1	16	1
Group 6	1	8	2	4	4	2	8	1	8	1	8	1	8	1	8	1	8	1
Group 7	1	4	2	2	4	1	4	1	4	1	4	1	4	1	4	1	4	1
Group 8	1	2	2	1	2	1	2	1	2	1	2	1	2	1	2	1	2	1
number of loads	8		16		30		54		94		158		254		382		510	

The impulse distributions for run 1 and run 5 are presented in figure 3.21 and 3.22 respectively. The loads have been randomly distributed for all runs except for run 1A which will be used as a “worst case scenario”.

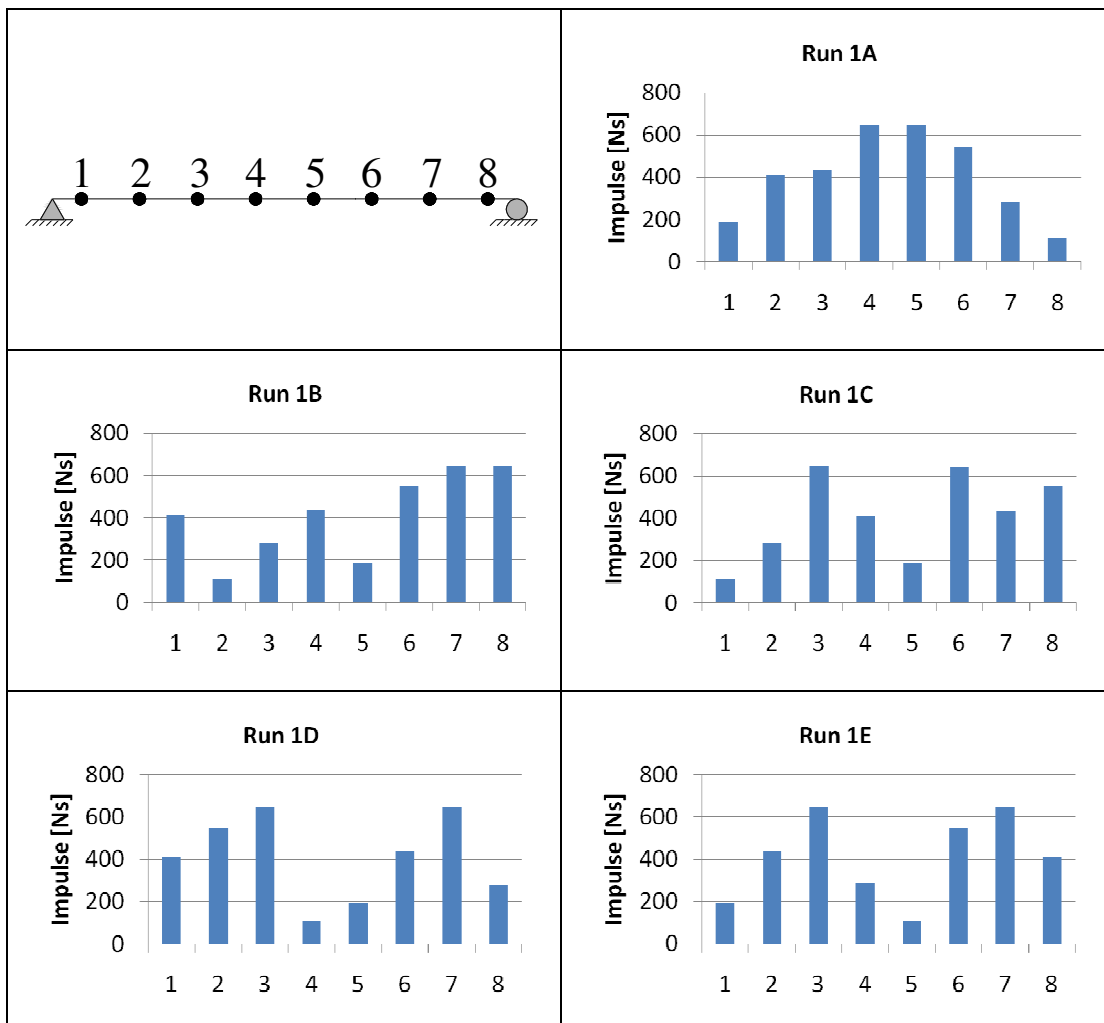


Figure 3.21 Impulse distribution for the various cases in run 1.

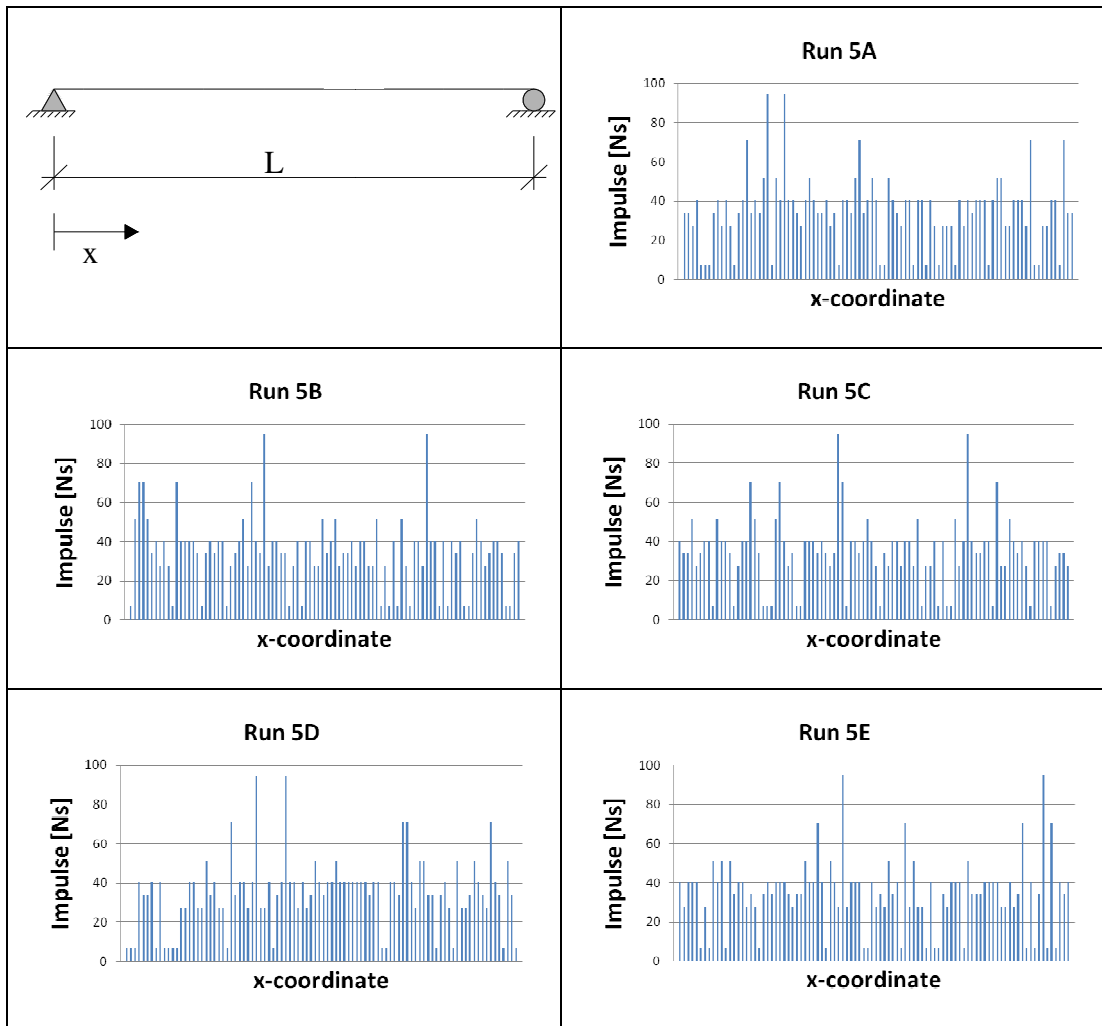


Figure 3.22 Impulse distribution for the various cases in run 5.

### 3.6.4 Fragmental load angle

As a first step, all fragments will be assumed to strike the beam at an angle of  $90^\circ$  regardless of where on the beam a fragment strikes. This is, in reality, only true for fragments that strike in the middle of the beam. This assumption will therefore somewhat overestimate the forces acting closer to the support and totally ignore the horizontal resultant of the force. Figure 3.23a presents one of the load cases in run 1 with the 8 fragment groups represented as forces which all acts perfectly perpendicular to the beam. Figure 3.23b presents the same load case but where the load angle has been taken into consideration.

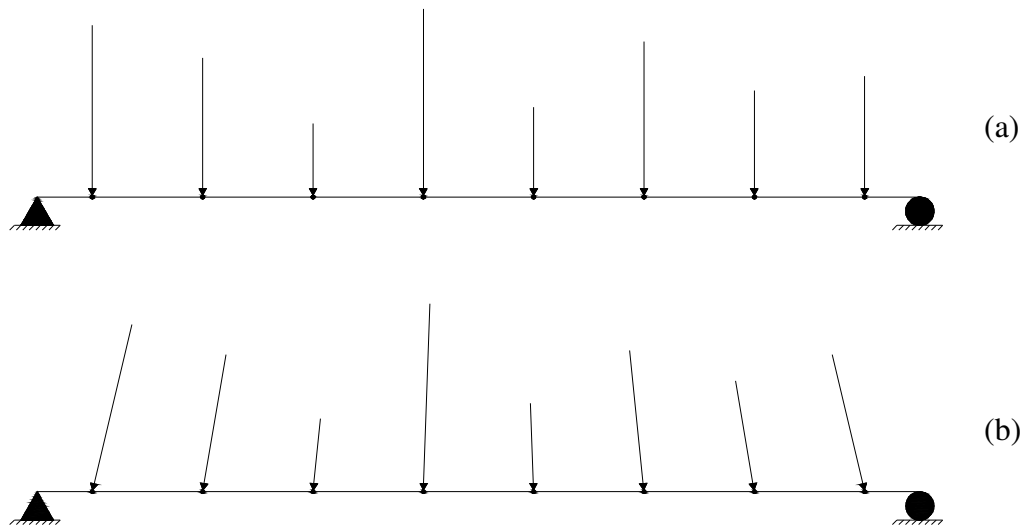


Figure 3.23 Fragment load where load angle has, and has not been taken into consideration, (a) and (b) respectively.

If the load angle is taken into consideration, each load can be subdivided into two resultants according to Figure 3.24.

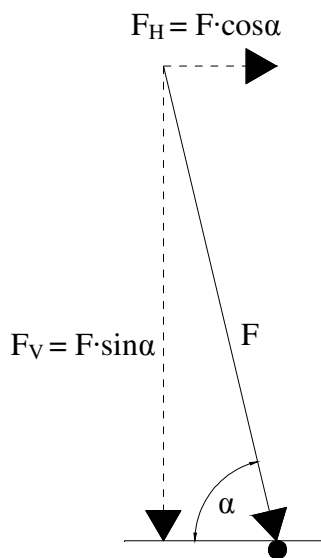


Figure 3.24 Fragment load subdivided into two resultants with a certain load angle.

### 3.6.5 Fragment arrival time

The time from when the bomb detonates until a fragment reaches the wall has been simplified by assuming that the distance from the center of the bomb to the striking points,  $R$ , is equal to five meters. This is, as for the load angle, only true for fragments hitting the mid section of the beam as can be seen in Figure 3.25.

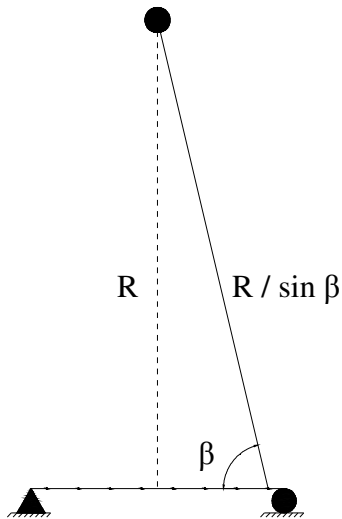


Figure 3.25 Distance from the bomb to any point on the beam.

Since the distance will be underestimated for fragments closer to the supports, the time from when the bomb detonates until a fragment reaches this point will also be underestimated. Fragments hitting closer to the supports will also have somewhat lower velocity when they arrive, since the distance is longer, which results in less impact for these fragments.

### 3.6.6 Comments about load angle and arrival time

A simplified model where the fragment load angle is constantly equal to  $90^\circ$  and where the fragment arrival time is independent of where the fragment hit the beam (i.e. based on  $R = 5$  m) will be used as a standard case in the simulations. The difference in load angle and arrival time will however be considered in order to see deviations compared to the simplified assumptions.

## 4 The FE-model

### 4.1 General description

The concrete wall strip is analysed numerically by using the finite element program ADINA (2008). Two different models are created, one simplified beam element model and a 2-D solid element model. Both these models are analysed with elastic, plastic and elastic-plastic material properties as described in section 3.3. For both models, an equivalent elasto-plastic material is used with the same simplified load-displacement curve as for the real material, Figure 3.4. The beam can in this way be modelled by only one material instead of two; one for concrete and one for reinforcement. By using an equivalent material, the FE-models will also be much more stable, since the simulation of cracking is not considered.

The beam element model is used to investigate how the beam's behaviour differs when the fragmental load is either applied as various numbers of point loads or as a uniformly distributed. The 2-D solid element model, though, is mainly used to simulate removal of concrete due to the fragmental impact when penetrating the concrete.

The beam is exposed to a blast load which is acting as a uniformly distributed load, while the fragment loads are either applied as a uniformly distributed load or as randomly distributed point loads corresponding to run 1,5 and 9. The fragment loads can vary between uniformly distributed load and point loads because the beam's difference in behaviour is to be checked.

In ADINA the loads are applied by using time functions to make the simulation more realistic. In the first case, the blast- and fragment loads are applied as uniformly distributed loads in such a way that they hit the beam at the same time. In the other case, the fragment loads are applied with varying arrival times, depending on the fragment mass and velocity.

Plastic material response is modelled in the same way as elastic-plastic response but the stiffness for the elastic part is increased by using rotational constraints for the elastic elements. The support nodes are used as master nodes and the elastic nodes in between the supports and the plastic element are used as slave nodes in order to constrain the beam's deflection to imitate that assumed according to yield theory.

To use the linear elastic, plastic and elastic-plastic material responses, a fictive young's modulus and fictive yield strength needs to be calculated. The fictive Young's modulus is calculated with the equations (4-1) and (4-2), this is achieved by reducing the Young's modulus with a constant  $\gamma$ , which is the quotient of the moment of inertias from state I and state II to get a representative value for the two states, see Figure 2.21. This will be input data for the FE-models in the elastic as well as the elastic-plastic analysis.

$$\gamma = \frac{I_I}{I_{II}} \quad (4-1)$$

$$E_{c,II} = \frac{E_{c,I}}{\gamma} \quad (4-2)$$

$\gamma$  Reduction factor for the Young's modulus

$I_I$  Moment of inertia in state 1

$I_{II}$  Moment of inertia in state 2

$E_{c,1}$  Young's modulus for concrete in state 1

$E_{c,II}$  Fictive Young's modulus

The ultimate capacity of the beam is calculated in Appendix B according to the theory presented in chapter two. The fictive yield strength can now be calculated according to equation (4-3).

$$f'_y = \frac{M_u}{Z} \quad (4-3)$$

$M_u$  Ultimate moment capacity

$f'_y$  Fictive yield stress used to describe when the beam goes from linear elastic to ideally plastic response

$Z$  Flexural resistance

## 4.2 Beam element model

### 4.2.1 Material properties

A beam element model is used to model the beam in a simplified way. The beam element is a two node element, which in ADINA may be provided with a maximum of seven integration points over the height. This means, that the cross-section can not be fully plasticized, but at most acquire a stress state as that shown in Figure 4.1. Therefore the flexural resistance will be modified on the basis of the seven integration points and be used in the input file for FE-analysis.

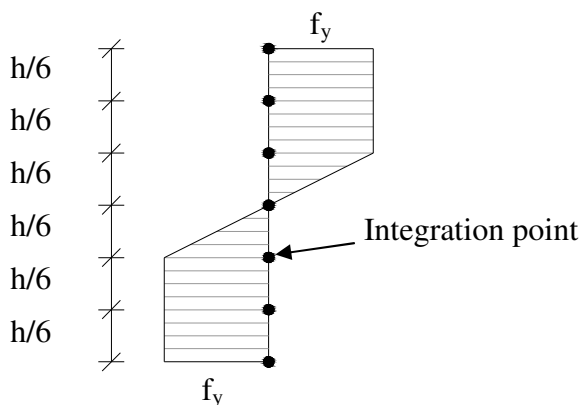


Figure 4.1 Maximum stress state over cross section with seven integration points in ADINA.

The flexural resistance has been calculated by using equation (2-11) and the following expression is obtained:

$$Z' = \frac{13}{54} b \cdot h^2 \quad (4-4)$$

The flexural resistance obtained by equation (2-11) differs approximately 4 % compared to the flexural resistance when the cross-section can reach its full plastic capacity, i.e.  $Z=bh^2/4$ .

During the analysis, the models were deformation controlled by point loads at the plastic nodes. It turned out that the expected internal resisting force when the beam reached yielding was not obtained. The reason for this is unknown but in order to describe a correct moment capacity of the beam the yield strength is increase with another 4 %, i.e.

$$f'_y = 1.04 \cdot f_y \quad (4-5)$$

where

$$f_y = \frac{M_{Pl}}{Z'} \quad (4-6)$$

In Table 4.1 the modified input data, concerning the material properties for the elastic and plastic elements are presented. The values for the Young's modulus and the yield stress are calculated and described in Appendix B.

*Table 4.1 Modified input data for the beam elements for the elastic elasto-plastic response.*

Elements	Young's modulus [GPa]	Yield stress [MPa]
Elastic	3.86	-
Plastic	3.86 (constraints)	5.358
Elasto-Plastic	3.86	5.358

Since the runs have different numbers of point loads, the subdivision of elements will be different for all the runs, since the points where the fragment loads hit must agree with the nodes in the mesh.

#### 4.2.2 Elastic analysis

In Table 4.2, the number of elements is presented for run 1, 5 and 9 for the elastic analysis.

*Table 4.2 Number of elastic beam elements in runs 1, 5 and 9.*

Run	Number of elements
Run 1	48
Run 5	188
Run 9	510

The beam elements model can be seen in Figure 4.3 and is only consisting of linear elastic elements.

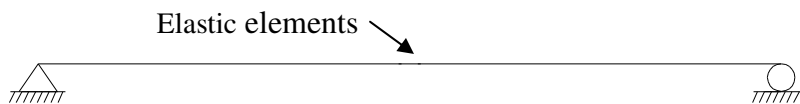


Figure 4.2 Beam element model for the linear elastic material response.

### 4.2.3 Elasto-plastic analysis

The plastic hinge phenomenon, discussed in section 2.4.2 is modeled with one elasto-plastic element in the midsection and the rest of the beam with linear elastic elements. The elasto-plastic element is approximately ten times smaller than the elastic elements. The numbers of elastic- and elasto-plastic elements are presented for run 1, 5 and 9 in Table 4.3.

Table 4.3 Number of elastic- and plastic beam elements in runs 1, 5 and 9.

Run	Number of elastic elements	Number of plastic elements
Run 1	32	1
Run 5	188	1
Run 9	510	1

In Figure 4.3 the concept of the beam model is visualized with the elastic and elasto-plastic parts.

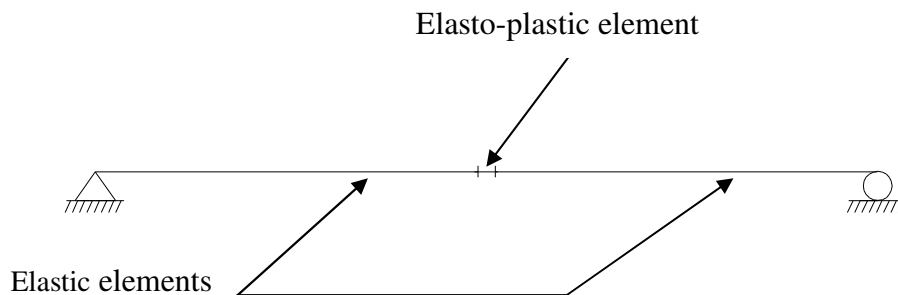


Figure 4.3 Beam element for the beam element model in the elasto-plastic analysis.

### 4.3 2D-solid element model

#### 4.3.1 Element mesh and material properties

A 2D-solid, plane stress model is used to be able to analyze the wall strip in a more advanced way. The main aim with this model is to simulate the removal of concrete after the fragmental impact has destroyed parts of the concrete surface.

To avoid stress concentrations in the support area, two support blocks are used to distribute the stresses and the support conditions are applied to the lower face of them, see Figure 4.4. These blocks are modelled with steel material properties.

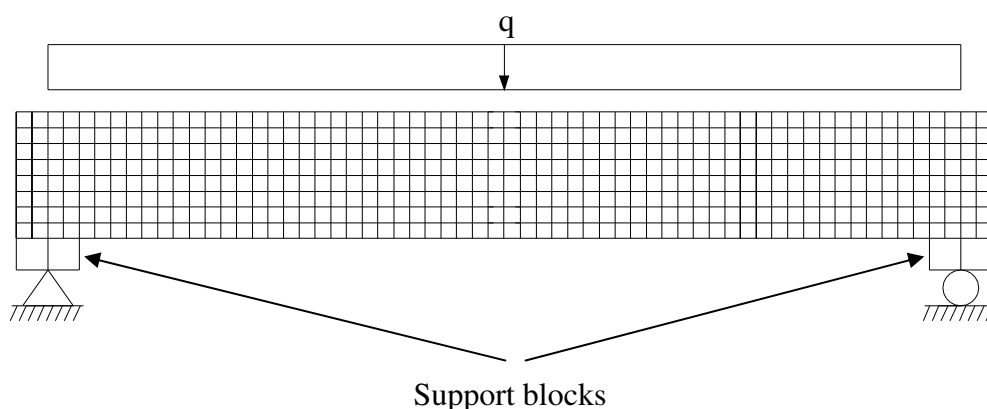


Figure 4.4 2-D solid model with support blocks to avoid stress concentrations.

In the 2-D solid model, four node elements are used, this means that the flexural resistance depends on the number of elements, since the number of elements affects the total number of integration points over the cross sections height. But it turned out that, for 8 elements or more over the height, the cross section can be assumed to reach its fully plastic capacity.

The input data concerning material properties for the elastic as well as the elasto-plastic analysis is presented in Table 4.4.

*Table 4.4 Input data for the 2-D solid elements for the elastic and elasto-plastic response.*

<b>Elements</b>	<b>Young's modulus [GPa]</b>	<b>Yield strength [MPa]</b>
Elastic	3.86	-
Elasto-Plastic	3.86	4.95

### **4.3.2 Elastic analysis**

In the elastic analysis the mesh is equally sized throughout the beam and the number of elements can be seen in Table 4.5. In Figure 4.5 the 2-D solid model can be seen with the exception of the plastic part.

*Table 4.5 Number of elastic 2-D solid elements.*

<b>Number of elastic elements</b>	<b>Number of plastic elements</b>
441	none

### **4.3.3 Elasto-plastic analysis**

In the elasto-plastic analysis the mesh is divided into two elastic parts and one elasto-plastic part placed in the middle of the beam, see Figure 4.5. This is done to achieve the plastic hinge phenomenon as discussed in section 2.4.2. The number of elements can be seen in Table 4.6.

*Table 4.6 Number of elastic- and plastic 2-D solid elements in the elasto-plastic analysis.*

<b>Number of elastic elements</b>	<b>Number of plastic elements</b>
434	7

In Figure 4.5, the 2-D solid model can be seen with the division of the elastic and elasto-plastic parts and as can be seen the elastic- and elasto-plastic elements are equally sized.

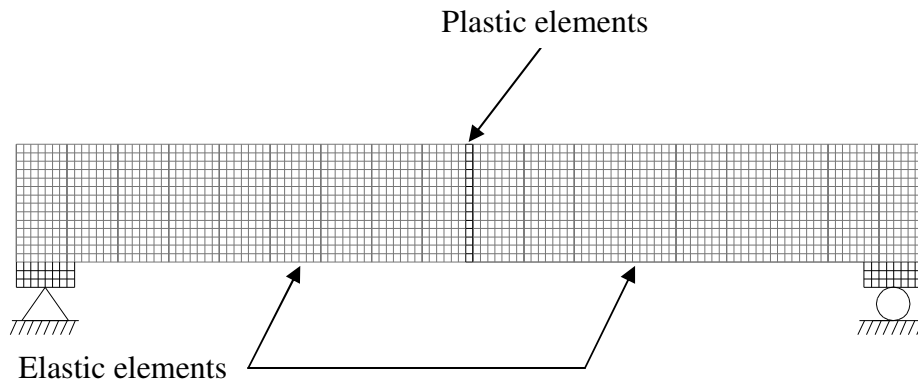


Figure 4.5 Element mesh for the 2-D solid model in the plastic analysis with the elastic- and elasto-plastic parts marked out.

#### 4.4 Simulation of removal of concrete due to fragmental impact

In this section, a simulation of removal of concrete due to the fragmental impact is presented. To be able to calculate the penetrations depth for the fragmental impact, equations are taken from section 2.2.3.2.

When fragments hit the wall strip, penetration will occur and concrete material will be partly destroyed. This phenomenon causes serious local damage to a certain depth in the concrete depending on the fragments mass and velocity. The material in regions close to the holes and in between the holes can no longer contribute to the stiffness. This loss of stiffness is to be modelled, and to achieve this behaviour in ADINA, elements on the outer edge of the wall strip will be removed.

The 2-D solid element model is used to model this behaviour, since these elements enable the removal of the outer edge elements with the remaining elements still contributing to the stiffness. Both the blast- and fragment load are applied and both loads are only applied as uniformly distributed loads.

In this project, three methods for simulating the removal of material when the fragments hit the wall strip have been analysed. A value for all the fragments has been calculated and a value of about 50 mm is obtained. The different methods for analyzing the removal are presented below:

1. The cross-section is initially reduced which means that the beam's moment capacity and internal resisting force decreases, also the yield strength needs to be changed to a somewhat higher value, see calculations in Appendix D. Hence, the beam is analysed with a height of 300 mm instead of the original 350 mm, i.e. an initial removal of 50 mm of concrete, see Figure 4.6.
2. The cross-section is reduced by removing the concrete layer that gets directly hit by the fragment load at a certain time. This means that the beam's stiffness

will decrease substantially and the loss of mass will also influence the behaviour of the beam. The removal consists of 50 mm concrete at a time during loading, when the fragmental load duration is over,  $t_{remove} = 0.22$  ms, See Figure 4.7.

3. The cross-section is reduced by removing stiffness material in the top layer, while the remaining part will consist of a mass material with a significantly lower Young's modulus to simulate destroyed concrete. This means that the top layer's stiffness will disappear while the mass will decrease depending on how much of the mass that is to be removed. The layer that is to be removed is modelled with two different materials. The concrete which is called the stiffness material has its original material properties except the weight, will be removed at the time when the fragmental load duration is over, i.e.  $t_{remove} = 0.22$  ms and another material here called mass material with a low Young's modulus will remain. This enables to avoid reduce all the mass of the 50 mm layer. A removal of 0, 25, 50 and 100 % of the mass is to be analysed. The amount of removed material for the various cases can be seen in Table 4.8. In Figure 4.8, a schematic description explains how the removal of stiffness and mass takes place.

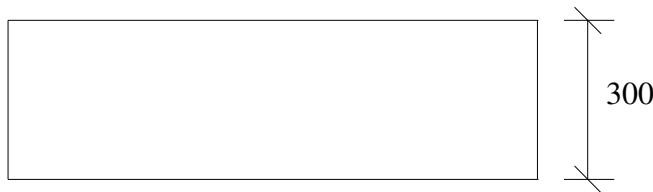


Figure 4.6 Initially reduced cross section with a height of 300 mm.

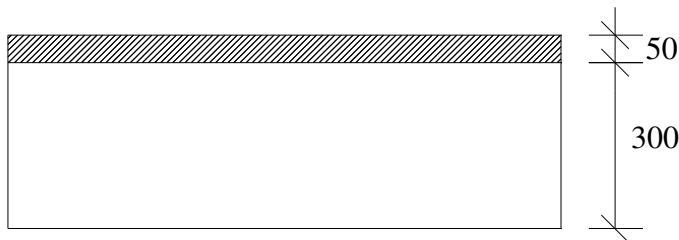


Figure 4.7 Cross section when removing all mass and stiffness of the top layer.

All the cross sections that is analysed when simulating the removal of concrete due to the fragmental impact, have the same cross section and material properties as the beam with a height of 300 mm. These properties can be seen in Table 4.7.

Table 4.7 Material data concerning yield stress and Young' modulus for the analysed beam with a height of 300 mm.

$f_y$	5.36 MPa
E	4.15 GPa

For the beam, which is modelled with two materials in the top layer, the cross section with the different layers is clarified in Figure 4.8. The material and cross section data

for the different layers are presented in Table 4.9. The stiffness material is modelled with bilinear elasto-plastic material properties in the midsection and the rest with linear elastic material properties, while the mass material is modelled with linear elastic material properties throughout the entire length.

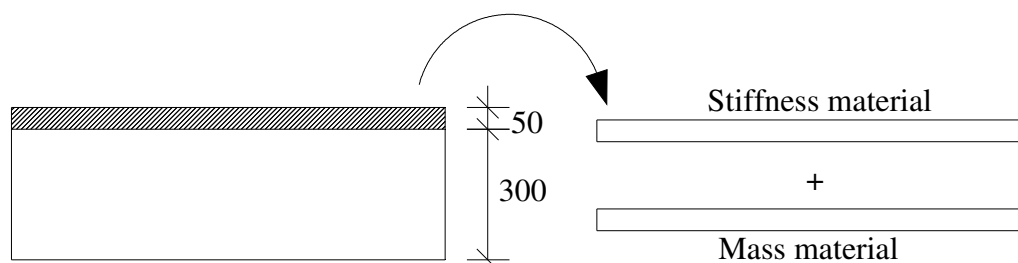


Figure 4.8 Cross section when the top layer consisting of a stiffness material and a mass material and the stiffness material layer will be removed to simulate the fragmental impact.

Table 4.8 Masses in the top layer that is to be removed and the remaining masses for the different cases.

Removal of mass [%]	Removed material	
	Mass [kg]	Modified density [kg/m <sup>3</sup> ]
0	0	2400
25	81	1800
50	162	1200
100	324	0

Table 4.9 Material properties for the two materials which are modelled in the top layer.

Material	Young's modulus	Yield stress (elasto-plastic element)
Stiffness material	4.15 GPa	5.36 MPa
Mass material	0.4 MPa	-

## 5 Results

### 5.1 Orientation

In this chapter the results from the different analysis are presented and discussed. The results obtained using ADINA have been compared and verified with the SDOF results and with simplified hand calculations which also are presented in this chapter.

In all the results presented in this section, the blast load is applied as a uniformly distributed load and the fragment load is either applied as various numbers of point loads or as a uniformly distributed load and the difference in behaviour is to be checked. All figures concerning displacement as a function of time are treating the midpoint displacement.

The results from linear elastic and ideally plastic analysis are mainly used to verify the model and to get a better understanding for the structural behaviour. Focus will be on the results obtained when using bilinear elasto-plastic material response which is the response closest to reality.

### 5.2 Linear elastic analysis

#### 5.2.1 Beam element model

As a first step to verify the beam element model, the displacement is compared to the ones obtained by SDOF and hand calculation. In Figure 5.1, the comparison between the beam element model, SDOF and hand calculation is presented. As can be seen the results between the different analysis methods is agreeing very well.

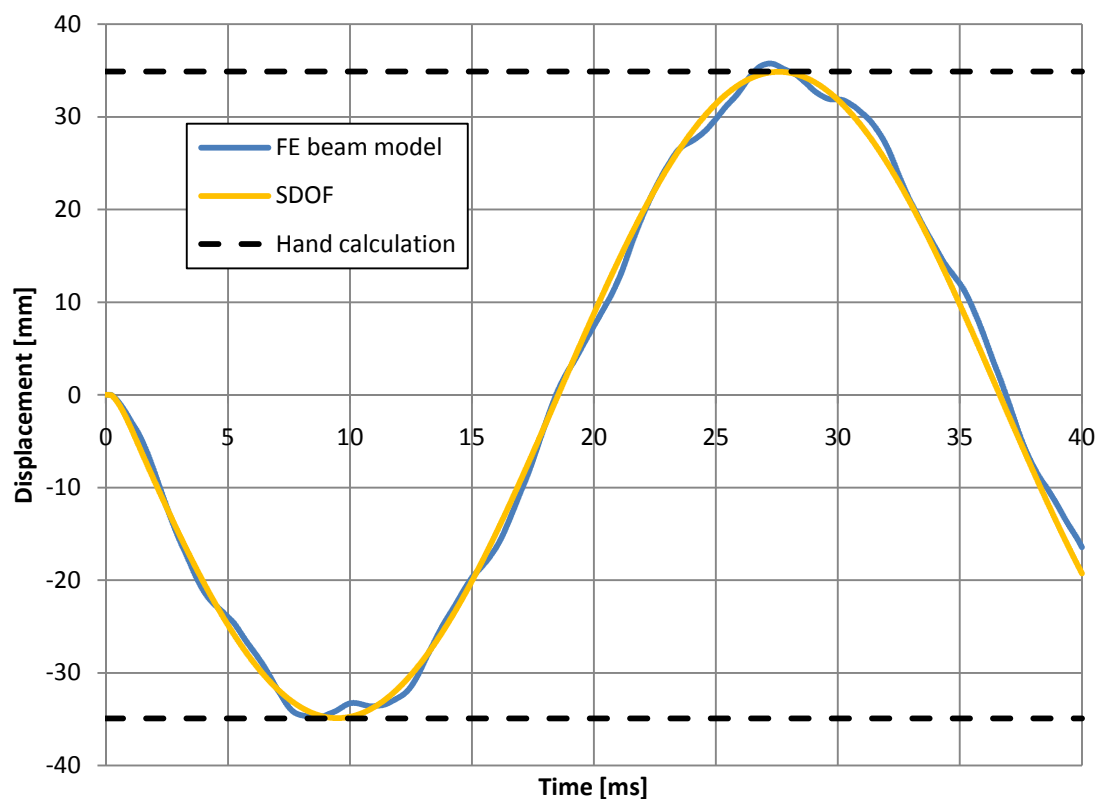


Figure 5.1 Comparison of midpoint displacements for the beam model in ADINA, SDOF and hand calculation. Blast- and fragment load is applied as a uniformly distributed load.

In linear elastic analysis, it is possible to super position different loads and get an identical result as if the loads were applied together at the same time. This can be explained by the following expression which calculates the elastic displacement:

$$u_{el} = \frac{I_1}{C_{el}} + \frac{I_2}{C_{el}} = \frac{I_1 + I_2}{C_{el}} \quad (5.1)$$

where

$$C_{el} = \sqrt{\kappa_{MF.el}} \cdot \sqrt{M \cdot K_{II}} \quad (5.2)$$

In Figure 5.2 this is presented for the blast- and fragment load and by adding the contribution from the single responses, the total response is obtained.

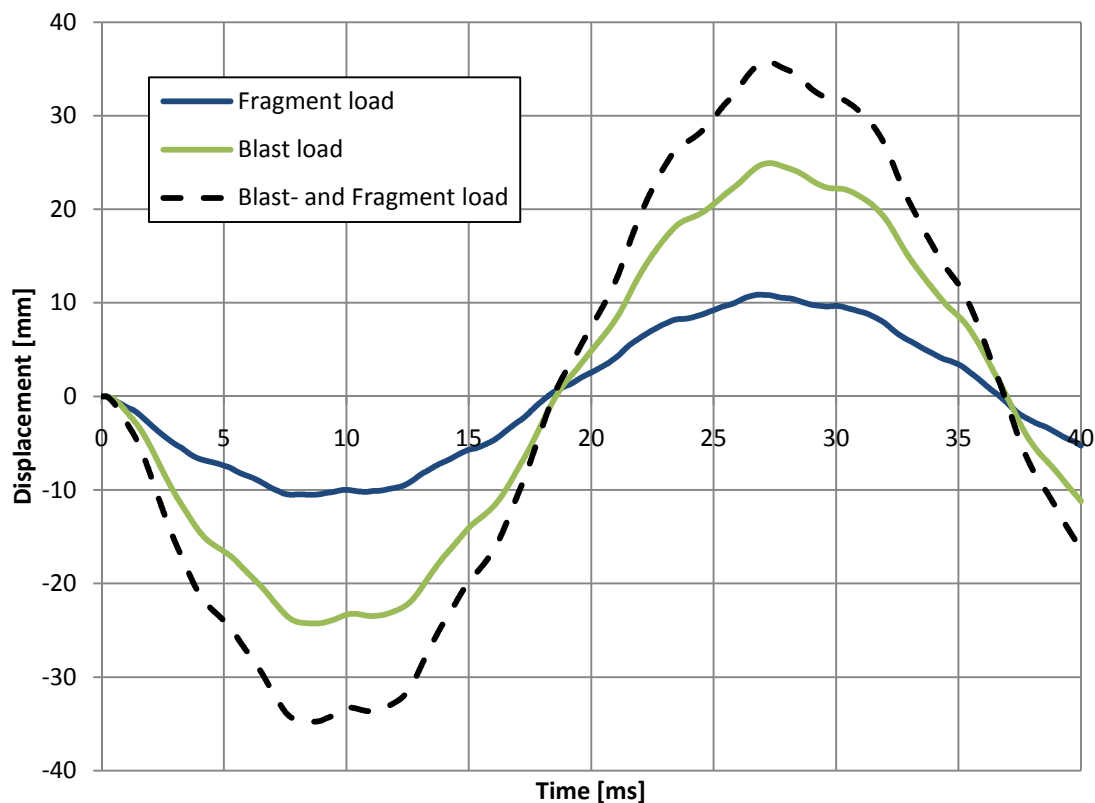


Figure 5.2 Midpoint displacements for the single response of the blast- and fragment load and the blast- and fragment load acting together for the FE beam element model.

A comparison in displacement between when the fragment load is applied normally and when the true arrival time, true distance and the inclination of the fragment loads are considered has been performed. The blast load is in both cases applied as a uniformly distributed load. In Figure 5.3, run 1B is presented for the two cases, and as can be seen, the difference is negligible. The small difference can be explained by the fact that the force inclination is small and therefore the reduced force perpendicular to the beam strip is almost the same as the original one. The fragment loads are also less

influencing regarding the displacement compared to the blast wave. In further analysis, the true arrival time, distance and inclined force will not be considered.

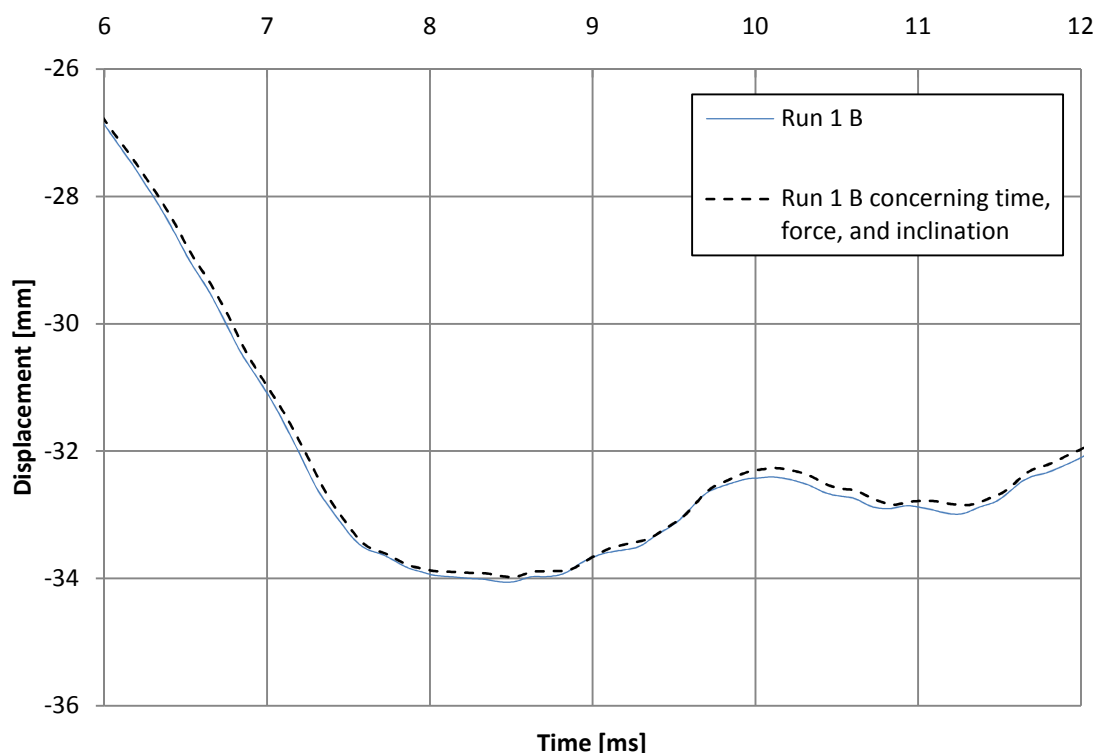


Figure 5.3 Comparison in displacement for run 1 B when the load is applied normally and when the true arrival time, force and inclination are taken into consideration.

In Figure 5.4 the results from the linear elastic analysis are presented for run 1. As can be seen, the difference in displacement between the various runs and when the fragment load is applied as a uniformly distributed load is small. Run 1 A is a worst case scenario, see section 3.6.3, where the largest fragments are applied in the middle of the beam with decreasing size towards the supports and that is why this displacement curve differs somewhat from the other ones.

Since the difference in displacement between the various runs and the uniformly distributed is so small, a zoomed version of the original results is needed to be able to distinguish the various curves. The zoomed version is presented in Figure 5.5 and as the figure shows once again, the difference in displacement is rather small.

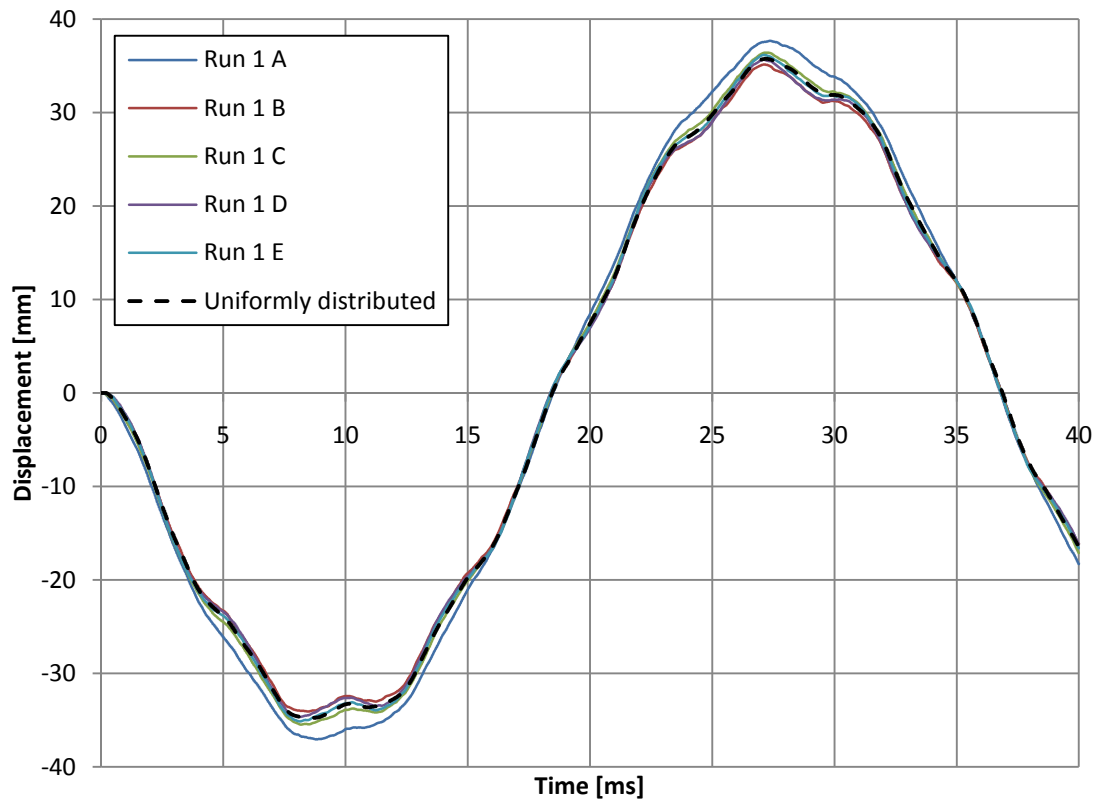


Figure 5.4 Displacement for the linear elastic analysis Run 1 and when the fragments are applied as uniformly distributed.

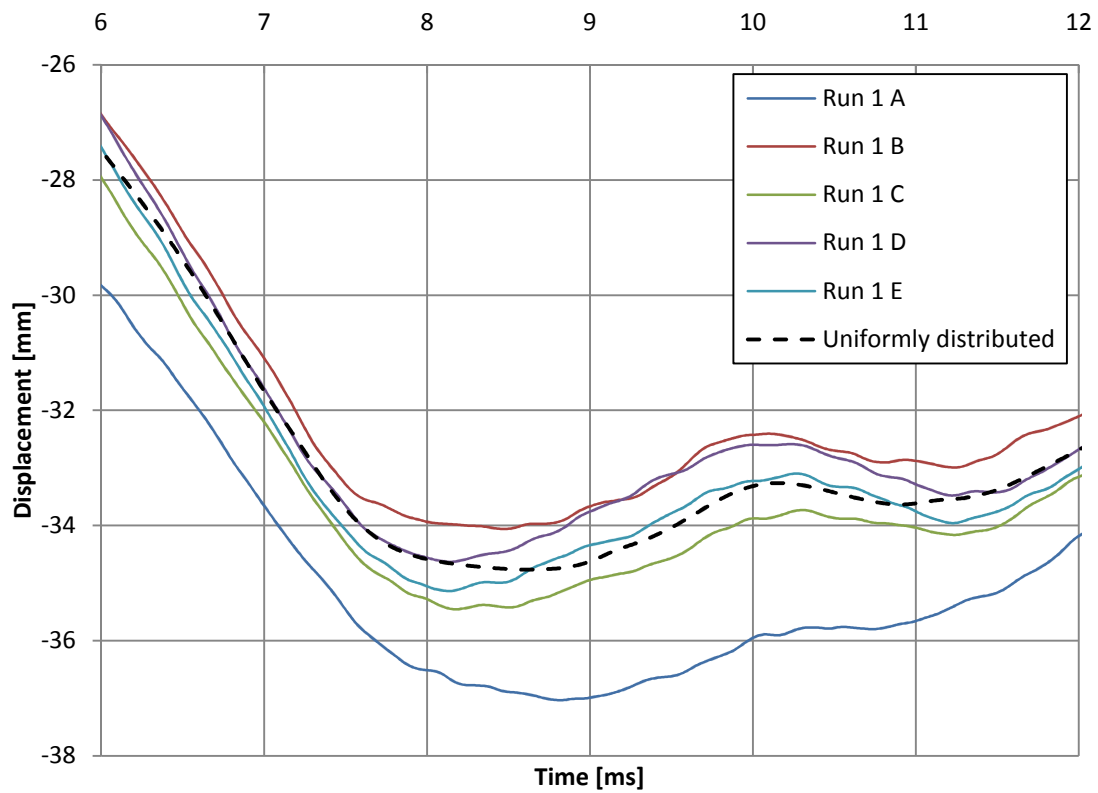


Figure 5.5 Zoomed displacements for the linear elastic analysis, Run 1 and when the fragments are applied as uniformly distributed.

In Figure 5.6 the displacements for Run 5 are presented and it should be noticed that the difference among the curves are now much smaller compared to Run 1. It depends on that it is many smaller point loads applied compared to Run 1 and therefore it looks more or less like the uniformly distributed case.

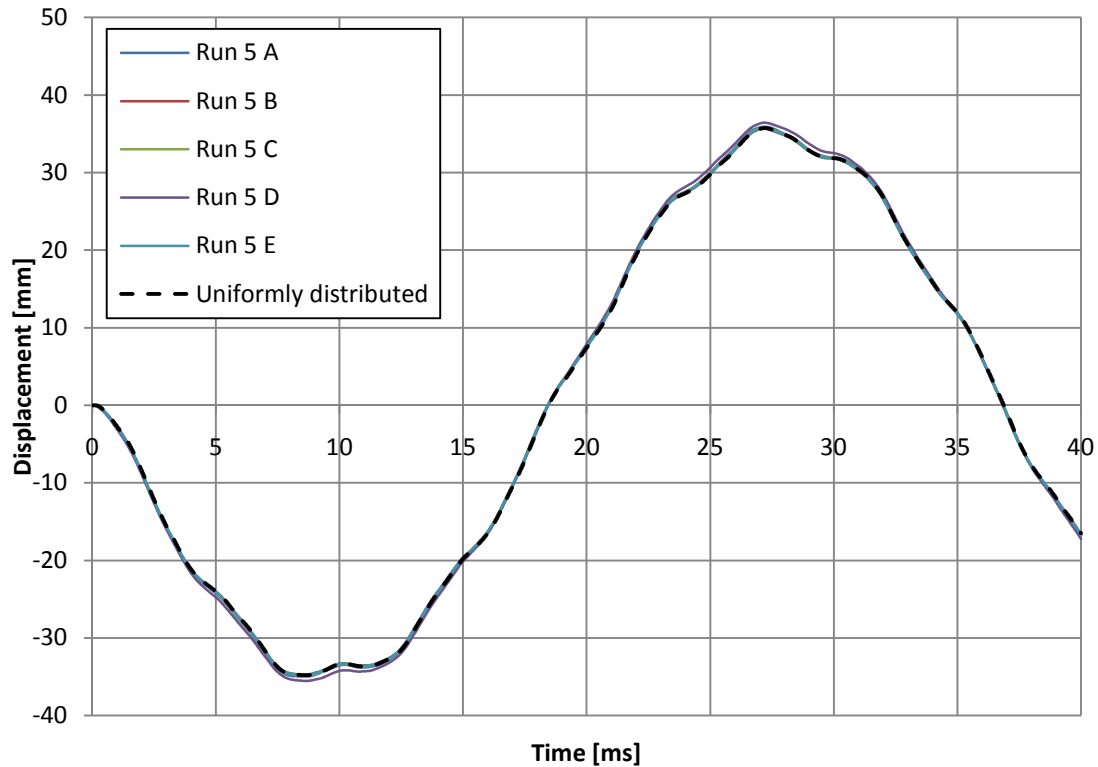


Figure 5.6 Displacements for Run 5 and when the fragment loads are applied as uniformly distributed.

In the zoomed version of Figure 5.6, Figure 5.7, the displacements are presented once again. The magnitude differences in displacement are approximately 1 mm for Run 5 compared to run 1 where it is approximately 2 mm. Run 5 D has significantly larger displacement than the other cases which can be described by the subdivision, since the largest fragment group cannot be further divided than into one single fragment. And if these large fragments strike in the middle of the beam the displacement will be somewhat larger.

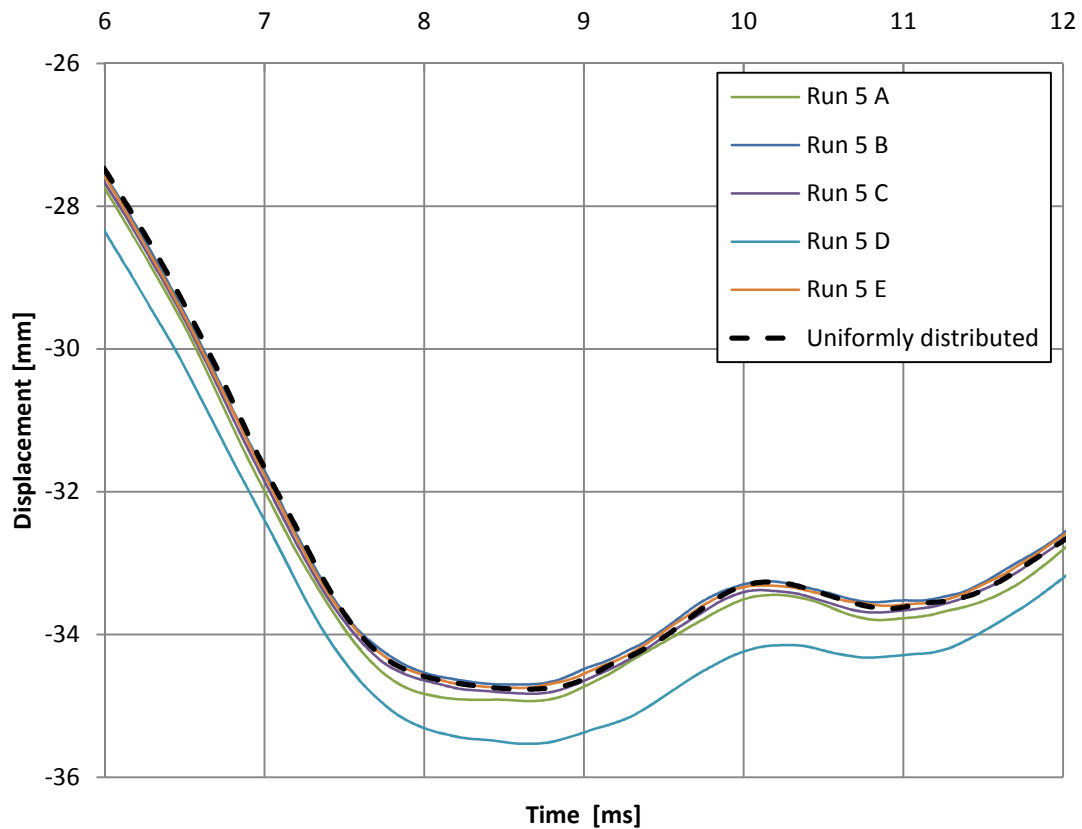


Figure 5.7 Zoomed displacements for Run 5 and when the fragment loads are applied as uniformly distributed.

The displacements for Run 9 are presented in Figure 5.8 and it reminds much of the results obtained in run 5. Still there is some difference between the cases which can be described by the subdivision once again. However, all cases are though very close to the uniformly distributed curve, which can be more easily seen in Figure 5.9.

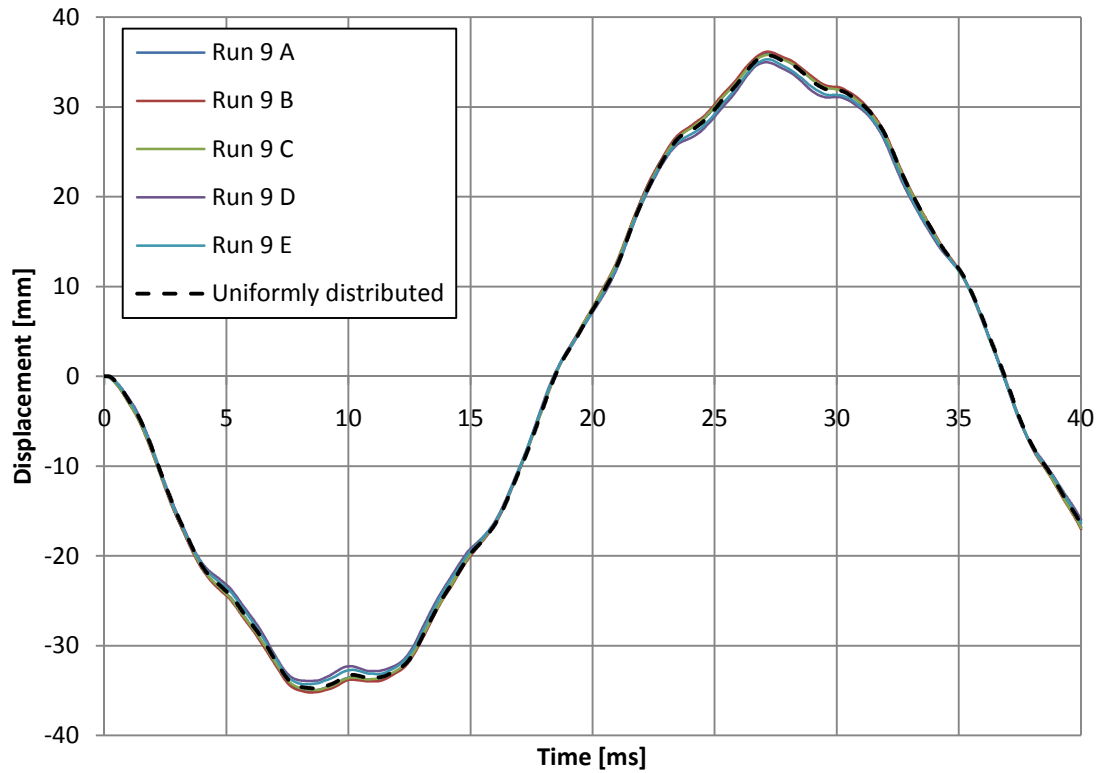


Figure 5.8 Midpoint displacements for Run 9 and when the fragment loads are applied as uniformly distributed.

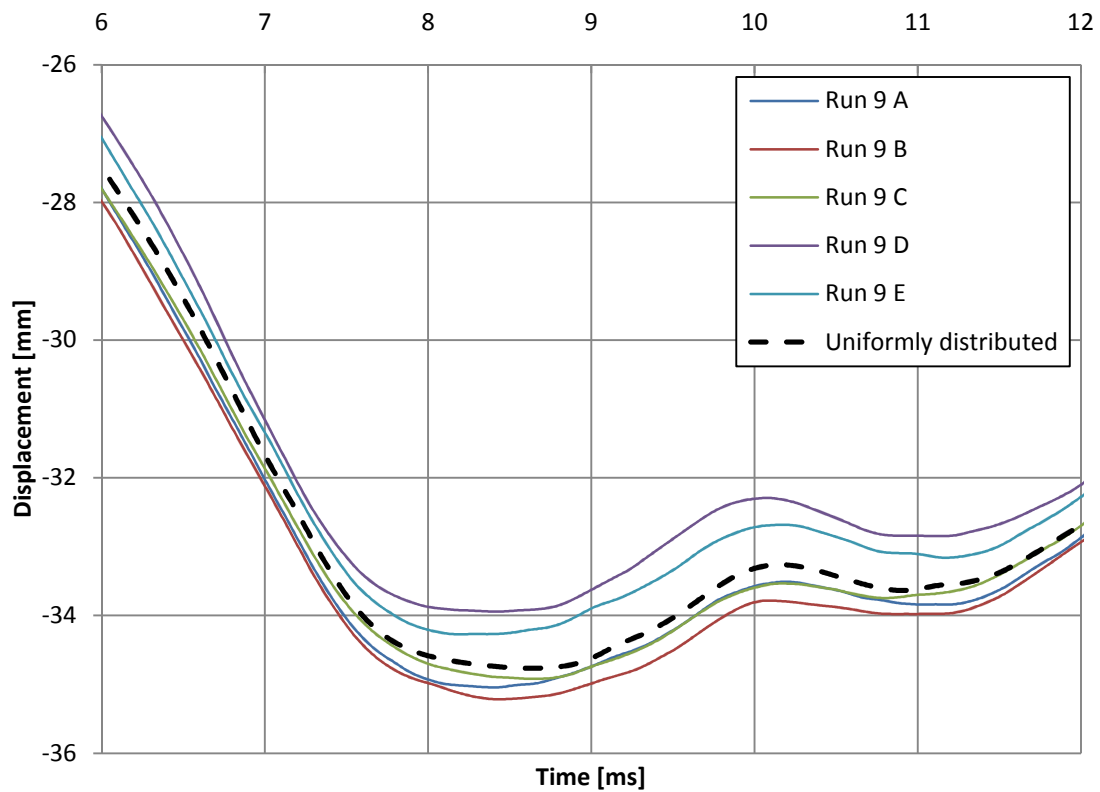


Figure 5.9 Zoomed midpoint displacements for Run 9 and when the fragment loads are applied as uniformly distributed.

### 5.2.1.1 Solid element model

In this chapter, the results from the 2-D solid model with linear elastic material properties are presented. Since the 2-D solid model mainly is used for simulating the removal of concrete, it will only be presented with the fragment loads applied as a uniformly distributed load. The displacements are compared to the ones obtained by the beam element model in order to verify the model.

In Figure 5.10, the displacements for the 2-D solid model and beam element model are presented and as can be seen, the curves are similar, but differ marginally concerning displacement and period.

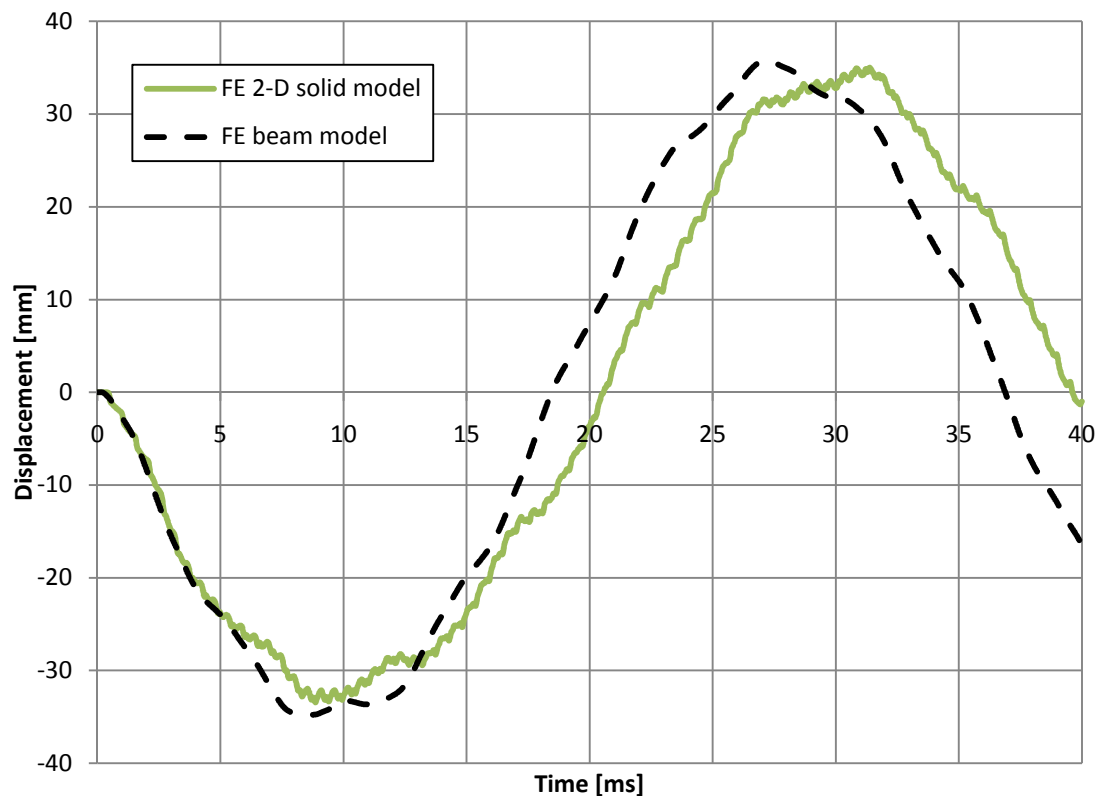


Figure 5.10 Midpoint displacements for the 2-D solid- and the beam element model when the fragment loads are applied as uniformly distributed.

### 5.2.2 Conclusion

The different analyses methods that have been used: beam element model, 2-D solid model, SDOF and hand calculation have all generated agreeing results in the linear elastic analysis.

For all the runs and cases that have been performed in the linear elastic analysis it seems to be a good estimation to apply the fragmental point loads as a uniformly distributed load. For each further subdivision, the results among them tend to differ less and come closer to the uniformly distributed one.

### 5.3 Plastic analysis

A first step in the plastic analysis is to verify the results obtained by the FE-analysis, this is achieved by comparing them with the results from SDOF and hand calculation. In Figure 5.11 the displacements are presented for the blast- and fragment load separately and the two loads applied together for the three analysis methods.

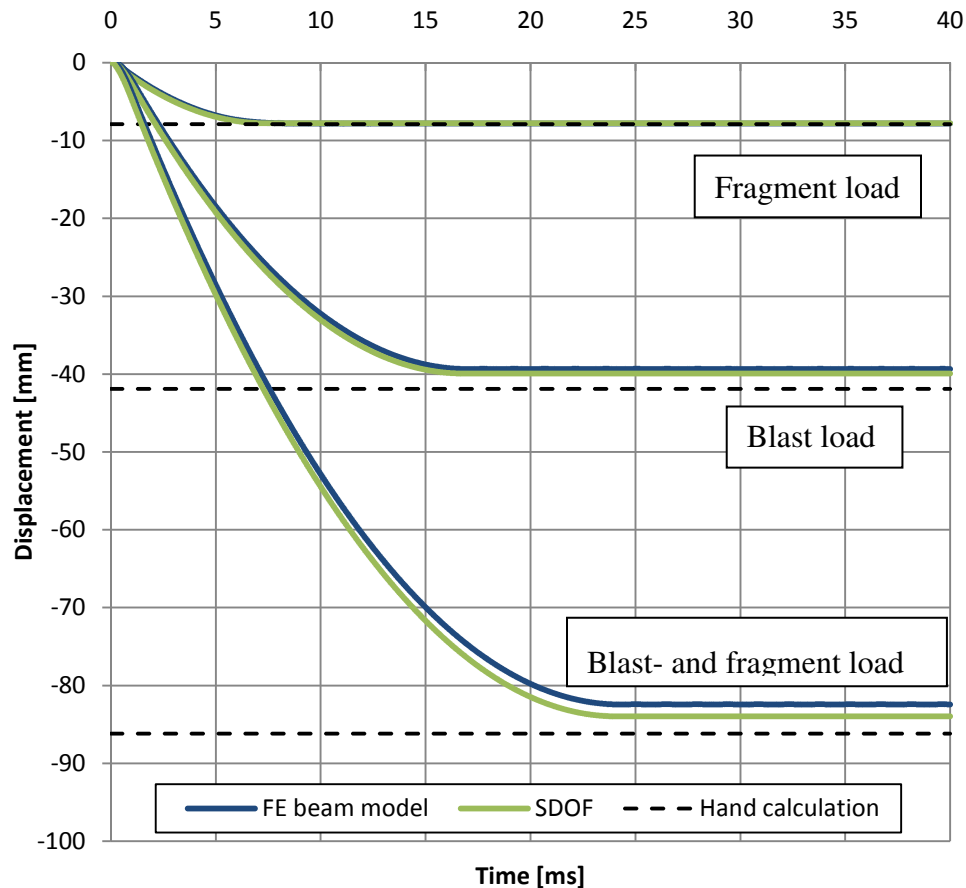


Figure 5.11 Midpoint displacements with ADINA-,SDOF- and hand calculation results for the fragment load, the blast load and the blast and fragment load applied together (c).

In section 5.2.1, it was concluded that for linear elastic material properties it is possible to super position the contribution from various loads independently of the load type. This is not possible when analyzing a structure with plastic material properties, as equation (5.3) describes.

$$u_{pl} = \frac{(I_1 + I_2)^2}{C_{pl}} \neq \frac{I_1^2}{C_{pl}} + \frac{I_2^2}{C_{pl}} \quad (5.3)$$

where

$$C_{pl} = \kappa_{KF} \cdot \kappa_{MF} \cdot 2 \cdot R_{pl} \cdot M \quad (5.4)$$

If the plastic displacements from different impulse loads are first taken to the power of two and divided by  $C_{pl}$  and then added, the term  $\frac{2I_1I_2}{C_{pl}}$  is not taken into account, which results in a much smaller displacement.

This can also be verified with Figure 5.11, where the blast- and fragment loads are applied separately and they do not, if summarized, correspond to the curve which both loads are applied at the same time.

During the analysis, problems occurred when trying to imitate an ideally plastic material behaviour, by increasing the Young's modulus by a factor hundred for both the elastic- and bilinear plastic elements. The result is presented in Figure 5.12 and as can be seen, the result differs much if compared to the curve which represents an increased Young's modulus and constraints for the elastic nodes. The difference is not expected and cannot be explained.

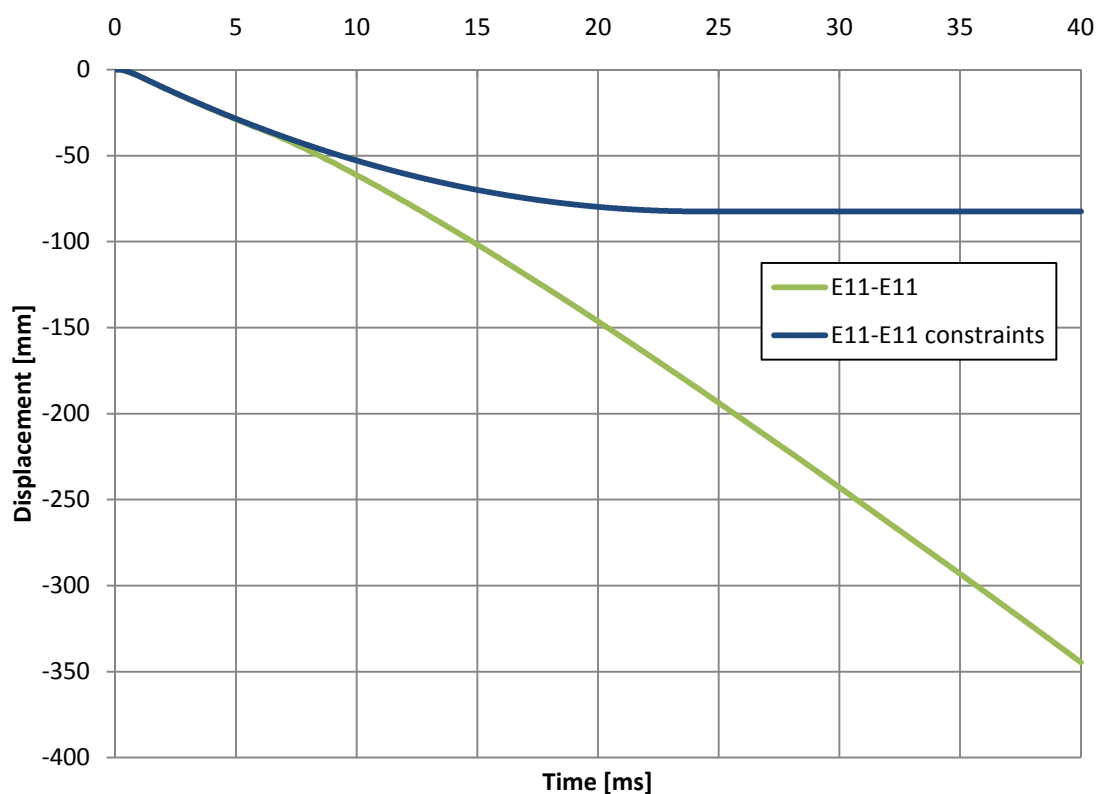


Figure 5.12 Midpoint displacements when the elastic- and bilinear elasto-plastic element's Young's modulus is increased with a factor hundred.

## 5.4 Bilinear elasto-plastic analysis

As a first step in the bilinear elasto-plastic analysis, the FE-results are compared to the results obtained in SDOF and by hand calculation in order to verify them. This is done for the blast- and fragment load separately and also when the two loads are applied together at the same time. The verification is presented in Figure 5.13, Figure 5.14 and Figure 5.15 and as the figures shows, the difference between the results obtained by the FE analyses differs to the ones obtained in SDOF analysis and hand

calculation. Worth mentioning, the SDOF and hand calculation result are agreeing well.

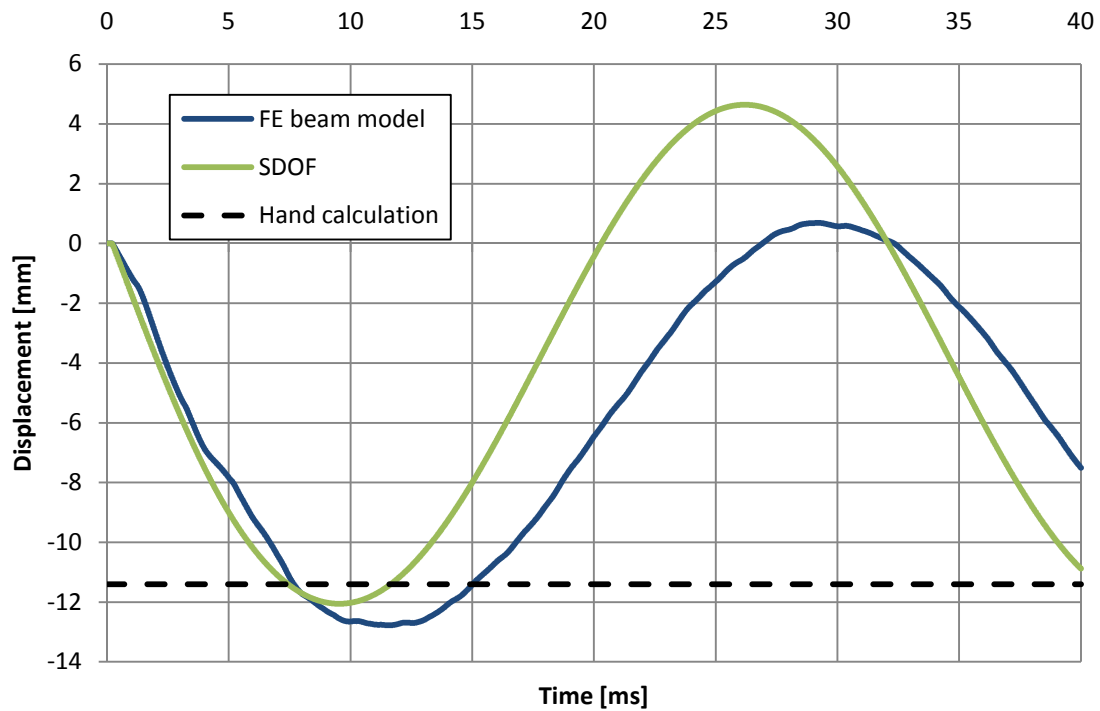


Figure 5.13 Comparison in midpoint displacement for the fragment load applied as uniformly distributed and analysed with ADINA, SDOF and hand calculation.

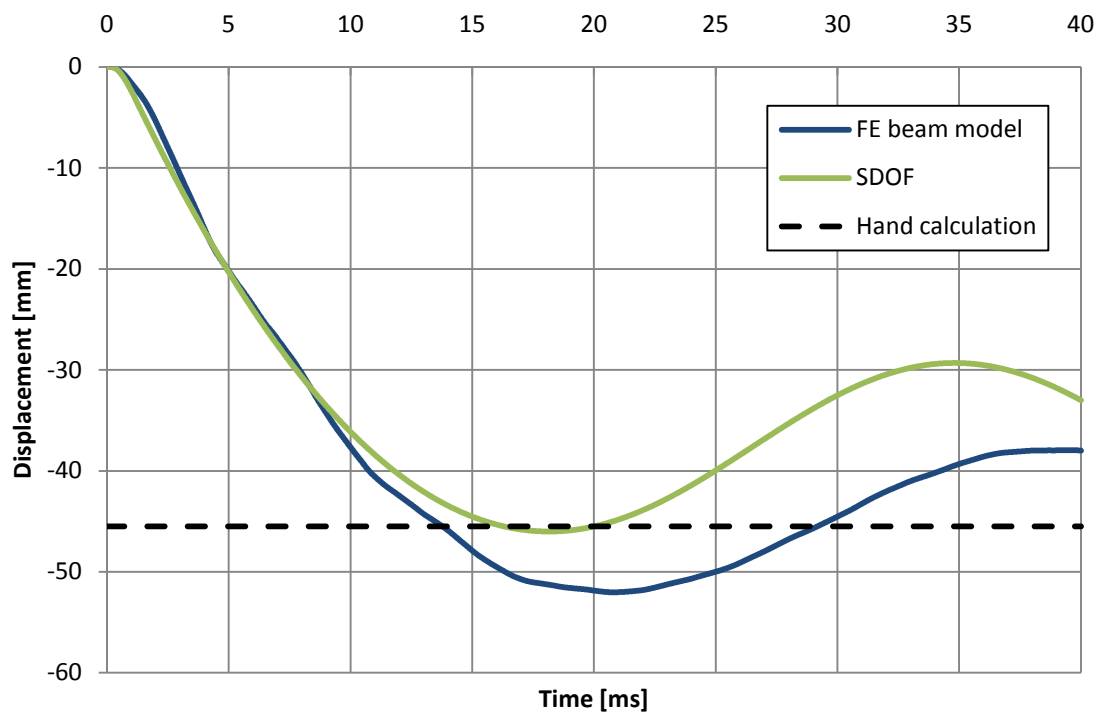


Figure 5.14 Comparison in midpoint displacement for the blast load analysed with ADINA, SDOF and hand calculation.

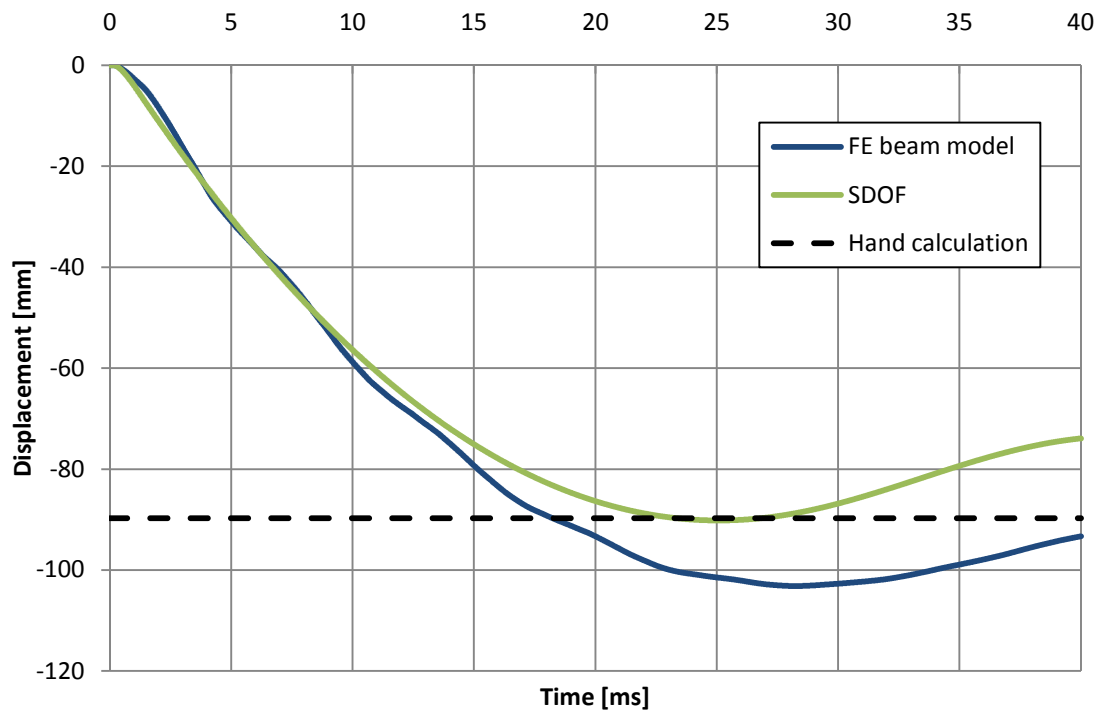


Figure 5.15 Comparison in midpoint displacement for the blast- and fragment load analysed with ADINA, SDOF and hand calculation.

The moment obtained in midsection of the beam is presented in Figure 5.16 and it is compared to the expected moment curve based on the displacements acquired in SDOF analysis. As can be seen, there are dips in the moment curve for the FE analysis, which means that the beam does not consume as much energy as the SDOF moment curve. This will influence the displacement, since the FE analysis needs larger displacement to reach the same amount of internal energy as the SDOF system, to level out the external energy. This can be one of the reasons for the substantial difference in displacement between the two analysis methods.

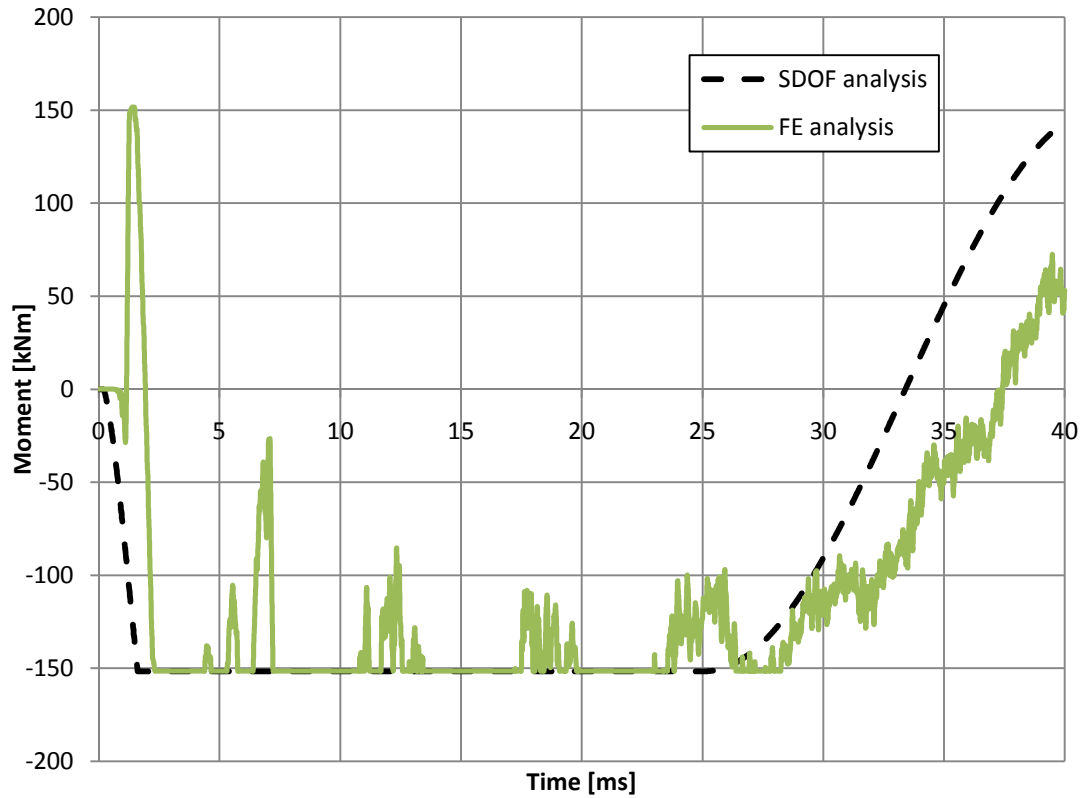


Figure 5.16 Midsection moment as a function of time obtained by the FE analysis compared to the intended moment obtained in the SDOF analysis.

As Figure 5.16 shows, yielding occurs with tensioned upper side in an early state of the analysis. The corresponding deformation shape when this happens is illustrated in Figure 5.17.

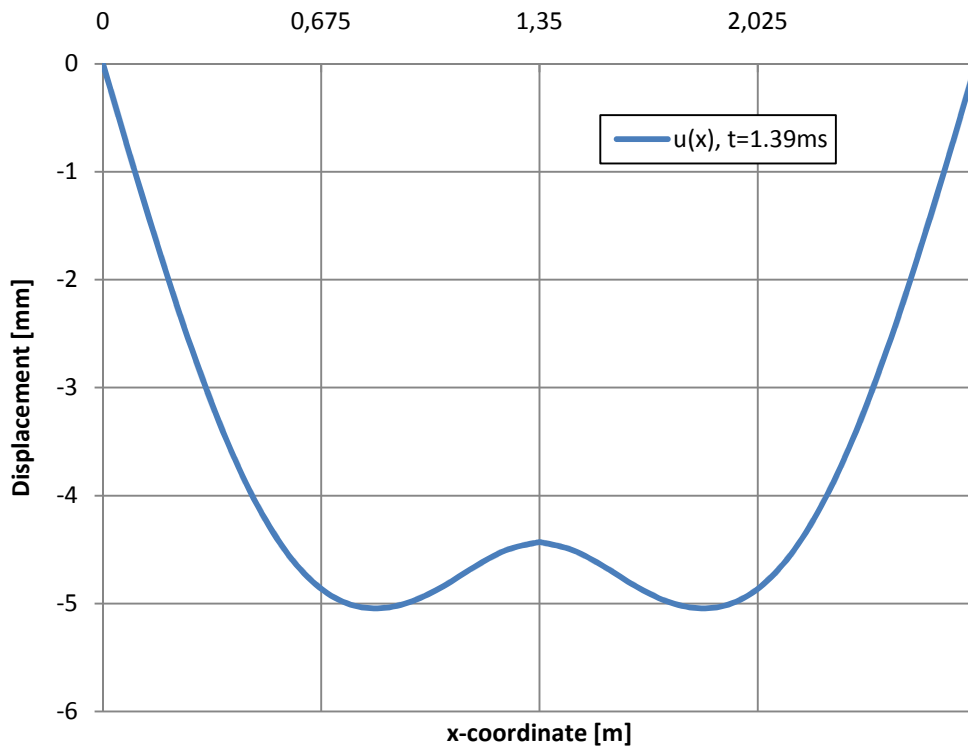


Figure 5.17 Yielding in the beam with tensioned upper side at time  $t = 1.39 \text{ ms}$ .

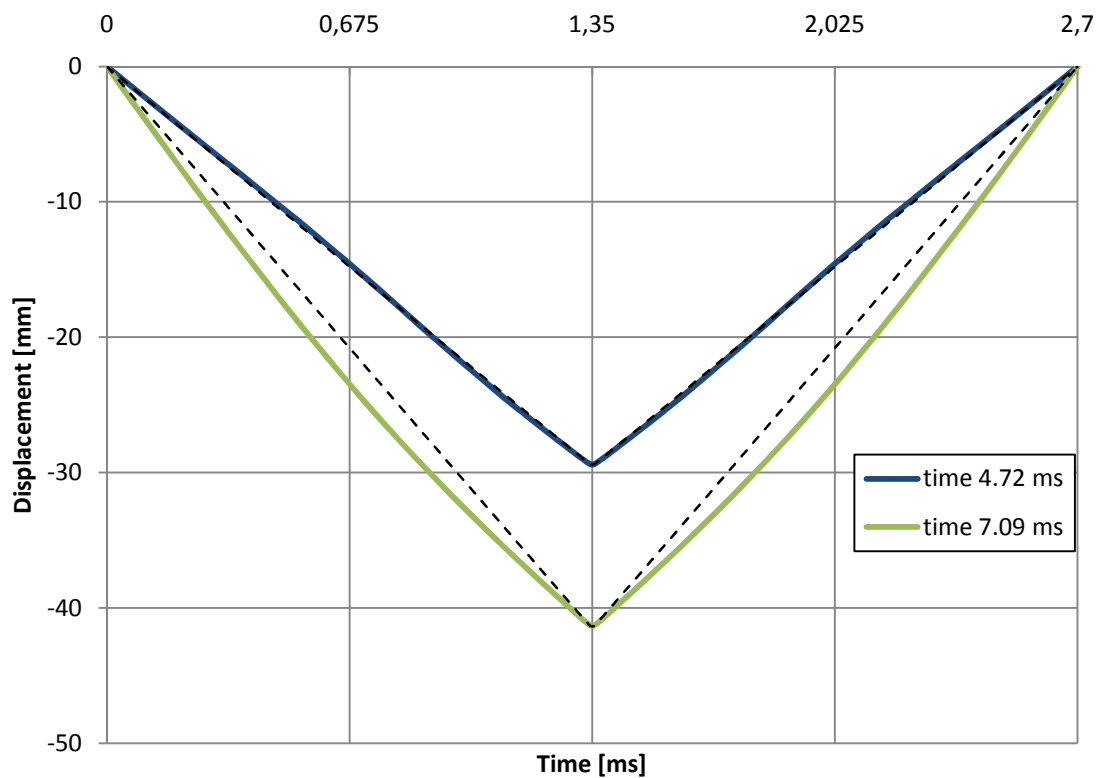


Figure 5.18 Deformation shapes at time  $t = 4.72 \text{ ms}$  and  $7.09 \text{ ms}$  where the dashed lines represents the elastic elements as completely straight.

Moment as a function of time for the sections  $x = 0.25L$  and  $x = 0.5L$  is presented in Figure 5.19 when both the blast- and fragment load are applied as uniformly distributed. The yield moment for the plastic element situated in the midsection is 151.6 kNm and as can be seen, the moment in the section  $x = 0.25L$  is by far exceeding this value in a few time intervals. This means, that the model is not behaving the way it is intended to do and this can also explain the difference between the FE beam model result and the SDOF-result and hand calculation result which is presented in Figure 5.15.

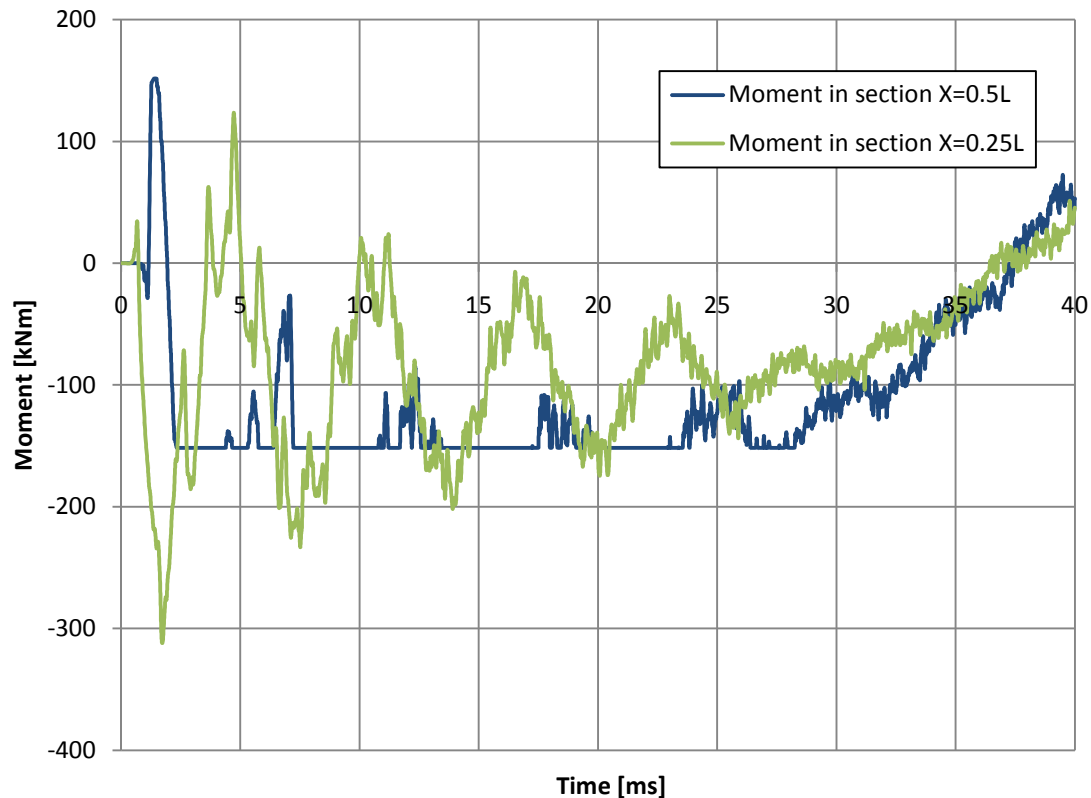


Figure 5.19 Moment when the blast- and fragment load are applied as uniformly distributed in sections  $X=0.25L$  and  $X=0.5L$ .

With the bilinear elasto-plastic analysis, it is as in the plastic analysis, not possible to super position loads. In case of an elasto-plastic material response, contribution from both the elastic- and plastic parts of the material response needs to be included to get the corresponding displacement. Equation (5.5) is used to calculate the displacement for the bilinear elasto-plastic response.

$$u_{el.pl} = u_{pl} + \frac{u_{el}^2}{4 \cdot u_{pl}} \quad (5.5)$$

where  $u_{pl}$  is calculated with equation (5.3) and  $u_{el}$  is calculated with equation (5.1).

The results from this analysis can be seen in Figure 5.22 with the blast- and fragment load applied separately and one curve represents the two loads applied together.

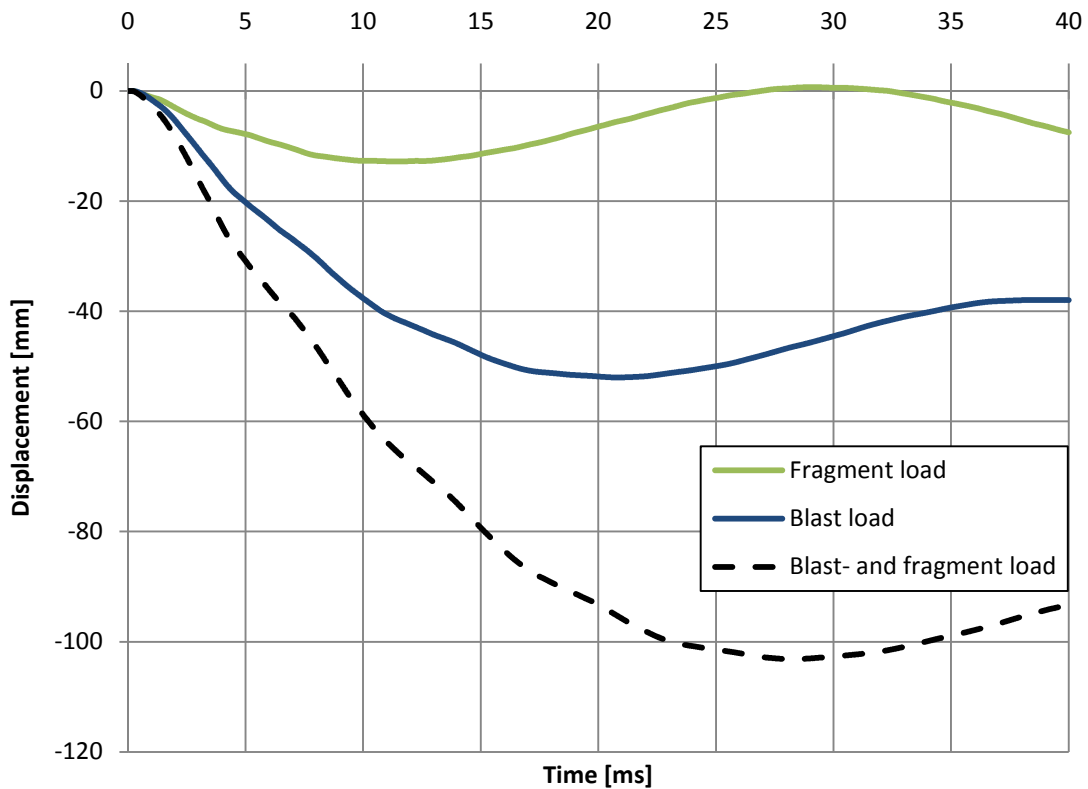


Figure 5.20 Midpoint displacements for the blast- and fragment loads separately and both the loads applied at the same time as uniformly distributed.

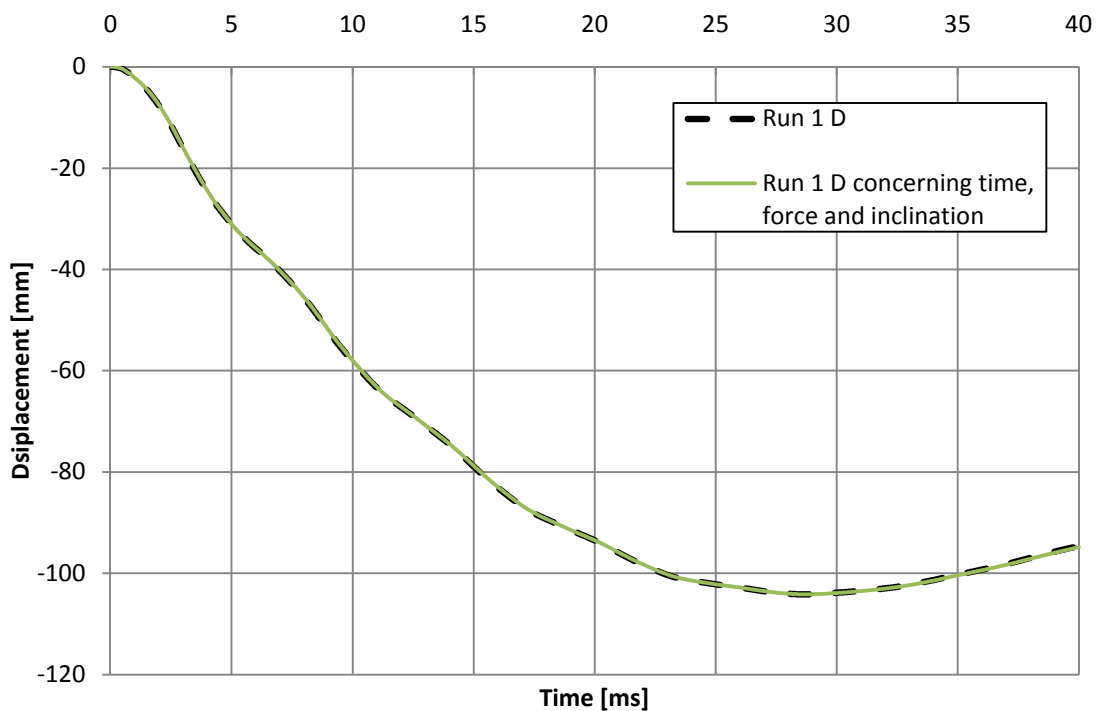


Figure 5.21 Midpoint displacements for run 1 D when the fragments are applied normally and when the true time, force and inclination of the fragments are considered.

When the fragment load is applied, concerning true time, true force and an inclination, the result is more or less the same as when the load is applied normally, this is presented in Figure 5.21. Hence, these factors will be neglected in further analysis.

The elasto-plastic displacements for run 1 are presented in Figure 5.22, where the broken line represents the fragment load applied as a uniformly distributed load. It should be noticed that run 1 A simulates a worst case scenario, where the largest point loads are placed in the middle, with decreasing size towards the supports, i.e. a triangle load, see section 3.6.3.

The difference in displacement between the various runs differs approximately 10 % with run 1 A not considered. Consequently, to apply the load applied as uniformly distributed seems to be a good estimation for the fragment point loads.

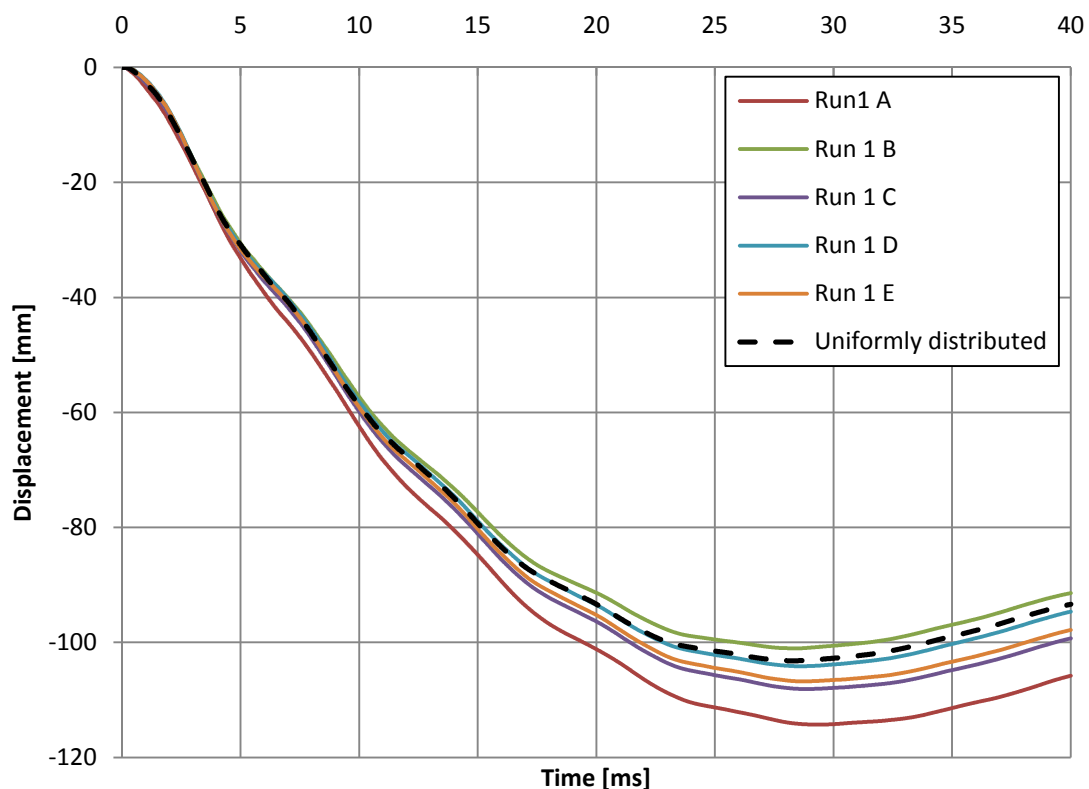


Figure 5.22 Midpoint displacements for run 1 with bilinear elasto plastic material properties.

In Figure 5.23 the displacements for run 5 are presented. If these results are compared to the ones obtained in run 1, the difference in displacement magnitude in between the runs is much smaller. The various runs seem to agreeing even better with the uniformly distributed line.

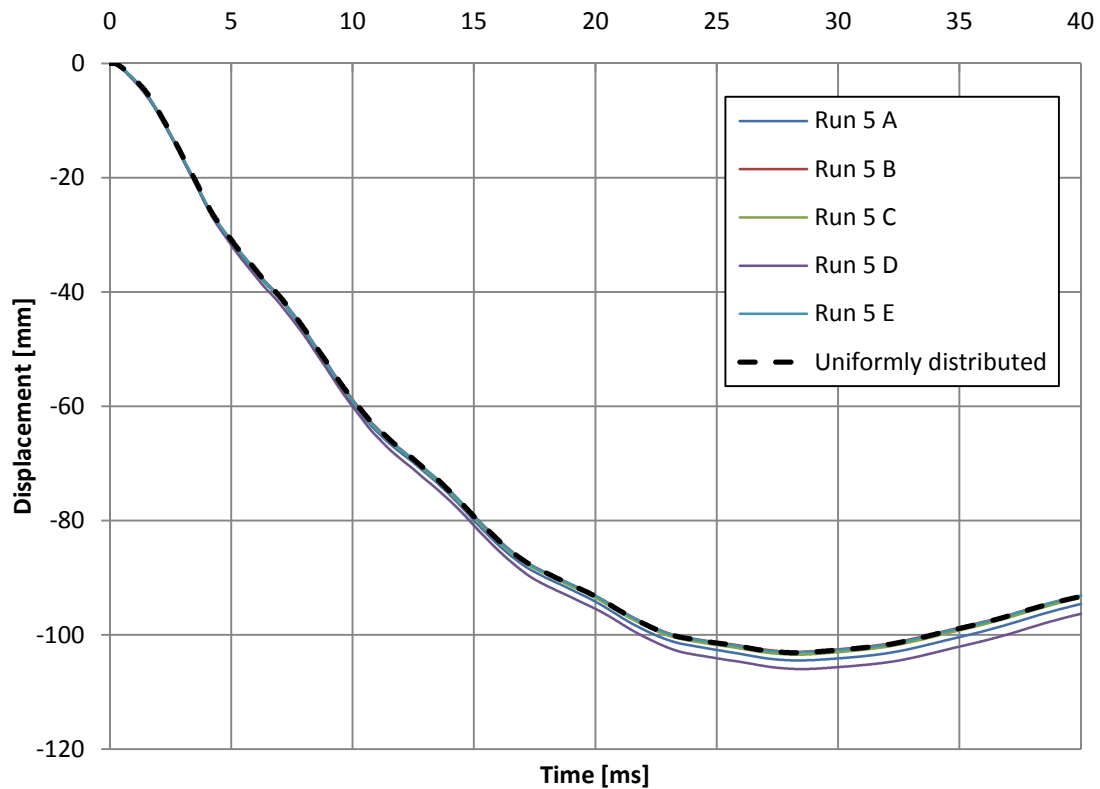


Figure 5.23 Midpoint displacements for run 5 with bilinear elasto plastic material properties.

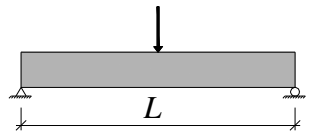
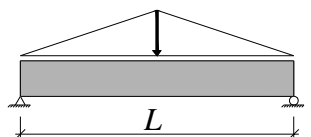
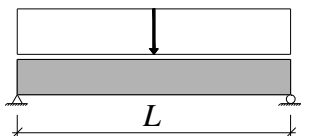
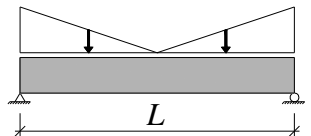
### 5.4.1 Conclusion

The FE-results in the elasto-plastic analysis did not agree well with the results obtained by SDOF and simplified hand calculation. Two possible reasons for the substantial difference were discussed previously in this section. Though, the results when applying the fragmental load as a uniformly distributed load still seems to be a good approximation.

## 5.5 SDOF results

Values for elastic and plastic transformation factors for the four different load cases presented in section 2.8.3.5 and the load cases can once again be seen in Table 5.1. The corresponding deflection curves when the beam is exposed to only the fragment load with the appearance according to the four different cases is present in and for elastic and plastic material response respectively.

Table 5.1 The cases which are analysed in SDOF.

Case 1		Case 3	
Case 2		Case 4	

Displacements for all the cases with the corresponding transformation factors are presented in Figure 5.24 and Figure 5.25 with linear elastic and ideally plastic material responses respectively.

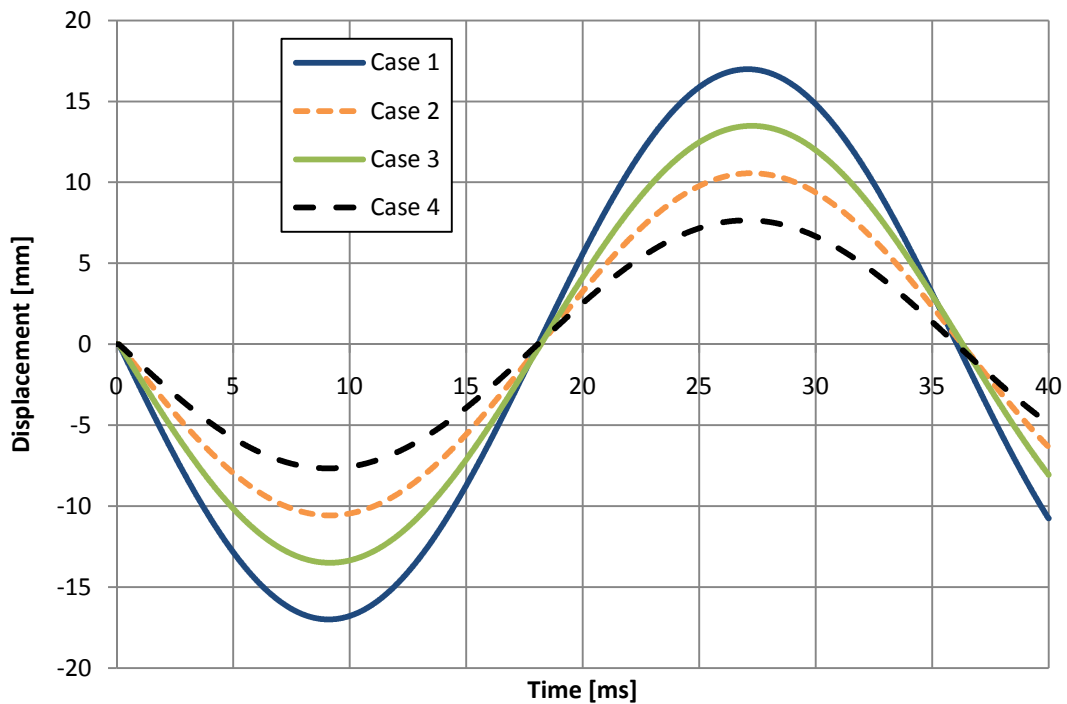


Figure 5.24 Elastic response for beam exposed to fragment load with appearance corresponding to four different load cases.

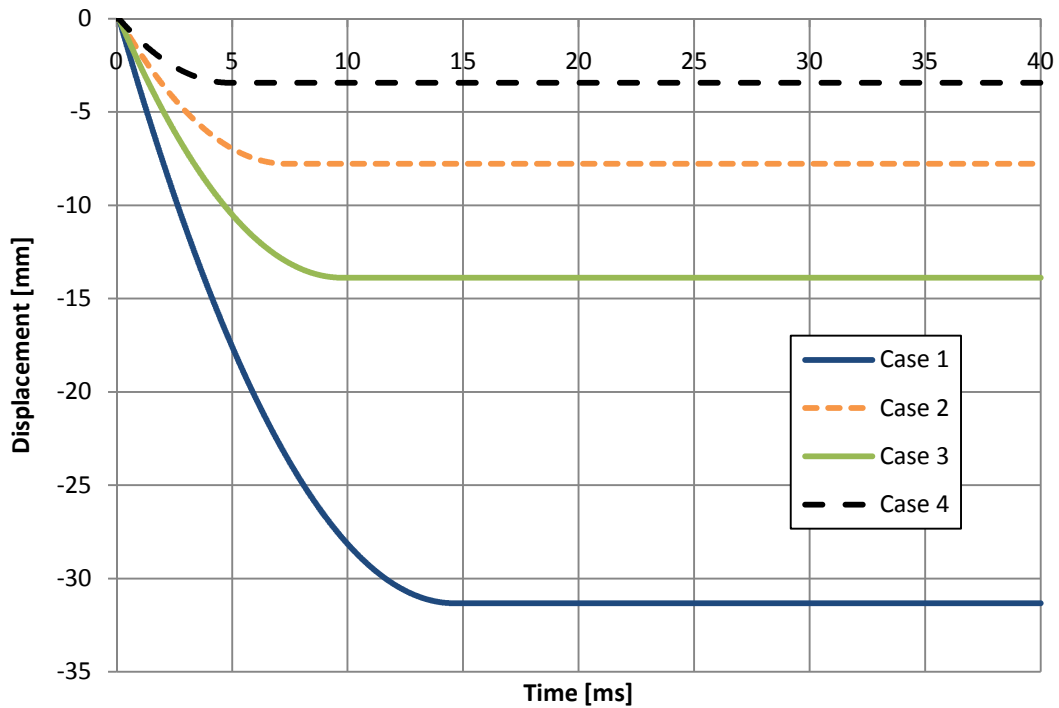


Figure 5.25 Plastic response for beam exposed to fragment load with appearance corresponding to four different load cases.

## 5.6 2-D solid model

### 5.6.1 Comparison with beam element

In order to verify the results obtained by the 2-D solid model, it is compared to the results obtained by the beam element model. This is presented in Figure 5.26 and as can be seen, the displacements from the two models differ somewhat.

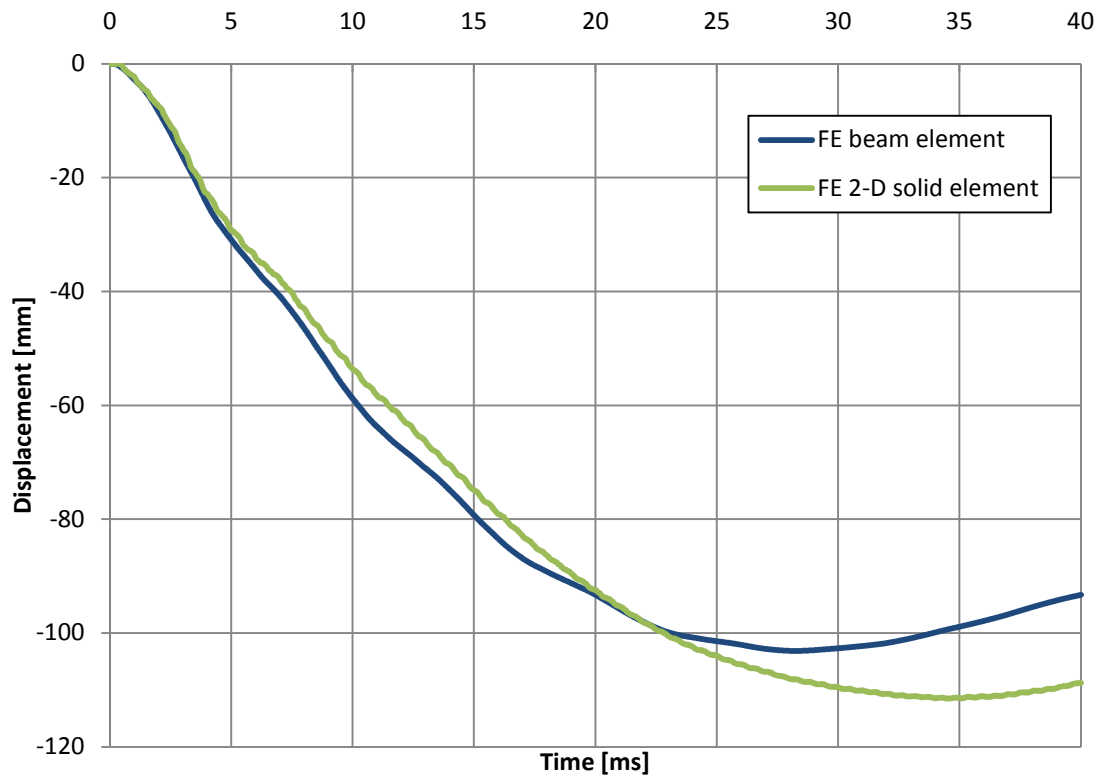


Figure 5.26 Midpoint displacement comparison for the beam- and 2-D solid element model.

Since removal of concrete is to be modelled due to the fragmental impact, it is required to use an explicit solver, because equilibrium conditions do not need to be fulfilled when this solver is used. Hence, a control is performed that the two solver methods, i.e. implicit and explicit integration schemes, give comparable results. As Figure 5.27 shows, the two solver methods do agree very well.

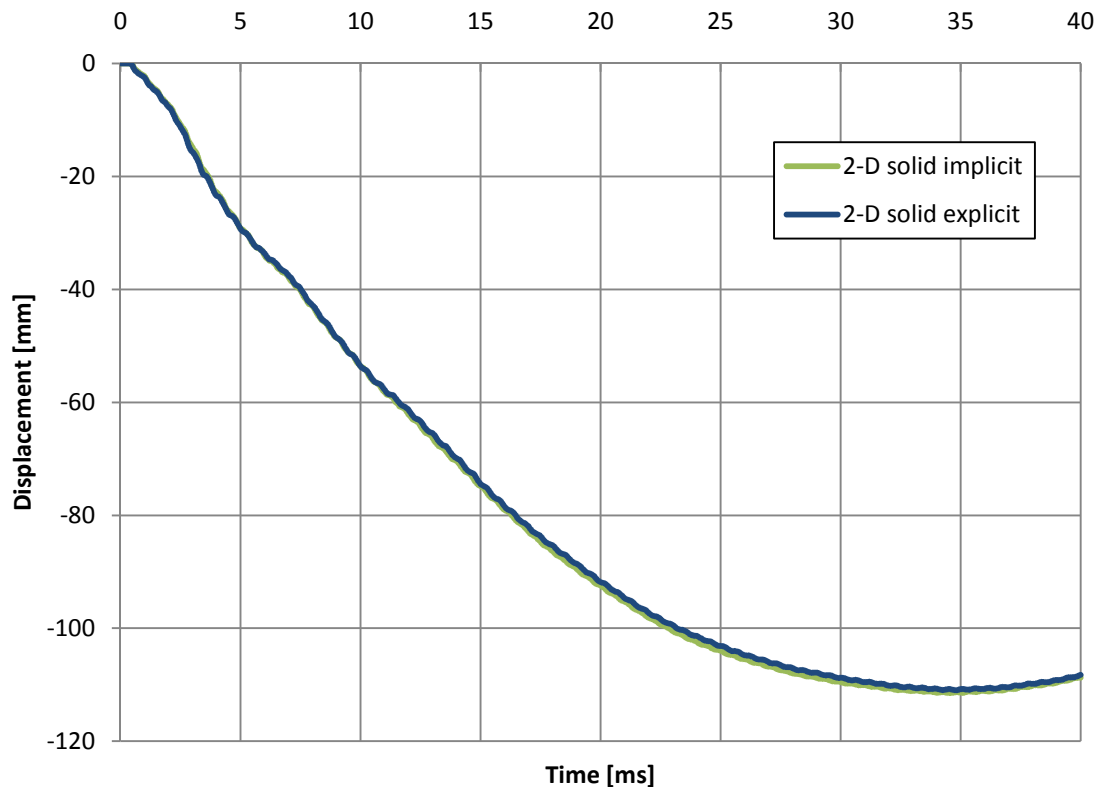


Figure 5.27 Comparison in midpoint displacement for implicit and explicit solver when using 2-D solid elements.

### 5.6.2 Results when removing concrete due to the fragmental impact

The FE-simulation of the removal of concrete due to the fragmental impact is illustrated in Figure 5.28. As can be seen, the loss of mass in the top layer seems to be positive for the beam, since the displacement decreases with increasing removed mass. A corresponding analysis has been performed in the SDOF-program. The result is illustrated in Figure 5.29, and it seems that the loss of mass has the opposite effect on the beam compared to the results obtained by the 2-D solid model.

Hand calculations have also been performed in order to understand the behaviour when beam loses stiffness and mass. The result from this analysis agrees with the results obtained by the SDOF program, i.e. the difference in displacement when removing different parts of the top layer should be small and tend to increase when the removed mass increases. For a detailed derivation of these calculations, see Appendix I.

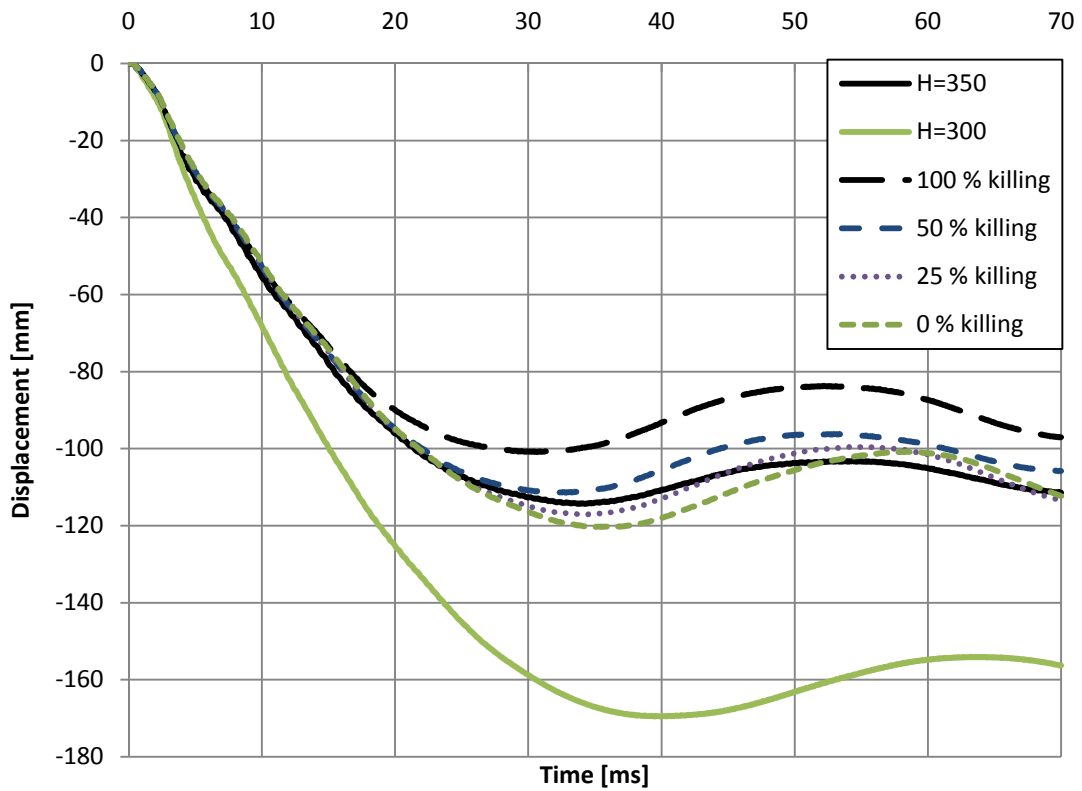


Figure 5.28 2-D solid displacements for the different analyse methods when removing material due to the fragmental impact.

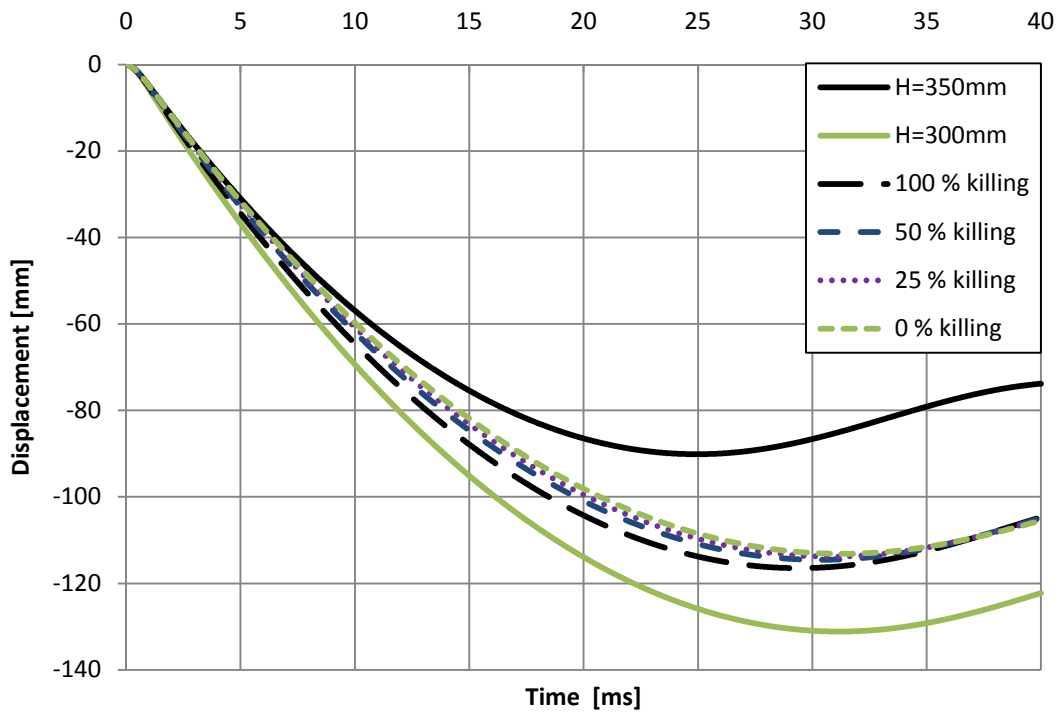


Figure 5.29 SDOF displacements for the different analyse methods when removing material due to the fragmental impact.

## 6 Conclusions

In all the analyses with different material responses it seems to be a good estimation to apply the fragmental load as a uniformly distributed load. For each further division of the fragment groups, the displacements in between the cases seems to differ less and is getting closer to the uniformly distributed displacement.

The force inclination and the true distance between the detonation and the wall have also been investigated, and the difference was very small compared to applying the fragments as a vertical load with a distance of 5 m between the bomb and the wall. Hence, the fragment load is well approximated assuming a uniformly distributed load with a constant distance between the wall and the bomb, i.e.  $R = 5$  m.

In the elasto-plastic analysis, the beam does not behave as it is intended to do. The elastic part of the beam is exposed to moments more than the doubled yield moment in the elasto-plastic element in the mid section. Using elasto-plastic elements over the entire length of the beam would probably result in a more realistic behaviour of the beam.

The simplified FE-methods for simulating the fragmental impact used in this thesis do not correspond to the expected behaviour which is generated by the SDOF and hand calculation. The analysis indicates that something is missing when using SDOF. The differences is probably due to that  $\kappa_{MP}$  in SDOF does not correspond to the real response. Hence, this simple way to model such a complex problem needs to be further investigated and in this thesis it is mainly presented as a way to simulate the fragmental impact.

Removing concrete in the FE analysis resulted in less displacement than if the concrete was not removed. However, SDOF and hand calculations resulted in the opposite effect, i.e. removal of concrete increases the displacements. This phenomenon cannot be explained in this thesis and further research is suggested.

## 7 References

- ADINA (2008): *Theory and Modelling Guide*, Vol 1: ADINA Solids & Structures Report ARD 08-7, ADINA R & D, Inc., Watertown, USA, 2008.
- Al-Emrani, M. Engstöm, B. Johansson, M. Johansson. P. (2006): *Bärande konstruktioner*. Chalmers University of Technology, Division of Structural Engineering, Göteborg, Sweden, 2006.
- Craig, R. Kurdila, A. (2006): *Fundamentals of Structural Dynamics*. John Wiley & Sons, Inc, New Jersey, USA.
- Engström. B. (2008): *Design and analysis of continuous beams and columns*. Chalmers University of Technology, Division of Structural Engineering, Göteborg, Sweden, 2008.
- Johansson. M. Laine. L. (2009): *Bebyggelsens motståndsförmåga mot extrem dynamisk belastning, Delrapport 3: Kapacitet hos byggnader*. MSB 2009. Avdelningen för utbildning, övning och beredskap. Karlstad. Sweden 2009.
- Lundh, H. (2000): *Hållfasthetslära*. Studentlitteratur, KTH, Stockholm. Sweden
- Nyström, U. (2008): *Concrete Structures Subjected to Blast and Fragment Impacts*. Thesis for the Degree of Licentiate of Engineering 2008:4. Division of Structural Engineering, Chalmers University of Technology, Göteborg, Sweden, 2008.
- Nyström, U. (2006): *Design with regard to explosions*. Master Thesis 2006:14. Division of Structural Engineering, Chalmers University of Technology, Göteborg, Sweden, 2006.
- Räddningsverket (2006) *Skyddsrumregler SR*, SR 06. Räddningsverket, Karlstad, Sweden.

## Appendix A      Input data in analysis

Table A.1 Material properties for concrete quality C25/30

C25/30	
Compressive strength, $f_{ck}$	25 MPa
Tensile strength, $f_{ctm}$	2.6 MPa
Ultimate strain, $\epsilon_{cu}$	0.0035
Modulus of elasticity, $E_{cm}$	31 GPa

Table A.2 Material properties for reinforcement quality B500B

B500B	
Yielding stress, $f_{yk}$	500 MPa
Yielding strain, $\epsilon_{yk}$	0.0025
Modulus of elasticity, $E_s$	200 GPa

Table A.3 Geometrical properties of the beam

Length of beam, $L$	2.7 m
Height of beam, $h$	0.35m
Width of strip, $w$	1 m
Area of reinforcement in compression, $A_s'$	1005 mm <sup>2</sup> /m
Distance from compressed edge to reinforcement in compression, $d'$	0.05 m
Area of reinforcement in tension, $A_s$	1005 mm <sup>2</sup> /m
Distance from compressed edge to reinforcement in tension, $d$	0.3 m

## Appendix B.1 Calculation of cracking moment

The cracking moment for the concrete section in figure B.1 will be calculated according to the equations presented in the thesis.

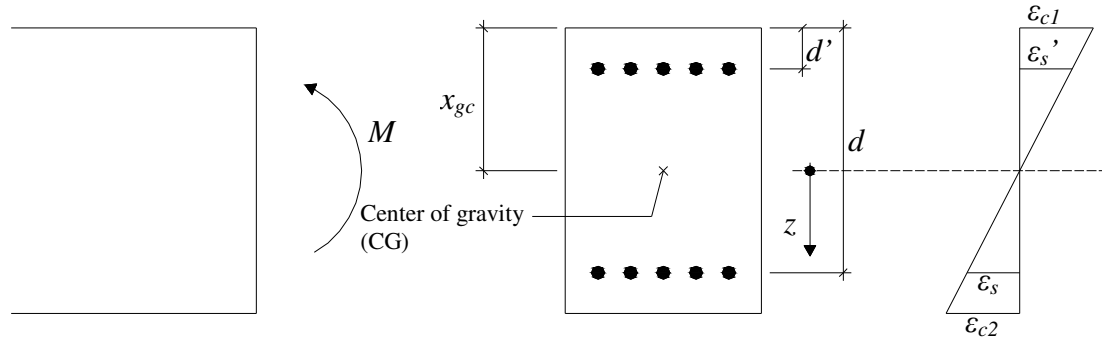


Figure B.1 Double symmetric cross section in state I with strain distribution, subjected to pure bending.

The location of the centre of gravity for a double symmetric, uncracked section is:

$$x_{cg} = \frac{h}{2} = \frac{0.35}{2} = 0.175 \text{ m} \quad (\text{B-1})$$

The moment of inertia is calculated without consider the reinforcement as:

$$I_I = \frac{BH^3}{12} = \frac{1 \cdot 0.35^3}{12} = 3.57 \cdot 10^{-3} \text{ m}^4 \quad (\text{B-2})$$

The cracking stress in concrete is equal to:

$$\sigma_{ct,max} = f_{ctm} = 2.6 \text{ MPa} \quad (\text{B-3})$$

The cracking moment can now be calculated as:

$$M_{cr} = \frac{f_{ctm} \cdot I_I}{x_{cg}} = \frac{2.6 \cdot 10^6 \cdot 3.57 \cdot 10^{-3}}{0.175} = 53.1 \text{ kNm} \quad (\text{B-4})$$

## Appendix B.2 Calculation of yielding moment

The moment for when the tension reinforcement yields in the cracked section seen in figure B.2 will here be calculated.

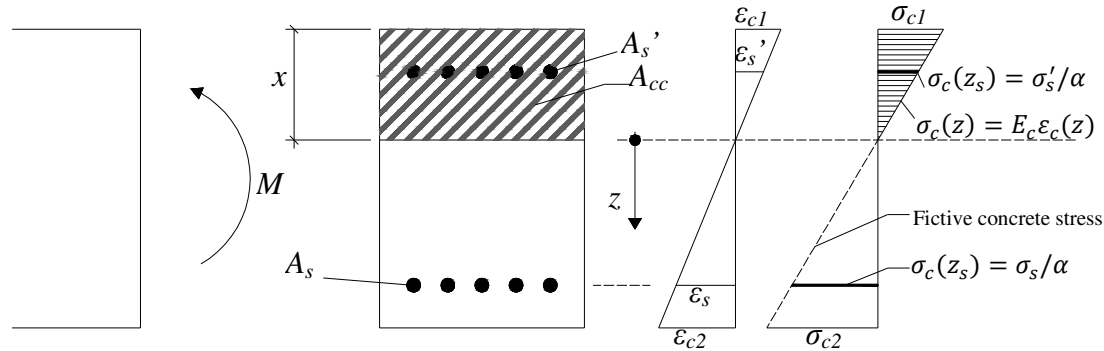


Figure B.2 Double symmetric cross section in state II with strain distribution, subjected to pure bending.

The expression for the location of the neutral layer for a cracked section was derived in section (xx) and can be calculated as:

$$b \cdot \frac{x^2}{2} + (\alpha - 1)A'_s(x - d') - \alpha \cdot A_s(x - d) = 0 \quad (\text{B-5})$$

$$\rightarrow x = 0.056 \text{ m}$$

where  $\alpha$  is the ration between the modulus of elasticity of steel and concrete:

$$\alpha = \frac{E_s}{E_{cm}} = \frac{200}{31} = 6.45 \quad (\text{B-6})$$

The moment of inertia for a concrete section in state II is calculated as:

$$\begin{aligned} I_{II} &= \frac{bx^3}{3} + (\alpha - 1)A'_s(x - d')^2 + \alpha A_s(d - x)^2 = \\ &= \frac{0.056^3}{3} + (6.45 - 1) \cdot 1005 \cdot 10^{-6} \cdot (0.056 - 0.05)^2 + 6.45 \cdot 1005 \\ &\quad \cdot 10^{-6} \cdot (0.3 - 0.056)^2 = 4.45 \cdot 10^{-4} \text{ m}^4 \end{aligned} \quad (\text{B-7})$$

The tensioned reinforcement is located at a distance  $z_s$  from the neutral layer:

$$z_s = d - x = 0.3 - 0.056 = 0.244 \text{ m} \quad (\text{B-8})$$

The moment for when the reinforcement yields can now be calculated as:

$$M_{spl} = \frac{f_{yk} I_{II}}{\alpha z_s} = \frac{500 \cdot 10^6 \cdot 4.45 \cdot 10^{-4}}{6.45 \cdot 0.244} = 141.146 \text{ kNm} \quad (\text{B-9})$$



$$\begin{aligned} &= 0.81 \cdot 25 \cdot 10^6 \cdot 0.037 \cdot (0.3 - 0.416 \cdot 0.037) - 0.001229 \\ &\quad \cdot 200 \cdot 10^9 \cdot 1005 \cdot 10^{-6} \cdot (0.3 - 0.05) \\ &= 151.6 \text{ kNm} \end{aligned}$$

## Appendix C Load-displacement relation

The internal force for when the ultimate moment (calculated in appendix B.3) is reached in the mid section can be calculated according to equation C-1.

$$R_{pl} = \frac{8 \cdot M_{pl}}{L} = \frac{8 \cdot 151.6}{2.7} = 449.2 \text{ kN} \quad (\text{C-1})$$

The stiffness can be calculated according to linear elastic theory, the modulus of elasticity and the moment of inertia in state II were calculated in Appendix B.

$$K_{II} = \frac{384E_{cm}I_{II}}{5L^3} = \frac{384 \cdot 31 \cdot 10^9 \cdot 4.45 \cdot 10^{-4}}{5 \cdot 2.7^3} = 53.8 \frac{\text{MN}}{\text{m}} \quad (\text{C-2})$$

The deflection in the mid section can now be expressed as function of the applied load and the stiffness as:

$$u_{pl} = \frac{P_{pl}}{K_{II}} = \frac{449.2 \cdot 10^3}{53.8 \cdot 10^6} = 0.00835\text{m} = 8.35\text{mm} \quad (\text{C-3})$$

## Appendix D Material and cross section constants

In this Appendix, a representative Young's modulus for state I and state II and the yield stress is calculated for both the wall strip with  $H = 350$  and  $H = 300$  mm.

$H = 350$  mm

The Young's modulus is calculated by reducing the Young's modulus for concrete with a factor  $\gamma$ , which is the quotient of the moment of inertias from state I and state II to get a representative value for the two states.

$$E_{c,II} = \frac{E_{cm}}{\gamma} \quad (D-1)$$

where  $\gamma$  is:

$$\gamma = \frac{I_I}{I_{II}} \quad (D-2)$$

$I_I$  and  $I_{II}$  are the moment of inertias for the state 1 and state 2 respectively and is calculated with expressions (D-2) and (D-7) respectively. This gives:

$$\gamma = 8.03 \quad (D-3)$$

And the corresponding Young's modulus for the two states becomes:

$$E_{c,II} = \frac{E_{cm}}{\gamma} = \frac{31 \text{ GPa}}{8.03} = 3.86 \text{ GPa} \quad (D-4)$$

The yield stress is calculated by the following expression:

$$f_y = \frac{M_u}{Z} \quad (D-5)$$

$M_u$  Ultimate moment capacity, calculated with expression (D-14)

$f_y$  Stress when the beam goes from linear elastic to ideally plastic response

$Z$  Flexural resistance

Since beam element in ADINA at maximum have seven integration points, the flexural resistance needs to be calculated with this kept in mind. The following expression is used:

$$Z = B \cdot \left( \frac{H^2}{4} - \frac{e^2}{12} \right) \quad (D-6)$$

With  $H = 0.35$  m,  $B = 1$  m and  $e = h/6$  the yield stress becomes:

$$f_y = \frac{M_u}{Z} = \frac{151.6 \text{ kNm}}{\frac{13}{54} \cdot bh^2} = 5.141 \text{ MPa} \quad (D-7)$$

It turned out that the beam element model in ADINA did not reach the intended internal resisting force, therefore the yield stress was further modified with 4.22 %:

$$f'_y = f_y \cdot 1.0422 = 5.358 \text{ MPa} \quad (\text{D-8})$$

The value above is used in the elasto-plastic analysis for the beam element model. For the 2-D solid element model, the same Young's modulus is being used as the one presented above in equation (D-4), but the yield stress is calculated by assuming a stress state corresponding to a fully plastic cross section. The yield stress for the 2-D solid model then becomes:

$$f_y = \frac{M_u}{Z} = \frac{151.6 \text{ kNm}}{\frac{bh^2}{4}} = 4.95 \text{ MPa} \quad (\text{D-9})$$

By using the same equations as presented above in this Appendix, but inserting H = 300 instead of 350, the following material and cross section parameters are obtained for the 2-D solid model:

$$E_{c,II} = 4.15 \text{ GPa} \quad (\text{D-10})$$

$$f_y = 5.36 \text{ MPa} \quad (\text{D-11})$$

## Appendix E Hand calculations for displacements

In this appendix, simplified hand calculations concerning displacement are presented in a more detailed way. The formulas used in this appendix are taken from Nyström, 2006 and for a more detailed derivation the reader is referred to Nyström, (2006).

In order to verify the results obtained by the FE model, hand calculations are performed for both the linear elastic analysis as well as the bilinear elasto-plastic material response. In table E.1, the data concerning the geometry, density and Young's modulus are presented.

Table E.1 Input data for the hand calculations concerning displacement.

Length (l)	2.7 m
Width (w)	1.0 m
Height (h)	0.35 m
Density ( $\rho$ )	2400 kg/m <sup>3</sup>
Young's modulus ( $E_{cm}$ )	31 GPa

The total mass, M is to be calculated as the volume of concrete times the density, see equation (E-1).

$$M = l \cdot w \cdot h \cdot \rho = 2268 \text{ kg} \quad (\text{E-1})$$

The loads generated by the reference bomb are in the hand calculations applied as impulse loads and the magnitude of these loads are presented in table E.2.

Table E.2 Impulse loads.

Blast load ( $I_{\text{Blast}}$ )	7546 Ns
Fragment load ( $I_{\text{Fragment}}$ )	3272 Ns

### Linear elastic analysis

In case of linear elastic material properties, the displacement for different load cases can be super positioned, which is not possible for the bilinear elasto-plastic material response. In table E.3, the transformations factors for mass, load and internal force are presented for the simply supported beam which is considered in this project.

Table E.3 Transformations factors for the linear elastic hand calculations.

$\kappa_P$	$\kappa_M$	$\kappa_K$	$\kappa_{MP}$	$\kappa_{KP}$
0.640	0.504	0.640	0.787	1.0

By following formula the displacement can be calculated:

$$u_{\text{elastic}} = \frac{I_{\text{Blast}} + I_{\text{Fragment}}}{\sqrt{\kappa_{MP}} \cdot \sqrt{M \cdot K_{II}}} \quad (\text{E-2})$$

where  $K_{II}$  is calculated by equation (E-3):

$$K_{II} = \frac{384 \cdot E_{cm} \cdot I_{II}}{5 \cdot l^3} = 53.814 \frac{\text{MN}}{\text{m}} \quad (\text{E-3})$$

$I_{II}$  is taken from Appendix B and is equal to:

$$I_{II} = 4.449 \cdot 10^{-4} \text{m}^4$$

This calculation gives a displacement of  $u_{\text{elastic}}=0.0349$  m and this value is compared to the results obtained by ADINA and SDOF in section 5.2.

### Ideally plastic analysis

In case of ideally plastic material properties, the transformations factors presented in table E.4 are being used.

Table E.4 Transformations factors for the ideally plastic hand calculations.

$\kappa_P$	$\kappa_M$	$\kappa_K$	$\kappa_{MP}$	$\kappa_{KP}$
0.5	1/3	0.5	2/3	1.0

The following equation is used to calculate the displacement:

$$u_{\text{plastic}} = \frac{(I_{\text{Blast}} + I_{\text{Fragment}})^2}{\kappa_{KP} \cdot \kappa_{MP} \cdot 2 \cdot R_m \cdot M} \quad (\text{E-4})$$

This gives a displacement of:

$$u_{\text{plastic}} = 0.0862 \text{ m} \quad (\text{E-5})$$

### Bilinear elasto-plastic analysis

When calculating the displacement with the bilinear elasto-plastic material response, the contribution from both the elastic and the plastic part is calculated and summarized. The transformation factors for the plastic material properties are presented in table E.4.

By use of the equation for displacement in case of ideally plastic material properties, the displacement for the plastic part is expressed as:

$$u_{\text{plastic}} = \frac{(I_Q + I_P)^2}{\kappa_{KP} \cdot \kappa_{MP} \cdot 2 \cdot R_m \cdot M} \quad (\text{E-6})$$

From the cross section analysis, the ultimate Moment capacity,  $M_{pl}$  is equal to:

$$M_{PL} = 151.6 \text{ kNm} \quad (\text{E-7})$$

The internal resisting force then becomes:

$$R_M = \frac{8 \cdot M_{PL}}{L} = 449.2 \text{ kN} \quad (\text{E-8})$$

This gives a plastic displacement equal to:

$$u_{\text{plastic}} = 0.0862 \text{ m} \quad (\text{E-9})$$

The total displacement taking both the elastic and plastic response under consideration is calculated by following expression:

$$u_{\text{elasto-plastic}} = u_{\text{plastic}} + \frac{u_{\text{elastic}}^2}{4 \cdot u_{\text{plastic}}} = 0.0897 \text{ m} \quad (\text{E-10})$$

## Appendix F Error in Adina when analyzing the dynamic problem with the explicit solver with beam elements

During the analysis, problems occurred in ADINA which resulted in values not comparable to the ones obtained by SDOF and hand calculations. To solve these problems many different things were tried and when using explicit solver instead of the implicit, it turned out that for beam elements with linear elastic material properties the explicit solution generates displacements around 14 % smaller compared to the ones obtained by the implicit solver. The curves for the two different solver methods and the displacement obtained by hand calculation can be seen in figure F.1. The maximum value obtained by the implicit method corresponds well to the hand calculated value. As the figure also shows, the period seems to be somewhat delayed for the explicit method compared to the implicit.

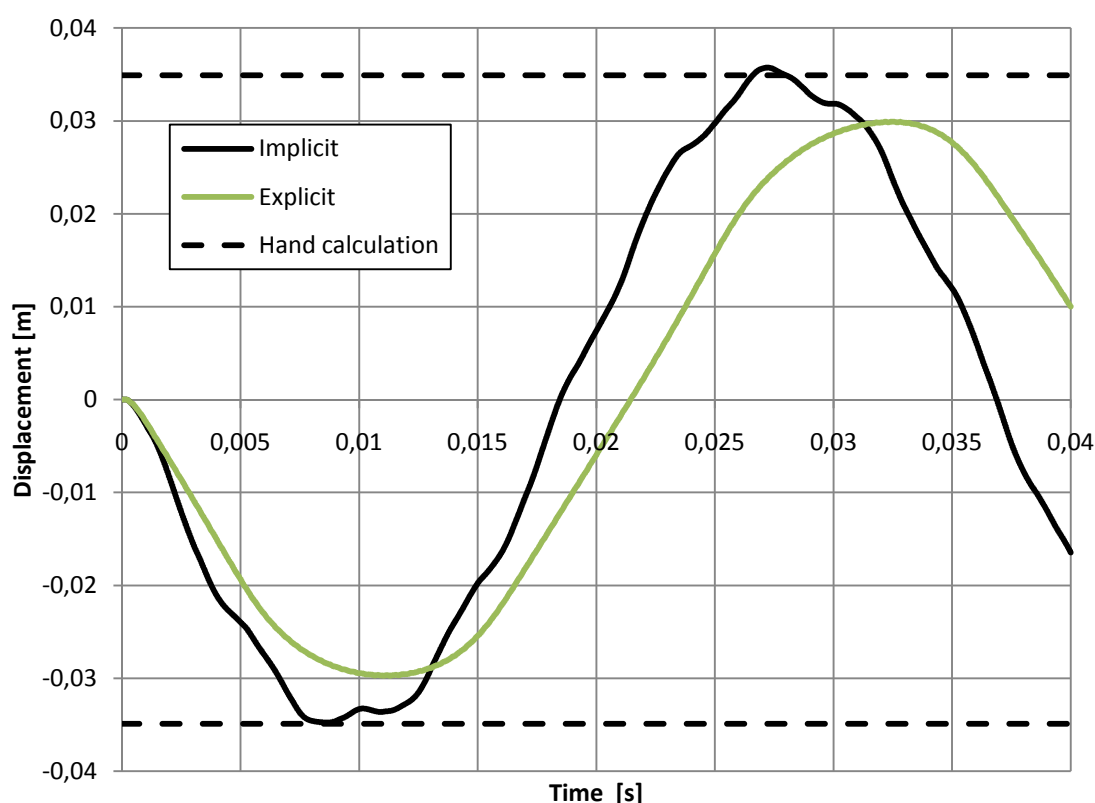


Figure F.1 Difference in displacements for implicit- and explicit solver with linear elastic material properties.

In theory, it is possible with a small difference between the two solver methods, but not as large as the results turned out to be in this project.

The results differ also for plastic- and for elastic material response as can be seen in figure F.2 and figure F.3.

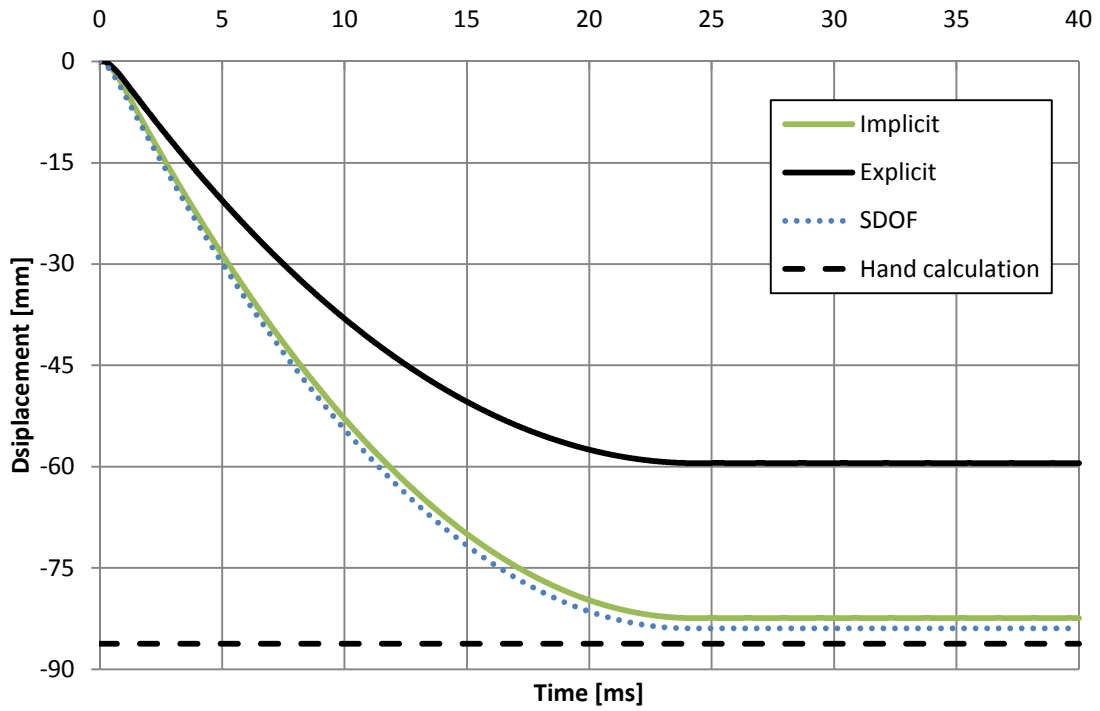


Figure F.2 Difference in displacements for implicit- and explicit solver with plastic material properties.

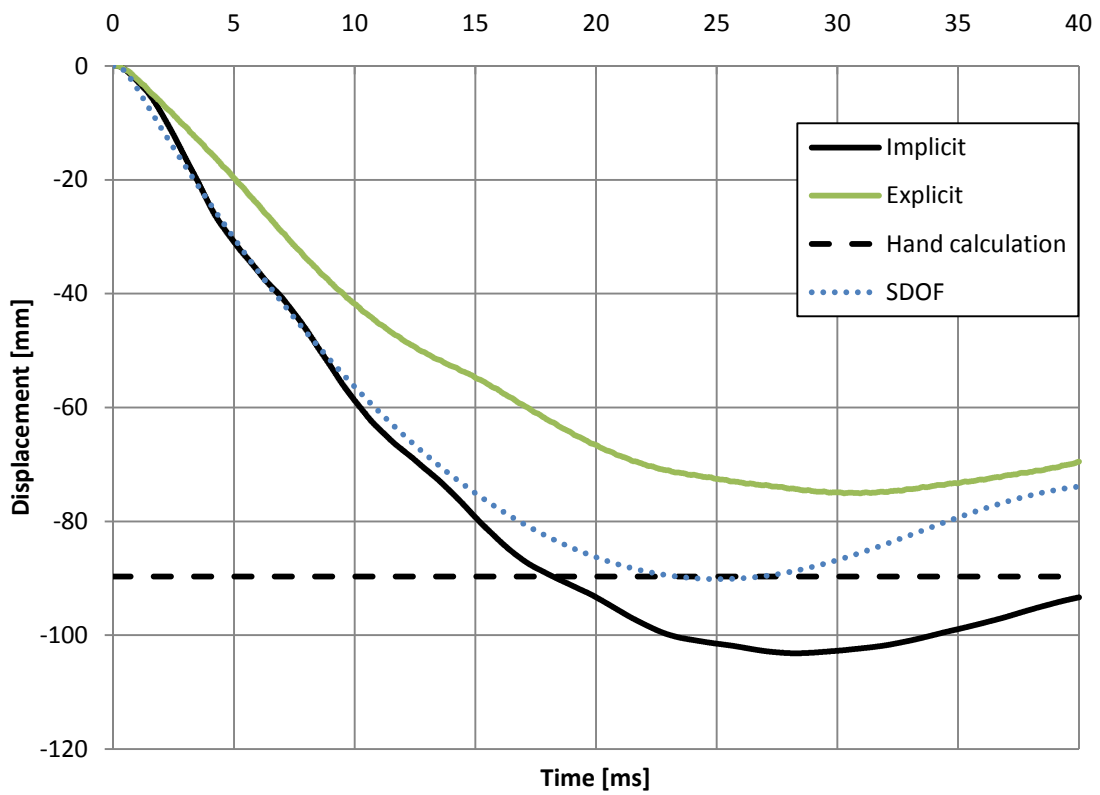
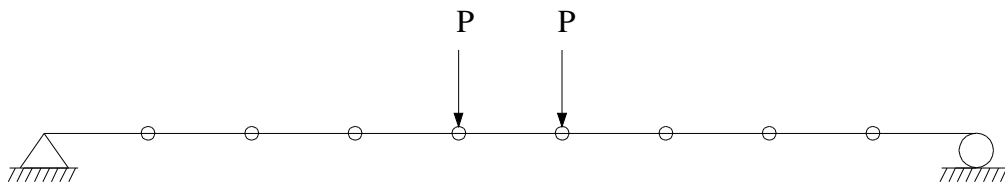


Figure F.3 Difference in displacements for implicit- and explicit solver with bilinear elasto-plastic material properties.

## Appendix G      **Different results obtained in ADINA when using different number of elements**

When the wall strip was analysed in ADINA, a controlled deformation was performed for the model with two controlled point loads acting on the plastic elements, see Figure G.1. This was done in order to control that the material properties correspond to the input data and was only analysed for the model with two linear elastic parts and one bilinear elasto-plastic in the middle.



*Figure G.1      Controlled deformation for the bilinear elasto-plastic model with two point loads acting on the elasto-plastic nodes.*

When controlling the behaviour for different number of elements, following numbers were used: 3, 5, 9, 27, 45, 75, 135, 225 and 375. The internal resisting forces for the corresponding number of elements are presented in Figure G.2. The resisting force obtained by the analytical solution is also shown in Figure G.2, and as can be seen, it differs approximately 4 % from the value that the curve tends to reach. This error in ADINA can not be explained and to be able to get accurate results the calculated yield stress is increased with a factor 0.0422.

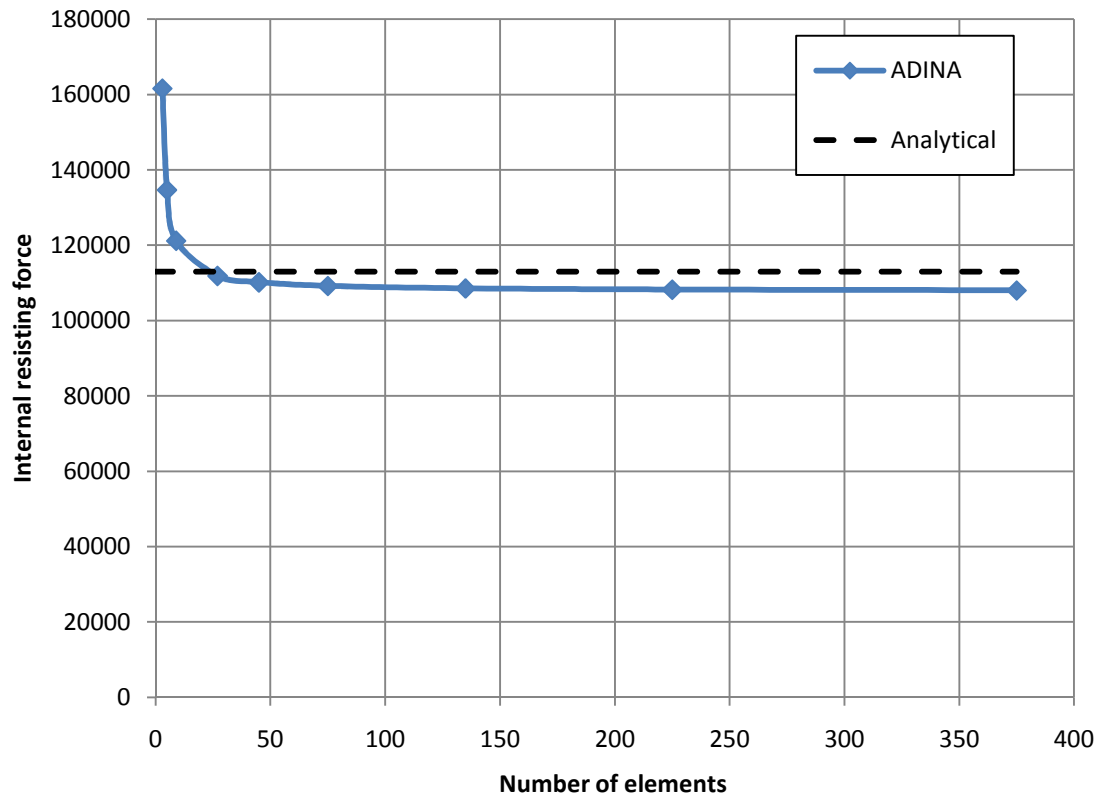


Figure G.2 Internal resisting force for the bilinear elasto-plastic model with different number of elements compared to the resisting force obtained by the analytical method.

## Appendix H Moment and reaction forces

In this appendix is moment and reaction forces presented in figures for the linear elastic and the bilinear elasto-plastic material properties. The moments are presented in three points along the beam as a function of time. The three are: the midpoint, a quarter of the beams length, i.e. 0.675 m and three quarters of the beams length, i.e. 2.025.

Due to amount of data, only a few runs chosen are and analysed. The following runs will be presented: run 1 A, run 1 B, run 5 D and uniformly distributed.

### Linear elastic results

In the elastic analysis, the fragmental load is applied separately to see how the beam's behaviour differs between the different runs and when the load is applied as a uniformly distributed.

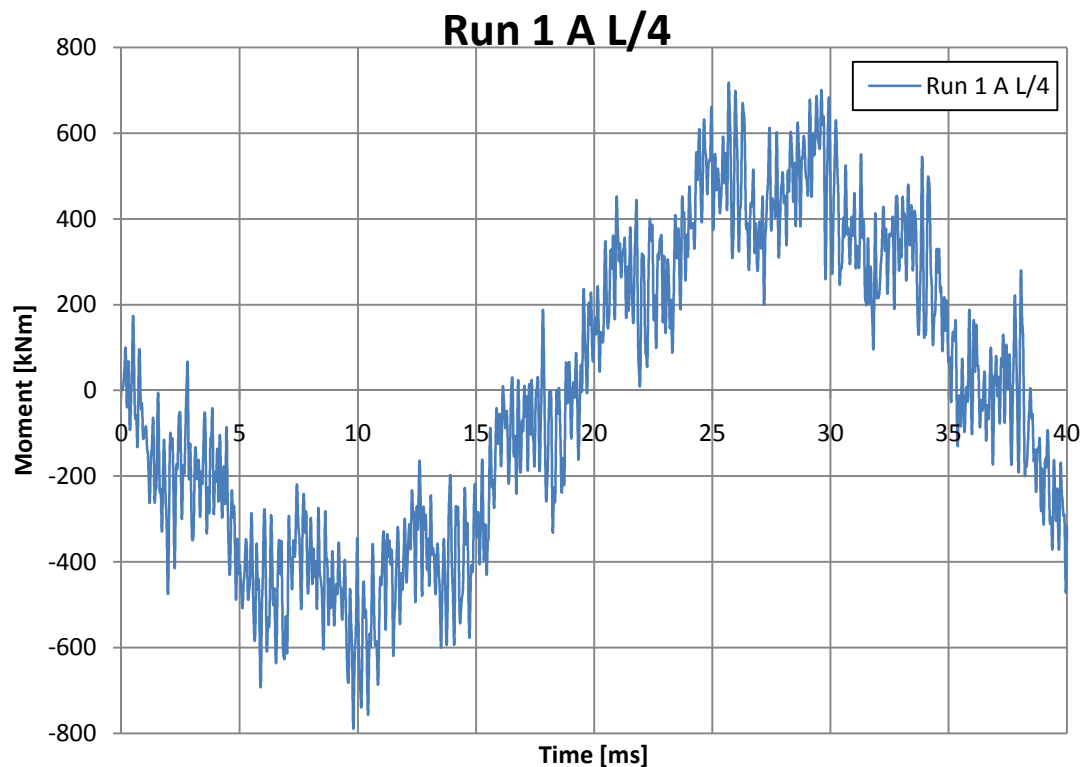


Figure H.1 Controlled deformation for the bilinear elasto-plastic model with two point loads acting on the elasto-plastic nodes.

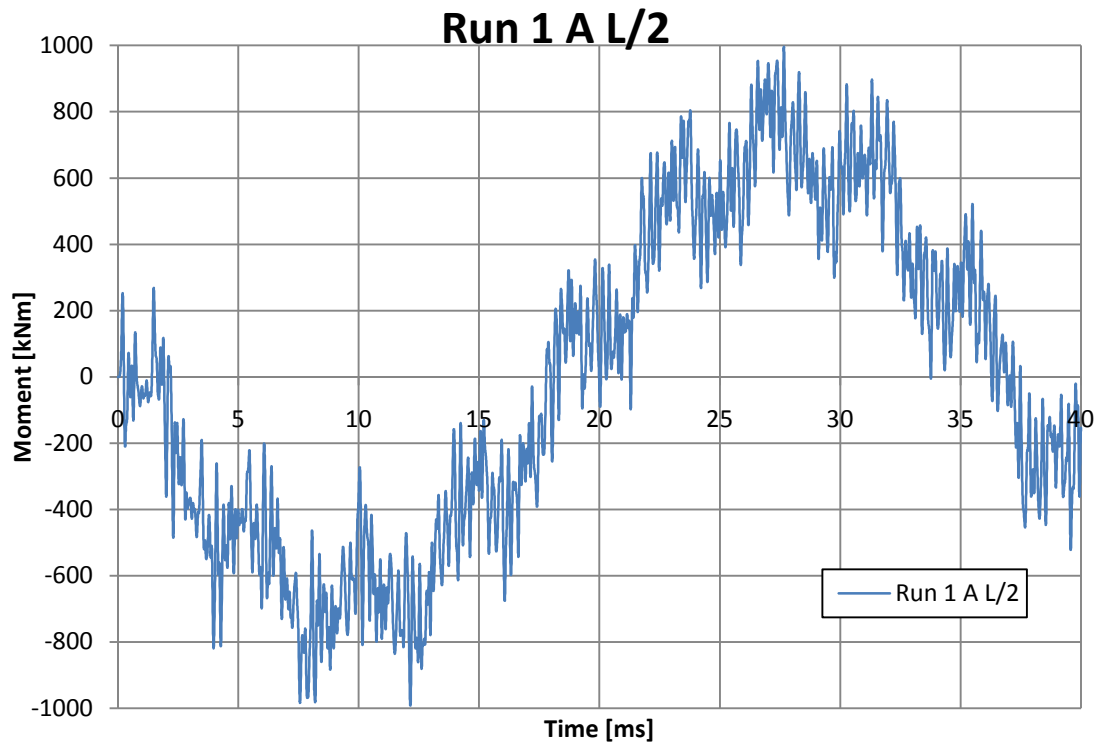


Figure H.2 Controlled deformation for the bilinear elasto-plastic model with two point loads acting on the elasto-plastic nodes.

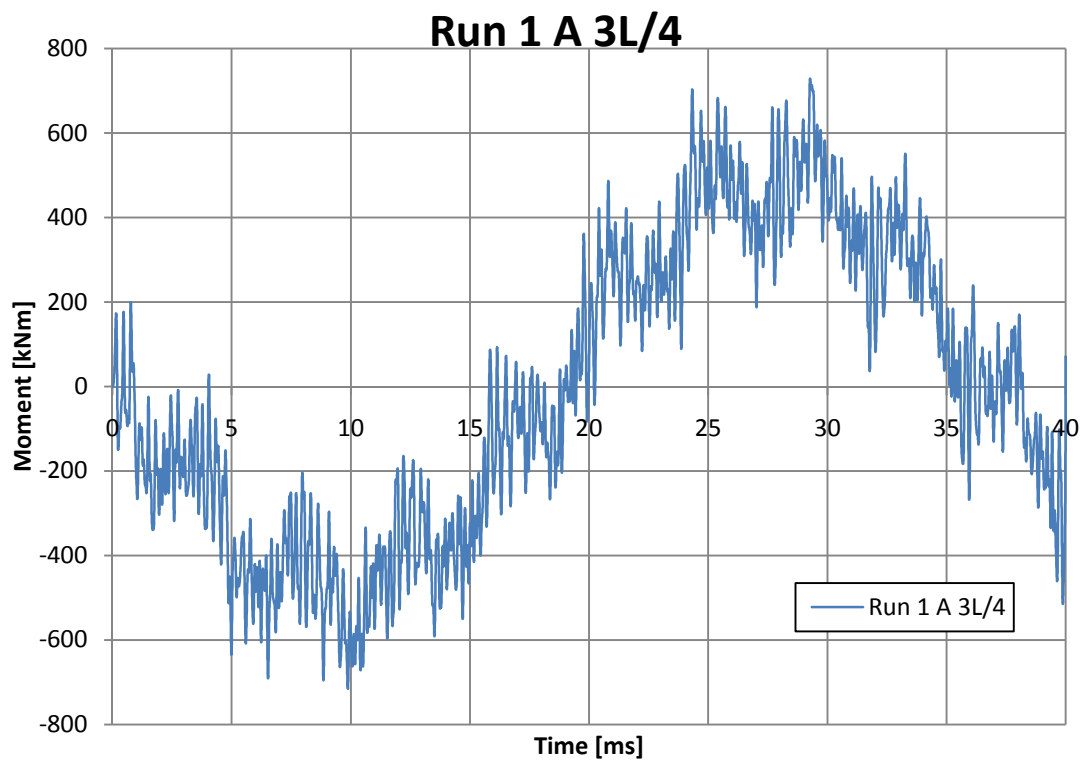


Figure H.3 Controlled deformation for the bilinear elasto-plastic model with two point loads acting on the elasto-plastic nodes.

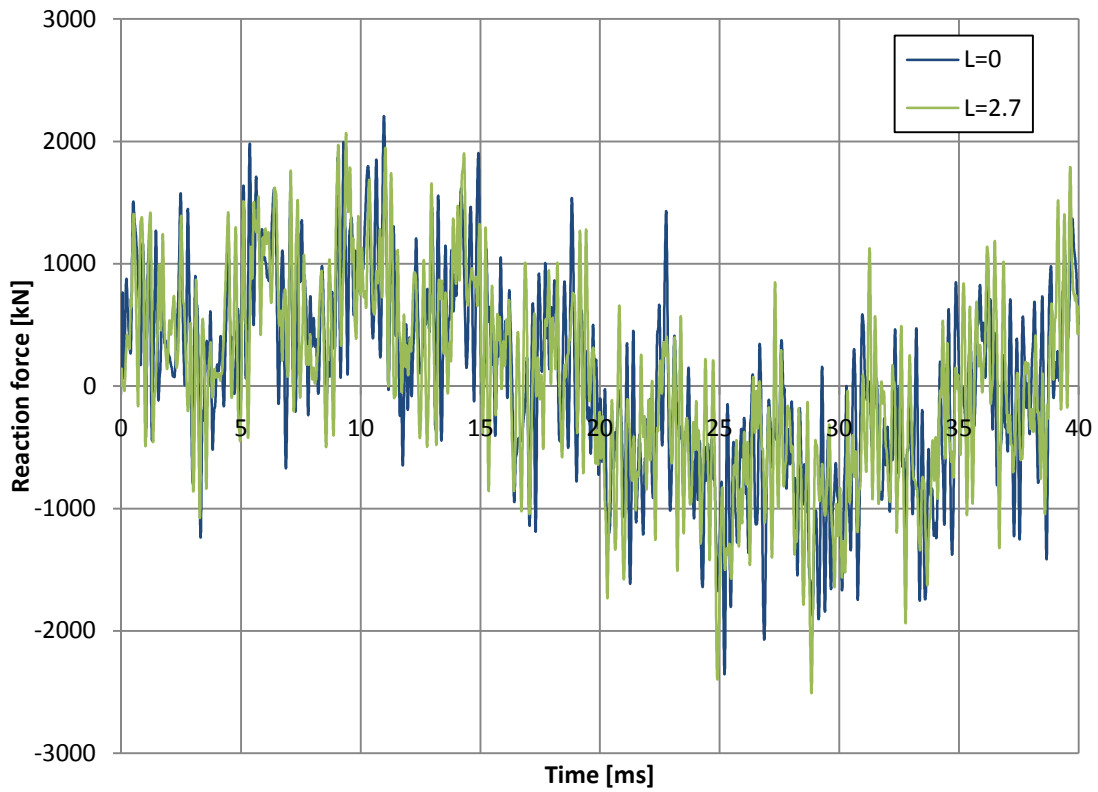


Figure H.4 Controlled deformation for the bilinear elasto-plastic model with two point loads acting on the elasto-plastic nodes.

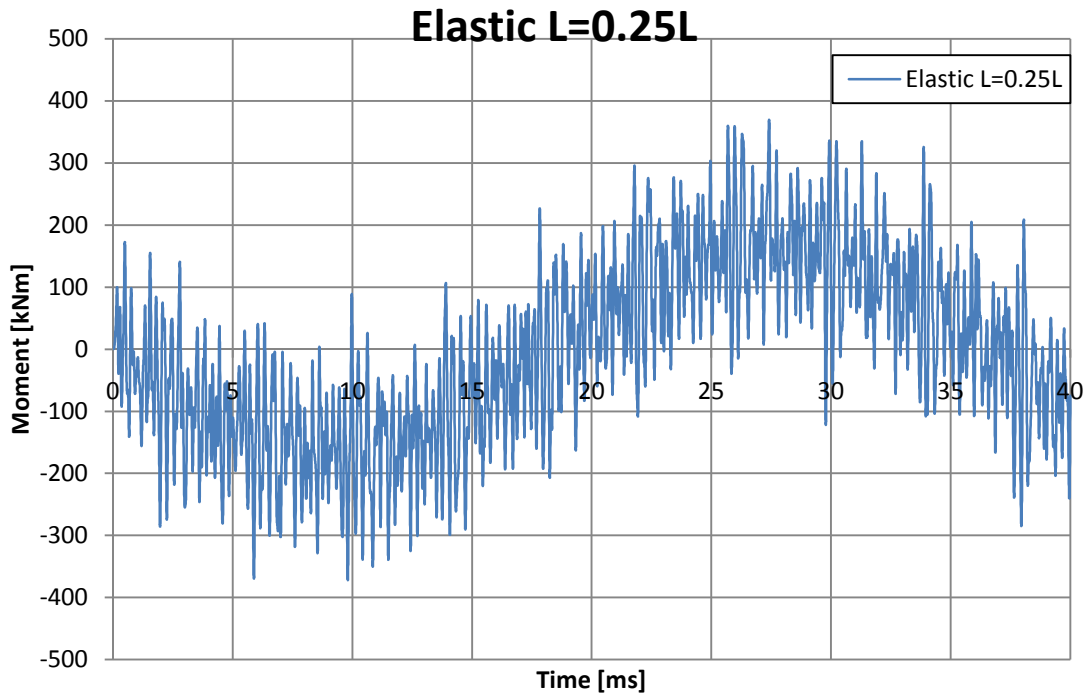


Figure H.5 Controlled deformation for the bilinear elasto-plastic model with two point loads acting on the elasto-plastic nodes.

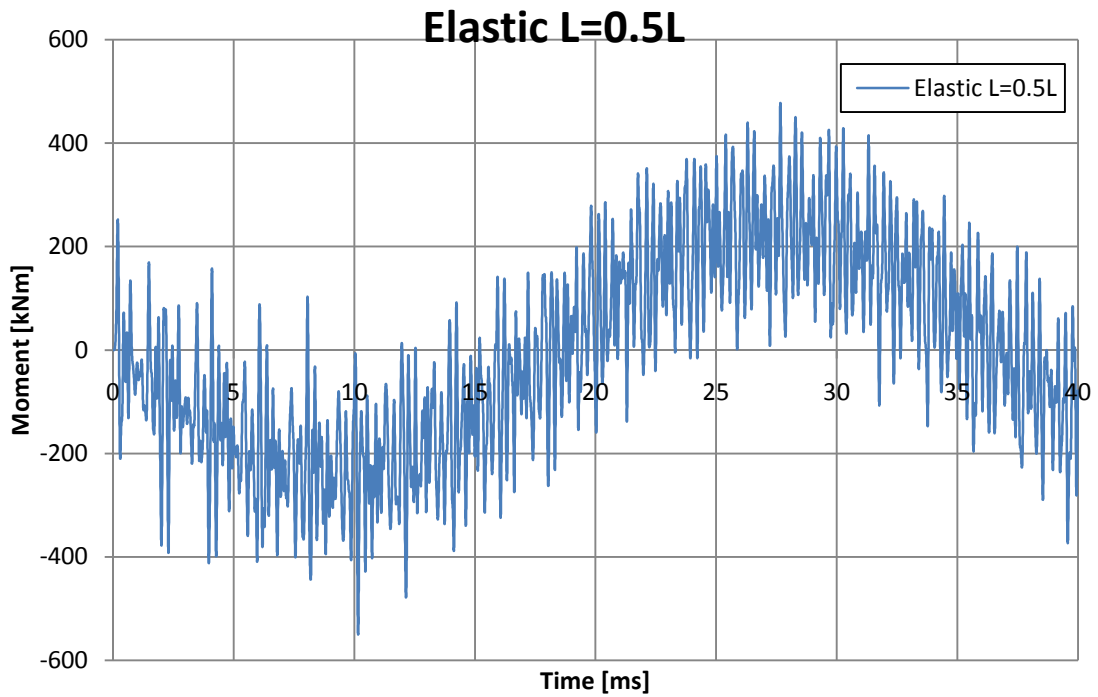


Figure H.6 Controlled deformation for the bilinear elasto-plastic model with two point loads acting on the elasto-plastic nodes.

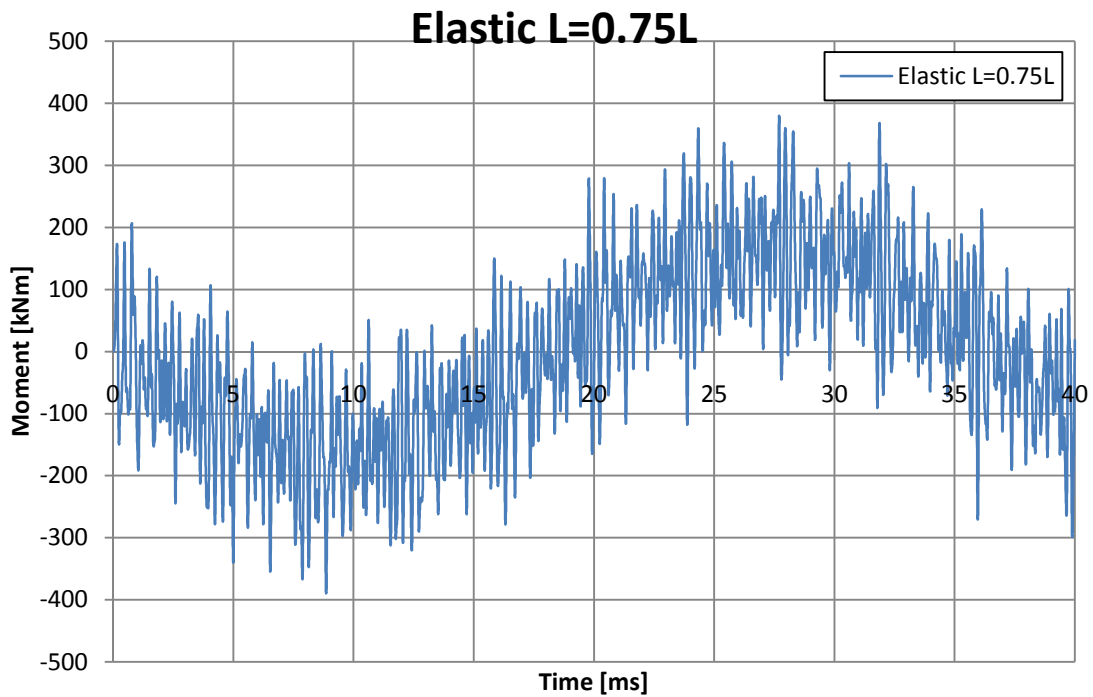


Figure H.7 Controlled deformation for the bilinear elasto-plastic model with two point loads acting on the elasto-plastic nodes.

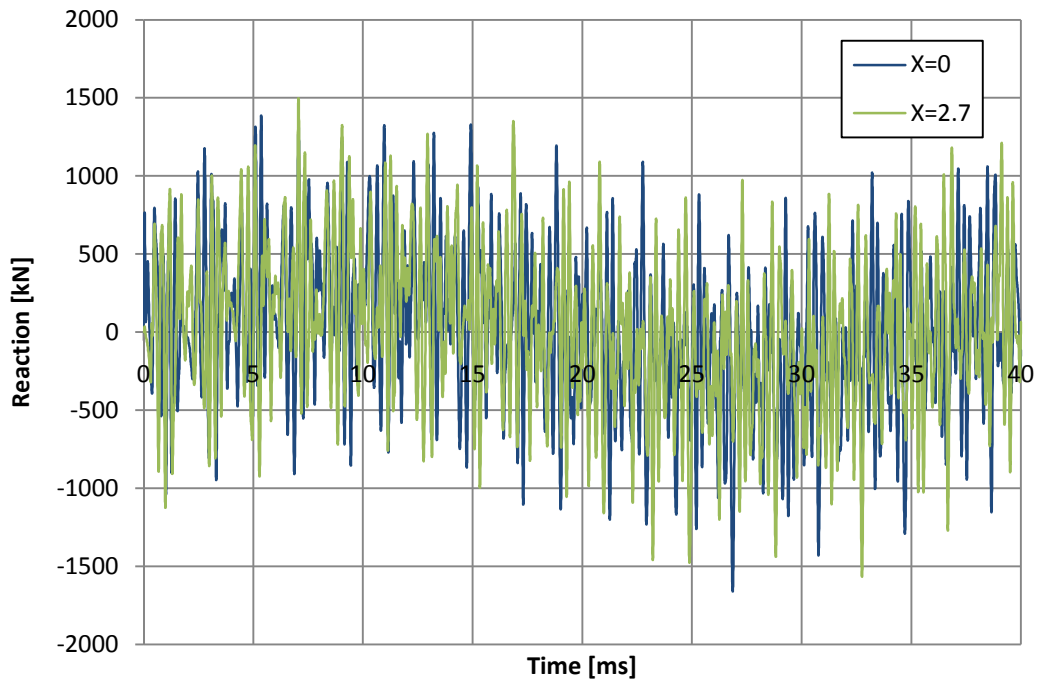


Figure H.8 Controlled deformation for the bilinear elasto-plastic model with two point loads acting on the elasto-plastic nodes.

## Appendix I Hand calculations for deflections when mass is reduced during impulse loading

Consider figure I.1 where a simply supported beam is exposed to a distributed load  $q(t)$ . The beam will, after a certain time  $t_1$ , lose a certain part of its mass. The total load can be subdivided into two parts; one where the mass is indifferent and the other where the mass has been decreased.

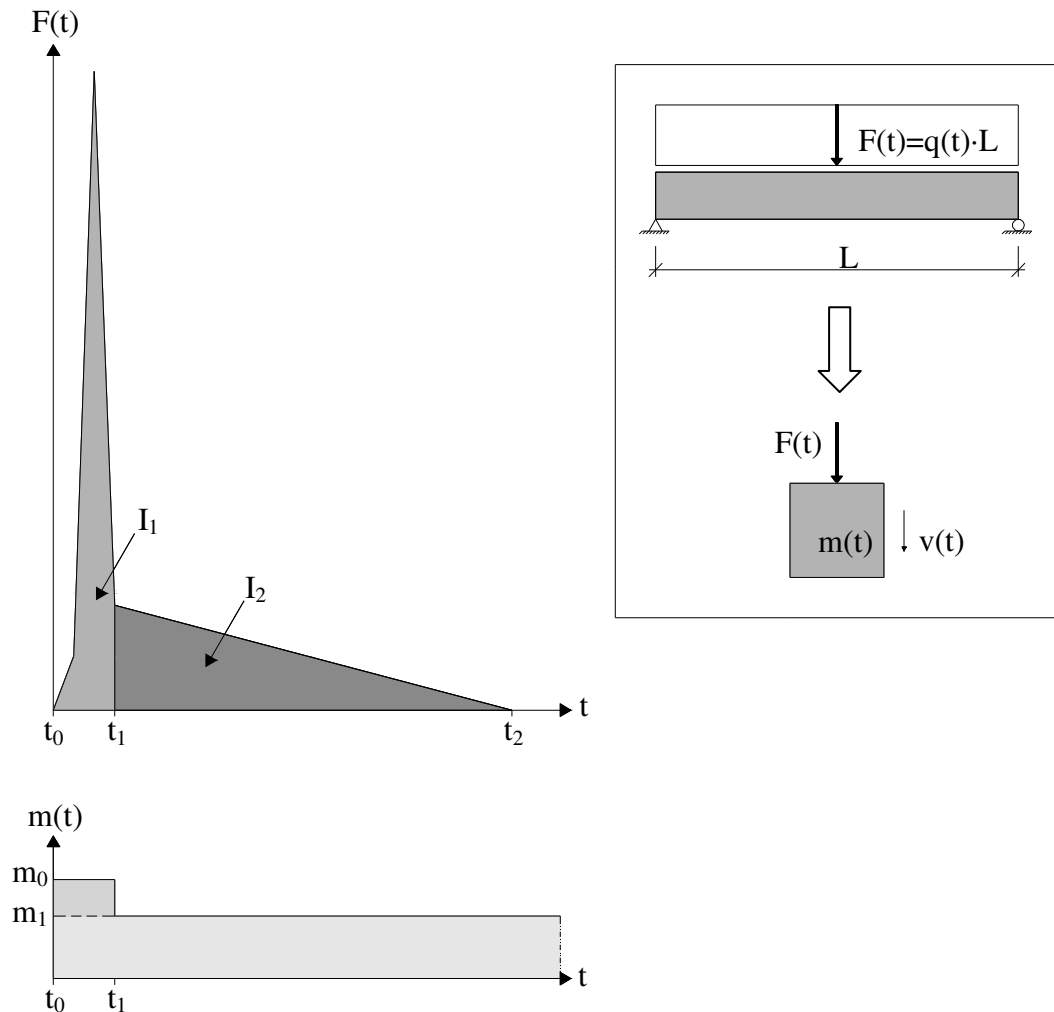


Figure I.1 Impulse loaded, simply supported beam where part of the mass is removed.

The impulse for each of the parts can be calculated as:

$$I_1 = \int_{t_0}^{t_1} F(t) dt \quad (\text{I-1})$$

$$I_2 = \int_{t_1}^{t_2} F(t) dt \quad (\text{I-2})$$

The momentum just before the beam loses a part of its mass can be written:

$$p_1 = m_0 \cdot v_1 = m_0 \cdot v_0 + I_1 = I_1 \quad \rightarrow \quad v_1 = \frac{I_1}{m_0} \quad (\text{I-3})$$

The kinetic energy at this energy can, at this time, be calculated as:

$$W_1 = \frac{m_0 \cdot v_1^2}{2} = m_0 \cdot \frac{I_1^2}{2 \cdot m_0^2} = \frac{I_1^2}{2 \cdot m_0} \quad (\text{I-4})$$

The beam will now lose a certain part of its mass. In this case one seventh of the height of the beam will be affected by the mass removal and a certain proportion  $\alpha$  of the mass in this layer will be decreased. The remaining part of the mass,  $m_1$ , is expressed by a factor  $\beta$  times the initial mass,  $m_0$ . The mass removal is illustrated by the equations below:

$$0 \leq \alpha \leq 1$$

$$\beta = \frac{7 - \alpha}{7} \quad (\text{I-5})$$

$$m_1 = \beta \cdot m_0$$

By assuming that the energy in the beam is uniformly distributed over the volume, the energy after the mass removal has to decrease with the same proportion as the mass was decreased. The energy after the loss of mass can now be written:

$$W_2 = \beta \cdot W_1 = \beta \cdot \frac{I_1^2}{2 \cdot m_0} \quad (\text{I-6})$$

We can now calculate the velocity of the remaining part directly after the mass loss as:

$$\beta \cdot \frac{I_1^2}{2 \cdot m_0} = \beta \cdot m_0 \cdot \frac{v^2}{2} \quad \rightarrow \quad v = \frac{I_1}{m_0} = v_1 \quad (\text{I-7})$$

We can see that the velocity will be conserved due to the fact that the kinetic energy is directly proportional to the mass.

The momentum in the body at time  $t_2$  when the load is removed can be expressed as:

$$p_2 = m_1 \cdot v_2 = m_1 \cdot v_1 + I_2 \quad (\text{I-8})$$

The velocity at time  $t_2$  can now, by combine equation (I-7) and (I-8) be written as:

$$v_2 = \frac{I_1}{m_0} + \frac{I_2}{\beta \cdot m_0} \quad (\text{I-9})$$

The kinetic energy, or the externally applied energy, can now finally be calculated as:

$$W_2 = W_y = \frac{m_1 \cdot v_2^2}{2} = \frac{\beta \cdot m_0 \cdot \left( \frac{I_1}{m_0} + \frac{I_2}{\beta \cdot m_0} \right)^2}{2} \quad (\text{I-10})$$

The displacements can now be calculated for elastic, plastic and elasto-plastic material response with the equations below.

$$u_{el} = \sqrt{\frac{\beta \cdot m_{0,el} \cdot \left( \frac{I_1}{m_{0,el}} + \frac{I_2}{\beta \cdot m_{0,el}} \right)^2}{K}} \quad \text{where} \quad m_{0,el} = m_0 \cdot \kappa_{MP,el} \quad (\text{I-11})$$

$$u_{pl} = \frac{\beta \cdot m_{0,pl} \cdot \left( \frac{I_1}{m_{0,pl}} + \frac{I_2}{\beta \cdot m_{0,pl}} \right)^2}{2 \cdot R_{pl}} \quad \text{where} \quad m_{0,pl} = m_0 \cdot \kappa_{MP,pl} \quad (\text{I-12})$$

$$u_{el,pl} = u_{pl} + \frac{u_{el}^2}{4 \cdot u_{pl}} \quad (\text{I-13})$$

## Appendix J Alternative method to derive transformation factors

Transformation factors for load and mass for a simply supported beam can usually be solved from the analytical expressions presented in Chapter 2. The expressions require however knowledge about the deformed shape which, for more complex load situations, can be hard to find.

Consider load case three and four in figure J.1. When having plastic material response, the deformed shape is known and the transformation factors can be solved from the equations presented in Chapter 2. For elastic material response however, the deformed shape is more complex and an analytical solution is not easy to find. An alternative solution for the transformation factors is however possible.

In commercial software for structure analysis, it is possible to plot the deflection along a simply supported beam with elastic response subjected to a certain load. In this case ADINA was used.

The shape of the deflection can then be satisfactory described by a 4<sup>th</sup> order polynomial. When the expression of the deformed shape,  $u(x)$ , is known for the actual load case, it can be inserted in the equations presented in Chapter 2 together with the expression for the load,  $q(x)$ , and the transformation factors can be solved.

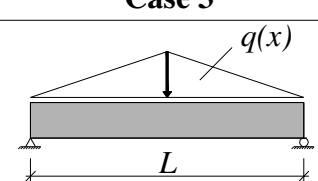
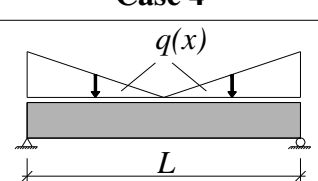
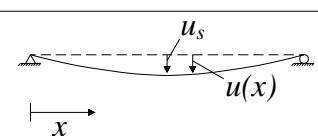
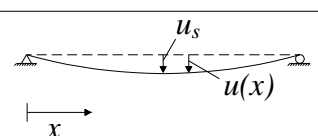
	Case 3	Case 4
		
<b>Plastic response</b>		
<b>Elastic response</b>		

Figure J.1 Load case 3 and 4.

## Appendix K Transition from elastic to plastic material response in SDOF

The transformation factors for ideal plastic and ideal elastic material response were derived from the condition that the deformed shape and the material response were the same independently of the magnitude of the load and the deflection.

When the material response changes during the deflection, as for an elastic-plastic material response, the transformation factor has to be changed in order to perform calculations based on the proper shape of deformation, i.e. the proper internal energy.

The transformation factor for the load  $\kappa_F$  is the same even if the material response changes but the transformation factor for the mass  $\kappa_M$  will change which result in a change of the combined transformation factor  $\kappa_{MF}$ .

The transformation factor for the mass is larger for elastic material response than for plastic material response which can be seen as that the effective mass will decrease when the response changes from elastic to plastic. When using the central difference method to calculate the deflection for an SDOF-system the effective mass has to be changed during the calculation. A sudden change of the effective mass will however result in a sudden loss of internal energy which might result in unwanted effects. This is why the transformation factor for the mass cannot be changed suddenly.

A better way to describe the transition from elastic- to plastic material response is to change the transformation factor and the effective mass gradually. Since the material response is a function of the internal resistance the transition should also be a function of the internal resistance.

Figure K.1 illustrates how such a transition can be done. For a certain resistance where the deformed shape starts to change from elastic towards plastic, the transformation factor starts its transition too. A linear transition is the simplest one but more advanced functions for the transition can of course be used, the linear transition is however used in this project.

Another choice that has to be considered is when, at what resistance, the transformation should start. The purpose of the transition is to imitate the reality as good as possible which is why the start point of the transition should be consistent with the behaviour of the material

For reinforced concrete, it can be assumed that the material response will start to go from elastic towards plastic at the same internal resistance as when the reinforcement yields.

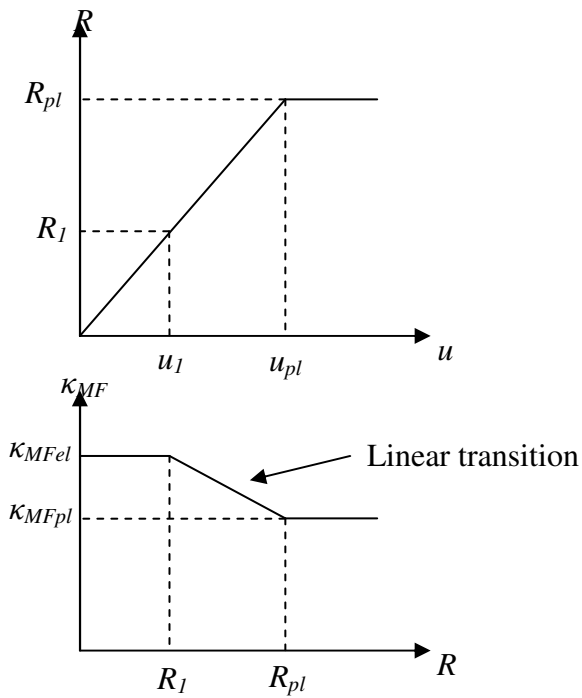


Figure K.1 Linear transition for transformation factors.

The results obtained for kappa plastic, kappa elastic and kappa as function of the resistance are presented in figure K.2

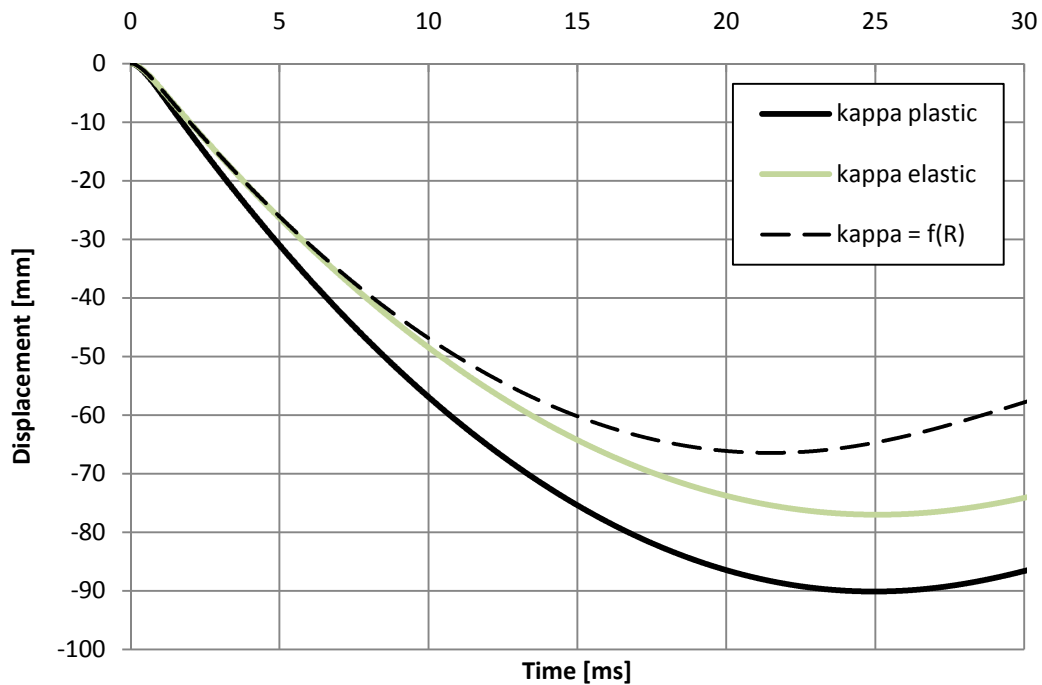


Figure K.2 Deflection as function of time when using kappa plastic, kappa elastic and kappa as function of the resistance. The same load is used.

The effective mass as function of time when changing the kappa value is presented in figure K.3. As can be seen, the duration of the transition is very short but it is still not a sudden loss of energy.

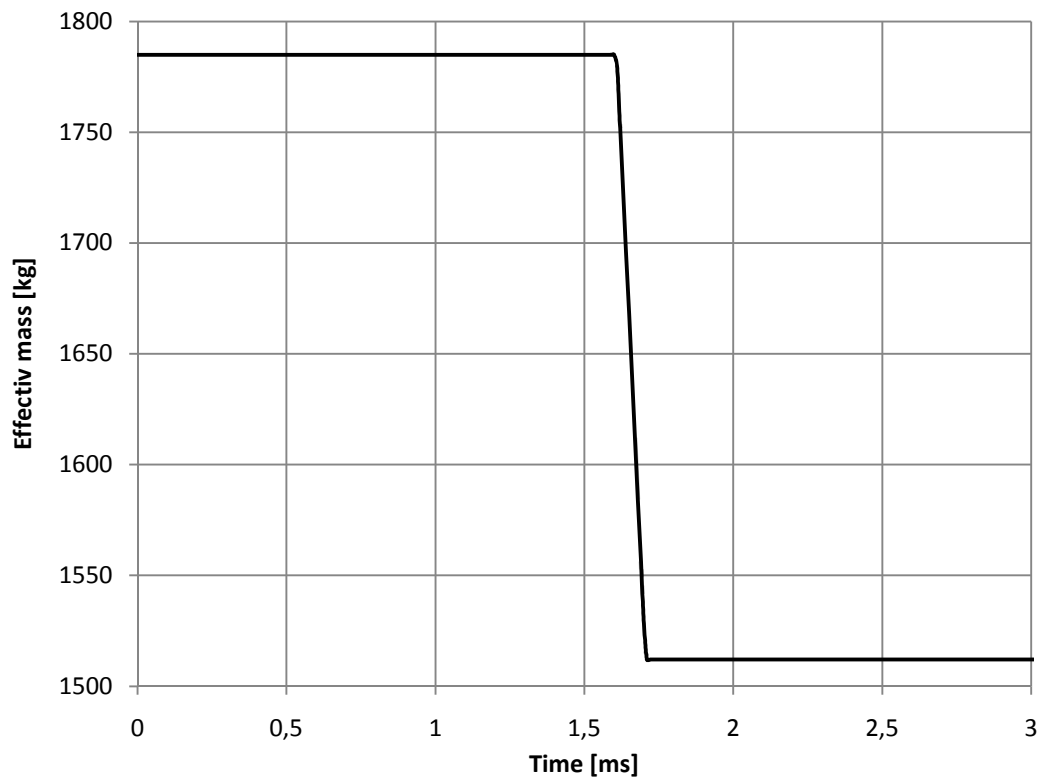


Figure K.3 Effective mass as function of time.

## Appendix L Indata file for ADINA with elasto-plastic material response

DATABASE NEW SAVE=NO PROMPT=NO

FEPROGRAM ADINA

CONTROL FILEVERSION=V85

\*

FEPROGRAM PROGRAM=ADINA

\*

COORDINATES POINT SYSTEM=0

@CLEAR

1 0 0 0 0

2 0 1.34 0 0

3 0 1.36 0 0

12 0 2.7 0 0

13 0 0 1 0

@

LINE STRAIGHT NAME=1 P1=1 P2=2

LINE STRAIGHT NAME=2 P1=2 P2=3

LINE STRAIGHT NAME=3 P1=3 P2=12

FIXITY NAME=SIMPLY1

@CLEAR

'X-TRANSLATION'

'Y-TRANSLATION'

'Z-TRANSLATION'

@

FIXITY NAME=SIMPLY2

@CLEAR

'X-TRANSLATION'

'Z-TRANSLATION'

@

FIXBOUNDARY POINTS FIXITY=ALL

@CLEAR

1 'SIMPLY1'

12 'SIMPLY2'

@

CROSS-SECTION RECTANGULAR NAME=1 WIDTH=0.3500000000000000,  
HEIGHT=1.0000000000000000 SC=0.0000000000000000 TC=0.0000000000000000,  
TORFAC=1.0000000000000000 SSHEARF=0.0000000000000000,  
TSHEARF=0.0000000000000000 ISHEAR=NO SQUARE=NO

\*\*\*\*\* MATERIAL \*\*\*\*\*

MATERIAL ELASTIC NAME=1 E=3.86E9 NU=0.2000000000000000,  
DENSITY=2400.000000000000 ALPHA=0.0000000000000000 MDESCRIP='concrete'

MATERIAL PLASTIC-BILINEAR NAME=2 E=3.86E9 NU=0.2 YIELD=5.358e6  
DENSITY=2400

\*\*\*\*\* ELEMENTS \*\*\*\*\*

EGROUP BEAM NAME=1 MATERIAL=1 RINT=7 SECTION=1

EGROUP BEAM NAME=2 MATERIAL=2 RINT=7 SECTION=1  
RESULTS=FORCES

SUBDIVIDE LINE NAME=1 MODE=DIVISIONS NDIV=14  
RATIO=1.0000000000000000 PROGRESS=GEOMETRIC CBIAS=NO

@CLEAR

1

3

@

SUBDIVIDE LINE NAME=2 MODE=DIVISIONS NDIV=1  
RATIO=1.0000000000000000 PROGRESS=GEOMETRIC CBIAS=NO

@CLEAR

2

@

GLINE NODES=2 AUXPOINT=13 NCOINCID=ALL GROUP=1

@CLEAR

1

3

@

GLINE NODES=2 AUXPOINT=13 NCOINCID=ALL GROUP=2

@CLEAR

2

@

\*\*\*\*\* DYNAMICS \*\*\*\*\*

KINEMATICS DISPLACE=small STRAINS=SMALL UL-FORMU=DEFAULT  
PRESSURE=NO INCOMPAT=AUTOMATIC RIGIDLIN=NO

MASTER ANALYSIS=DYNAMIC-DIRECT-INTEGRATION

MODEX=EXECUTE TSTART=0.000000000000 IDOF=0 OVALIZAT=NONE  
FLUIDPOT=AUTOMATIC CYCLICPA=1 IPOSIT=STOP REACTION=YES  
INITIALS=NO FSINTERA=NO IRINT=DEFAULT CMASS=NO  
SHELLNDO=AUTOMATIC AUTOMATI=OFF, SOLVER=SPARSE

CONTACT-=CONSTRAINT-FUNCTION, TRELEASE=0.000000000000  
RESTART-=NO FRACTURE=NO LOAD-CAS=NO,

LOAD-PEN=NO MAXSOLME=0 MTOTM=2 RECL=3000 SINGULAR=YES,

STIFFNES=0.0001000000000000 MAP-OUTP=NONE MAP-F§ORM=NO,

NODAL-DE=" POROUS-C=NO ADAPTIVE=0 ZOOM-LAB=1 AXIS-CYC=0,

PERIODIC=NO VECTOR-S=GEOMETRY EPSI-FIR=NO STABILIZ=NO,

STABFACT=1.00000000000000E-10 RESULTS=PORTHOLE FEF CORR=NO,

BOLTSTEP=1 EXTEND-S=YES CONVERT-=NO DEGEN=YES TMC-  
MODE=NO, ENSIGHT-=NO

ITERATION METHOD=BFGS LINE-SEA=DEFAULT MAX-ITER=50

PRINTOUT=ALL PLASTIC-=1

\*\*\*\*\* TIME FUNCTIONS \*\*\*\*\*

TIMESTEP NAME=DEFAULT

@CLEAR

4000 0.00001

@

\*\*\*\*\*Blast load\*\*\*\*\*

TIMEFUNCTION NAME=1 IFLIB=1

@CLEAR

0.0 0

0.00012 0

0.00022 1

0.00124 0

0.04 0

@

\*\*\*\*\*Fragment loads\*\*\*\*\*

TIMEFUNCTION NAME=2 IFLIB=1

@CLEAR

0.0 0

0.00017 0

0.00022 1

0.00027 0

0.04 0

@

\*\*\*\*\*Loads\*\*\*\*\*

\*\*\*Blast load\*\*\*

LOAD LINE NAME=1 MAGNITUD=4991071

\*\*\*Fragment load\*\*\*

LOAD LINE NAME=2 MAGNITUD=24234412

APPLY-LOAD BODY=0

@CLEAR

1 'LINE' 1 'LINE' 1 0 1 0.0000000000000000 0 -1 13 0 0 'NO',

0.0000000000000000 0.0000000000000000 1 0

2 'LINE' 1 'LINE' 2 0 1 0.0000000000000000 0 -1 13 0 0 'NO',

0.0000000000000000 0.0000000000000000 1 0

3 'LINE' 1 'LINE' 3 0 1 0.0000000000000000 0 -1 13 0 0 'NO',

0.0000000000000000 0.0000000000000000 1 0

6 'LINE' 2 'LINE' 1 0 2 0.0000000000000000 0 -1 13 0 0 'NO',

0.0000000000000000 0.0000000000000000 1 0  
7 'LINE' 2 'LINE' 2 0 2 0.0000000000000000 0 -1 13 0 0 'NO',  
0.0000000000000000 0.0000000000000000 1 0  
8 'LINE' 2 'LINE' 3 0 2 0.0000000000000000 0 -1 13 0 0 'NO',  
0.0000000000000000 0.0000000000000000 1 0  
\*\*\*\*\* THE END \*\*\*\*\*